POLITECNICO DI TORINO

Department of Mechanical and Aerospace Engineering

Master’s Degree Course

in Biomedical Engineering

EFFECTS OF BONE EROSION ON A TOTAL SHOULDER ARTHROPLASTY: FINITE ELEMENT ANALYSIS

Supervisors:

Prof. Cristina Bignardi

Prof. Alberto Audenino

Prof. Bernardo Innocenti

Candidate:

Emma Campopiano

232578

A.Y. 2017-2018

A Mattia,
che non si arrenda mai.

A mio padre,
il mio instancabile supporto.

A mia madre,
una forza della natura.

List of Contents

List of Figures

List of Tables

List of Graphs

Abstract

Anatomic total shoulder arthroplasty (aTSA) has markedly developed in the decades thanks to its efficacy in relieving patients' pain and restoring the correct function of arthritic shoulders [106] [107]. The main reason of its failure is glenoid component loosening, since it jeopardies stability and survival of the implant, chiefly in shoulders with preoperative erosion [15]. Posterior glenoid erosion is commonly found in some patients affected by osteoarthritis. That type of disorder can lead to an increase of complications and component loosening, affecting negatively on clinical outcomes after an aTSA [14] [15]. Eroded shoulders are difficult to deal with and correct because the glenoid components need sufficient bone support for the implantation so as to promote osseous integration or cement layer long-term survival. Therefore, predicting the possible consequences of implanting an anatomic component with incomplete bone support is crucial for long term stability of implant.

The adequate bone support to limit glenoid loosening has not yet been defined [56]. Thus, the aim of the present work is to analyse the effects of posterior bone erosion on the glenoid-component stability when anatomical shoulder prostheses are implanted and to provide indications on what could be the impact of bone support reduction on the strains and stresses both in the bone and in the prosthesis.

In order to do this, 3D Finite Element models were generated using a mean shape scapula and two types of implants: the former is an all PE cemented component and the latter is a T.E.S.S. cementless component. Five different type-B2 bone erosions (5°, 10°, 15°, 20° and 30°) were implemented through a 3D cutting procedure. A quasi-static analysis was performed simulating a worst-case scenario during a 90° abduction in the frontal plane. Two loading conditions were considered: concentric and eccentric compressive forces applied perpendicularly to the glenoid plane mimicking the actual clinical situations [100]. FEA results were compared in terms of glenoid loosening, bone stress and strain using three failure criteria.

All considered parameters showed an upward trend compared to the reference model (without posterior erosion) with the decreasing of bone support for both loading conditions. Even though, the values obtained in the eccentric condition were always higher than those in the concentric case for both implants. For the all PE implant a decrease of the backside support until 95% had no relevant effect on cement stress, however the high degree of CCV for the reference model should raise concern. In case of a cementless component interfacial micromotions increased starting from 97% bone support. Consequently, all of which leads to the conclusion that an anatomic glenoid component should always be implanted with full backside support. In case this is not possible without jeopardising other outcome related factors like glenoid orientation, other options should be investigated.

Chapter 1
Introduction

1.1 Shoulder anatomy

The shoulder is one of the most complex and mobile joints in the body. It is formed by several structures: bones and joints, ligaments and tendons, muscles, nerves, blood vessels and bursae (Figure 1). Such structures are linked and work together to control the typical motions of the upper limb. The scapula, the clavicle and the humerus are the three main bones in the shoulder. They are related through four joints [1]:

- *glenohumeral joint (GHJ)*: it is a ball-and-socket joint, characterized by the glenoid cavity in which the head of humerus articulates. The articular surfaces are covered by hyaline cartilage;
- *sternoclavicular joint (SCJ)*: it supports the connection of the shoulders and arms to the main skeleton on the front of the chest;
- *acromioclavicular joint (ACJ)*: it is a plane synovial joint, that connects the clavicle to the acromion process of the scapula;
- *scapulothoracic joint (STJ)*: it is considered a not true anatomic joint, that links the scapula to the ribs at the back of the breast.

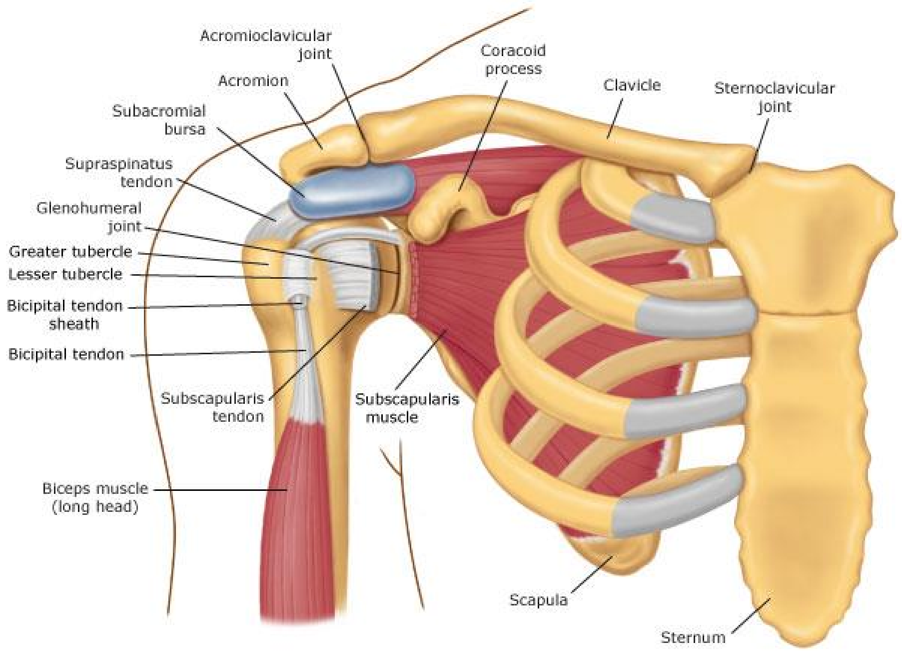

Figure 1 - Shoulder Anatomy [2].

Many muscles attach to the main bones of the shoulder and allow a wide range of motions of the upper arms. The most important muscles are:

- the *infraspinatus*: it is a rotator cuff muscle and links the humerus and the scapula through tendons;
- the *deltoid*: it is the largest muscle of the shoulder and covers the GHJ. Such muscle allows different motions of the scapula (extension, flexion and abduction);
- the *trapezius muscles*: it allows the elevation of the clavicle and consequently of the whole shoulder;
- the *pectoralis*: it connects the humerus, the clavicle and the sternum on the front of the chest.

The *rotator cuff* is a muscle-tendon system of the shoulder made up of four tendons and four muscles (subscapularis, infraspinatus, teres minor, supraspinatus). Such system has two important tasks: the former is to stabilize the upper limb and the latter is allow the rotation and the abduction [3].

1.1.1 Motions

Ligaments, tendons and muscles cooperate to allow stable motion through generating joint moments and stabilizing forces. The shoulder provides to the upper limbs a wide range of motion: flexion, extension, adduction, abduction, external and internal rotations, 360° circumduction in the sagittal plane, scapular retraction, protraction, elevation and depression (Figure 2).

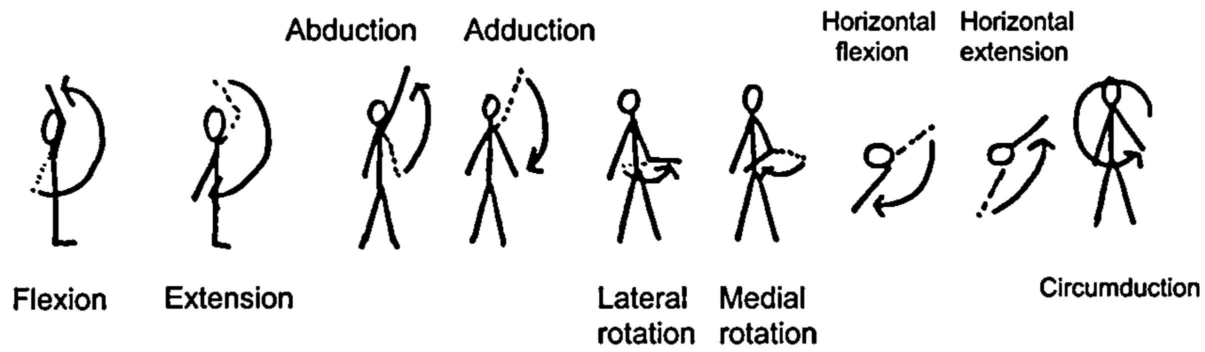

Figure 2 - Shoulder Joint Movements [4].

The abduction motion in the scapular plane is considered in the present work. The main muscles involved in the abduction motion are the deltoid, the trapezius and the supraspinatus.

1.2 Total Shoulder Arthroplasty (TSA)

Shoulder pain is a frequent disorder that occurs in many diseases of the glenohumeral joint. Generally, such symptomatology spreads to the neck and the hand leading to difficulties in the motion of the upper limb. The treatment of shoulder disorders is still a complex and challenging matter. When conservative or medical therapy do not carry out to effective results, the use of prosthesis represents a definitive solution to pain.

Total shoulder arthroplasty (TSA) is a surgical technique which involves the glenohumeral joint (GHJ) replacement in order to reduce patients' pain and to restore the correct function of the shoulder. Several reasons lead to TSA:

- *osteoarthritis*: it involves to the loss of cartilagine on the humeral head and on the glenoid with the subsequent disappearance of the joint space between the scapula and humerus, articular surfaces deformations and formations of osteophytes;
- *rotator cuff tear arthropathy*: a huge lesion of rotator cuff leads the humerus to lose the centering with the glenoid and to move upward;
- *rheumatic diseases*;
- *humeral head necrosis*: the humeral head deforms and degenerates as a result of the lack of the appropriate blood supply;
- *poorly established fractures* [5].

Figure 3 - Anatomical Total Shoulder Arthroplasty [10].

The GHJ replacement has the aim of reproducing the mechanics and anatomy of the joint through the insertion of prosthetic components chosen according to the specific requirement of each patient and pathology. The main components of a typical shoulder implant (Figure 3) are:

- *humeral component*: it consists in a cemented or cementless stem and a cap with a spherical surface. Before the positioning of the component, the humeral head is dissected and the degenerated portion is removed. Furthermore, the humeral canal is excavated to insert the stem;
- *glenoid component*: it is characterized by a concave surface, which can be all in polyethylene or composed of a metal baseplate and a polyethylene insert.

The shoulder arthroplasty has developed significantly over the last fifty years. According to Khatib *et al.* [6], the shoulder arthroplasty procedures have increased of 393% in the New York State between 2001 and 2010. Such increase reflects the improvement of prosthetic implants, the general success of the surgical techniques and the growing desire of patients to improve their quality of life.

The evolution and the increase of shoulder implants lead to a surgical revisions growth: they have risen of 29% over the last ten years. The revision rate for a TSA is higher than knee and hip arthroplasty over a 10-year observation period [7]. Many studies [8] shows a TSA success from 67% to 99.7% over a <10-year follow-up, while according to other researches [7] the success rate decreases significantly over a >10-year follow-up.

Total shoulder arthroplasty is not free from intra-, peri- and post-operative complications. A prosthetic shoulder can last from 10 to 20 years [5] and it presents some risks like all invasive surgical procedures. Such events include infections, instability of the prosthesis, fracture of the scapula or humerus, the formation of hematomas and paralysis of nerve.

Several causes affect shoulder prosthesis durability: implant design, size and positioning, bone structure and quality and forces. The main reasons of implants failure concern the glenoid cavity, in particular the bone erosion (20.6%) and glenoid component mobilization (14.3%) [9]. From what was previously said, a method to reduce the failure rate of glenoid component should be sought in the study of glenoid morphology and orientation and in the eventual correction of this last, in the choice of the most suitable implant for the patient and in the improvement of the surgical procedure.

1.3 Bone erosions

Glenoid pathology can change the structure of the glenoid cavity. Glenoid erosions represent a hard challenge to face for shoulder arthroplasty surgeons. Lack of sufficient bone support takes on particular importance in the TSA planning because glenoid bone loss can increase the glenoid component loosening [11]. Progressive bone loss leads to an increase of glenoid retroversion, which is correct when a TSA is performed. Thus, pre-operative planning is fundamental to quantify bone loss.

Several methods to assess posterior subluxation of humerus and glenoid erosion developed. Walch et al. [12] carried out a study on the possibility to classify the glenoid morphology in primary glenohumeral osteoarthritis (GHOA) and they developed a system based on the typology and severity of glenoid usury and version (Figure 4). The humeral head position in the glenoid cavity is an important element to predict the glenoid morphology evolution. Three kinds of glenoid were defined and identified by letters and numbers:

- *Type A*: in a type A glenoid the humeral head is well-centered and the forces are well-distributed on the glenoid surface. According to the erosion severity, the glenoid can be type A1 (minor erosion) or type A2 (major erosion).
- *Type B*: in a type B glenoid the humeral head is subluxated posteriorly and it leads to an asymmetric distribution of loads. According to the erosion severity, the glenoid can be type B1 (posterior subluxation without erosion) or type B2 (posterior erosion with a biconcave glenoid).
- *Type C*: a type C glenoid is characterized by a retroversion over 25° without taking into account the erosion.

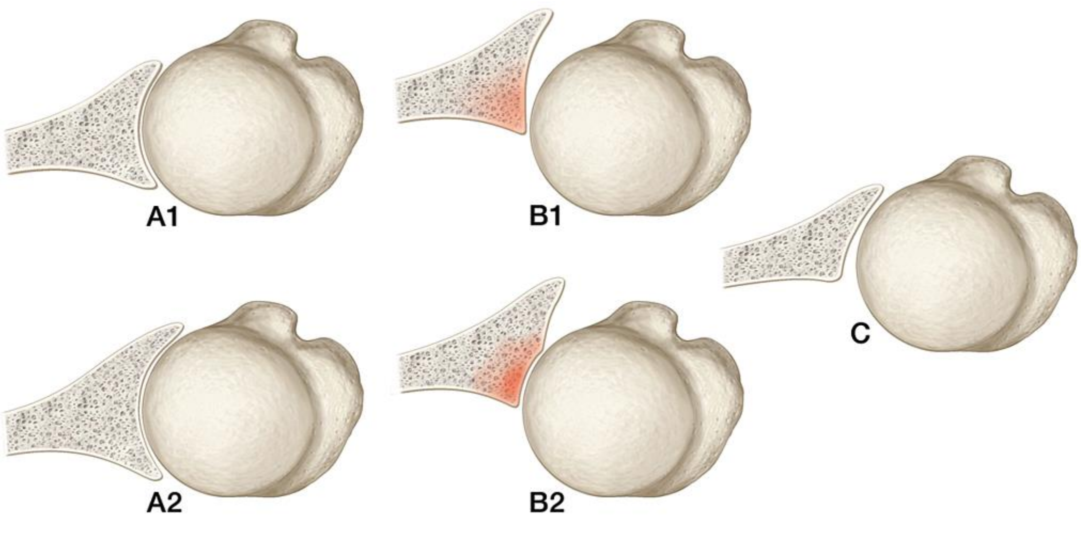

Figure 4 - Walch classification of glenoid morphology [13].

B2 glenoid morphology is difficult to deal with in an anatomic total shoulder arthroplasty. Many studies have shown an increase of complications and rates of glenoid component loosening and poor clinical outcomes after an anatomical total shoulder arthrosplasty (aTSA) in patients with B2 glenoids [14] [15].

B2 erosion occurs in more than 41% of patients [16] and the traditional surgical procedures are often inadequate to its treatment [17] [18]. The most widely used techniques to face B2 glenoid defects include: the asymmetric reaming of the glenoid and the use of a standard glenoid component if the bone loss is minimal; the bone grafting or the use of augments if the bone loss is considerable. In certain cases, reverse shoulder arthroplasty shall be used [19].

1.4 Aim of the work

The aim of the present work is to analyse the effects of posterior bone erosion on the glenoid component stability when anatomical shoulder prostheses are implanted and to provide indications on what could be the impact of bone support reduction on the strains and stresses both in the bone and in the prosthesis.

Two types of implants were considered in this study and they were compared in terms of glenoid loosening, bone stress and strain: the former is an all PE cemented component and the latter is a T.E.S.S. cementless component.

The study is organized into two main steps: firstly, a Finite Element model of the shoulder was implemented and several type B2 bone erosions were performed; secondly, the two prostheses were implanted and the FEA results were analysed.

Chapter 2
Glenoid Components

The first total shoulder implant was introduced by Neer in 1974 [20], and it included a cemented, all PE keeled component and a monoblock humeral stem. Prostheses designs have developed significantly over the last sixty years to try and solve the initial problems they presented: limited range of motions and functions and components loosening.

Each year around 23 000 shoulder prosthesis surgeries are performed compared to 343 000 hip prosthesis surgeries and 400 000 knee ones [21]. The limited number of shoulder replacement is due to the complexity of shoulder joint. Because of it, several shoulder implants, fixation methods and surgical procedures exist, they are used according to diseases and implicated tissue.

2.1 Glenoid classification

Modern glenoid components can be classified according to shapes, sizes, fixation methods and designs. Some components have a pear shape to fit well to glenoid cavity's shape, while others present an elliptical shape, which adapts better to glenoid after reaming.

Moreover, prostheses backsides can be one of two types: flat or convex. Anglin *et al.* [22] carried out a study to evaluate the resistance to loosening of flat of curved- and flat-back glenoid components. They observed favourable results for the curve-back components: these last allow to preserve more bone during the replacement surgery and they endure micromotions more efficiently than flat designs. Other research [23] through FEA demonstrated a minor susceptibility to malposition-related failure for the curved-back glenoids.

One of the main goal in TSA is reaching long-term fixation of the glenoid component, which can be limited by decrease of bone support in the glenoid cavity. For this purpose, several types of fixation methods have been developed, they include cemented, cementless, minimally cemented and hybrid devices.

Cemented components with pegs or keels are the most common and they provide a more predictable fixation, while cementless components are based on biologic integration: screws or press-fit pegs are used to obtain an initial fixation, which facilitates long-term bone ongrowth/ingrowth. However, even though uncemented components present theoretic benefits compared to those cemented, they show higher complication rates. Hybrid fixation is a combination of the two methods of fixation described above. These implants are minimally cemented, they maintain the thickness of traditional all-poly cemented components and they are fixed through pegs, sleeves or other features.

Glenoid implant designs can be divided into all-polyethylene and metal-backed components. The former are generally fixed through a cement layer and they are limited by the higher stresses, that occur in the cement, while the latter show a higher rate of failure due to the excessive micromotion at the interface bone-implant.

2.1.1 All Polyethylene Components

The majority of glenoid components used today are wholly constituted in polyethylene (PE) and designed to a cemented fixation around pegs or keels. This may be due in part to the good mechanical properties of all-PE components: they allow the translation of the humeral head, but they do not transmit excessive stress at the interface.

2.1.1.1 Keeled vs Pegged Components

Pegged components are made up of circular pegs that may differ in number, configuration and length (Figure 5a and Figure 5b), while keeled components are characterized by a tapered "fin" with roughly rectangular cross section (Figure 5c).

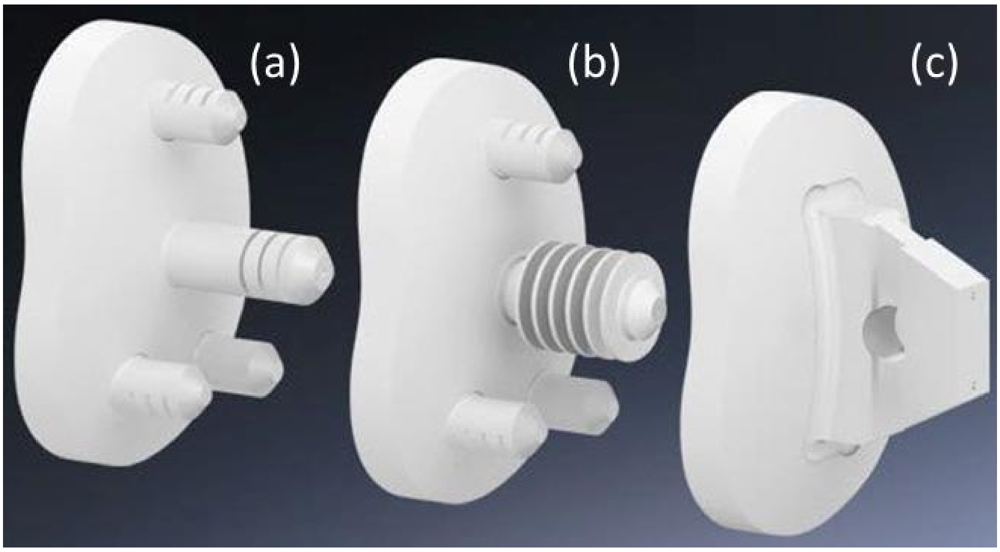

Figure 5 - All PE Glenoid Components: (a), (b) pegged glenoids; (c) keeled glenoid [24].

Many studies were carried out during the years to compare keeled and pegged components and to provide information about which of the two implants could present the better results. Some research through radiographic comparison [25] [26] demonstrated that keeled components are inferior radiographically to pegged components. Two-dimensional Finite Element Analyses [27] [28] also found that pegged implants showed a more physiological stress distribution, concluding that the use of pegged designs is the best approach for regenerating physiological bone stresses. A recent comparative study [29] through a three-dimensional Finite

Element Analysis showed different performances of the two implants depending on the bone quality. In particular, Lacroix *et al.* [29] demonstrated that cement stresses are lower in normal bone for a pegged component, whereas a keeled component provides lower cement stresses in rheumatoid arthritic (RA) bone.

2.1.1.2 Fixation

Both keeled and pegged implants are intended for cemented fixation. A great deal of research [30] has analysed the effect of cement preparation techniques and cement layer thickness on fixation thereof. Terrier *et al.* [31] evaluated how the stresses in the cement and the bone changed considering several uniform cement thicknesses (0.5, 1, 1.5 and 2 mm) and a flat-backed keeled glenoid. In their Finite Element Analysis, they used two types of loads, concentric and eccentric loadings, and two types of contact condition, namely debonded and bonded conditions. Therefore, they observed that cement stress decreased with the increasing of cement mantle thickness and a cement thickness of 1 or 1.5 mm allowed to minimize bone stress. Furthermore, they observed that the overall stress in the cement layer and bone were higher with eccentric loads and debonded condition. Accordingly, they suggested that a uniform cement layer 1.0 mm thickness was optimal for a better stability.

Anglin *et al.* [22] studied the correlation between cement fixation and glenoid surface finish. They compared the resistance to glenoid loosening with two implants: roughened- and smooth-back ones. The former resulted more stable resisting until 250 000 eccentric loading cycles, while the latter yielded during the first cycle.

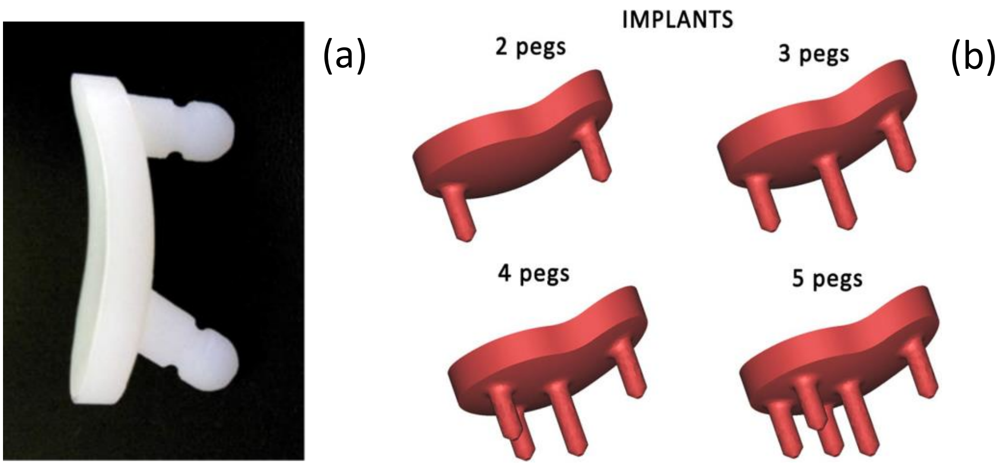

Figure 6 - Pegged Glenoid Designs: (a) glenoid component with divergent pegs [11]; (b) Wahab *et al.* [34] analysed designs.

In the last years, various version of the traditional all-poly pegged prostheses were developed with the aim of improving components stability. In fact, to achieve a better stability against micromotions, divergent pegs were introduced (Figure 6a). Besides, parametric studies have analysed how pegs design affected implant stability [33], since the existence of several prosthetic designs pointed out uncertainty relating to the optimal design able to decrease stress and relative micromotions at the bone-implant interface.

Giori *et al.* [33] performed mechanical tests to evaluate the sheer stability of five geometries with different size and shapes. The analysed parameters were the size, number and the aspect ratio (length/diameter) of the pegs. The results showed a more uniform stress distribution in the support material and a more sheer stability per unit volume in implants with multiple small pegs than those with fewer larger pegs.

A similar study was carried out by Wahab *et al.* [34] using a Finite Element Analisys. They compared the stability of four implants with different number of pegs (Figure 6b) in terms of relative micromotions and focal stress distributions. The results suggested that the micromotions for all implants remained within the acceptable limit without compromising the prosthesis stability, while the total focal stress volumes exceeding the specified threshold decreased with increasing number of pegs. Therefore, according to Wahab *et al.* [34] the optimal peg design was represented by four-peg glenoid implant because it provided lower stress volumes than lesser-peg components, reduced cement mantle usage and preserved more bone support than major-peg components.

2.1.2 Metal-backed Components

Metal-backed prostheses were developed to improve glenoid components stability. The first components were cementless and fixed to the bone through screws.

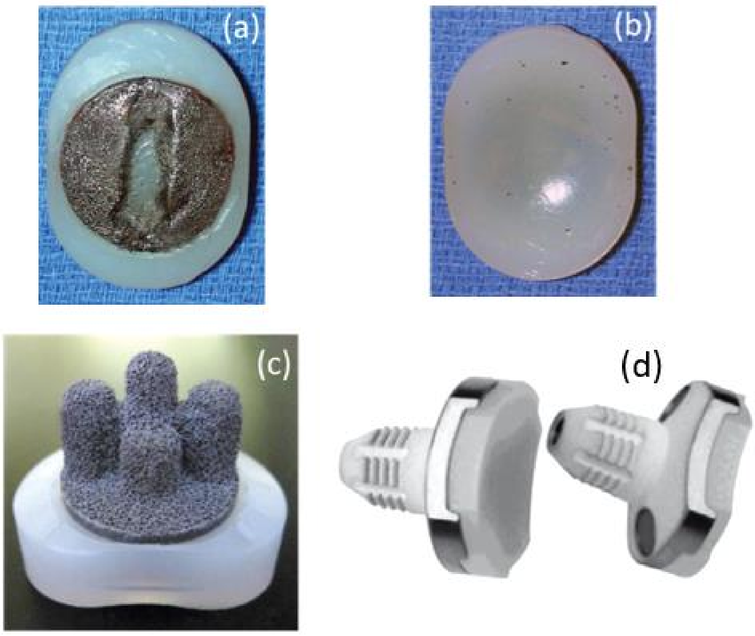

Figure 7 - Metal backed implants: (a), (b) failed glenoid components [41]; (c) trabecular metal glenoid component [41]; (d) new generation metal backed implant [9].

Originally the idea was to strengthen the polyethylene implant with metal in order to improve the stress distribution at the cement-bone interface. In 1978 Neer developed a metal back glenoid component called Neer Mark II [35]. However, several studies [36] [37] [38] demonstrated that the lucency rate did not decreased with the better loads transfer with the Neer

Mark II. In addition, the new implant had higher failure rate with shoulder pain and early loosening. Subsequently, a new concept of prosthesis started to develop widely: the aim was not just to improve Neer Mark II's problems, but also to realize a new method of cementless primary fixation, more durable and stable, that could replace the cemented implants. The Cofield MB implant was designed in 1981 and it consisted of a porous surface fixed by two screws and a central uncovered peg [35]. Many studies [38] [39] [40] demonstrated that, even though Cofield MB component was well-fixed to the bone, a number of complications occurred: polyethylene wear and dismantling, dissociation between this last and metal, instability, upward migration, off-centered strain and fragilization of the cuff. Nowadays Cofield MB implant is obsolete.

Over time metal-backed designs were modified, eliminating screw fixation and improving porous materials. These implants consisted of a polyethylene monoblock, that replaced the metal backing, and a porous central keel which allowed bone ingrowth [41]. However, the implants still presented high failure rate due to fractures at the keel-glenoid junction (Figure 7a and Figure 7b). To solve such problem, the bony ingrowth platform and the bond to the polyethylene monoblock were reinforce (Figure 7c).

Recently, Castagna *et al.* [42] studied a glenoid component different from the others by the fixation mechanism (Figure 7c). The implant was characterized by a convex bone-metal back interface and a polyethylene insert; its stability was achieved through a large cable central peg. Based on the obtained results, Castagna *et al.* [42] concluded that a metal-backed glenoid component was a good option in the TSA that could be used as an alternative to cemented all-polyethylene prostheses.

2.1.3 Cemented vs Uncemented implants

The choice of the right glenoid component in the TSA in terms of better adaptability to the patient, stability and durable biologic fixation method appears to be extremely difficult.

All-poly implants allow to reduce stress concentration and are more compliant than those metal-backed. These last are better in terms of lucency but the metal backing leads to a significant increase of stress concentration [43]. The critical zone of cementless component with two interfaces is the transition region where the metal baseplate meets the polyethylene insert. In this region high stresses develop that lead to polyethylene wear [44] [45] [46].

Boileau *et al.* [47] carried out a study of 40 shoulders in which they compared the results of cementless and cemented implants. The results showed an increased incidence of postoperative radiolucent lines after a TSA with a cemented component: 85% for the cemented glenoids compared to 25% of cementless ones. Nonetheless these last required more revision surgery due to the early loosening: 20% for uncemented glenoid compared to 0% for cemented ones. According to their outcomes, Boileau *et al.* [47] suggested two potential causes of metal-back loosening: biologic and mechanical, the former was due to metal and polyethylene wear debris that caused osteolysis, the latter was due to the lack of initial stability. Therefore, they concluded that uncemented glenoid fixation was inferior than that cemented.

Wallace *et al.* [48] analysed the outcomes of 26 cementless implants and 32 cemented components for a mean follow-up of 5 years. They observed that the intermediate results of cementless and cemented implants were comparable even though uncemented glenoids presented more early complications.

A great deal of research [38] [49] [50] analysed survival of metal-backed components. A retrospective analysis of 140 cementless implants conducted by Martin *et al.* [49] for a mean follow-up of 7.5 years showed that 11.4% of prostheses failed clinically. The failure causes were polyethylene dissociation, components fracture and aseptic loosening. So, Martin *et al.* [49] identified the potential factors associated with clinical failure: radiolucent lines on the implant backside, postoperative pain and male gender.

The comparison between cementless and cemented glenoid components has also been done through Finite Element Analyses. Gupta *et al.* [51] analysed a metal-back implant in several physiologic loading conditions and with different fixation (in the presence and in the absence of cement). Their results showed that higher Von Mises stresses occurred in the metal implant particularly during the abduction, while lower stresses occurred in the glenoid cavity under the implant. This indicated stress shielding phenomenon. However, the stresses in the cementless polyethylene component resulted 20% less than stresses in cemented polyethylene component, showing a better resistance to glenoid wear with a cementless fixation.

Stone *et al.* [52] through a FEA found that cemented all-poly components presented a more physiologic stress distribution, while the stress in the subchondral glenoid bone were lower with cementless components. In addition, they noted higher stresses at the metal-polyethylene interface in the cementless glenoids during eccentric loadings. They concluded that cementless implants had an increased failure rate compared to that associated with cemented components. The failure depended on stress shielding and high polyethylene wear.

The reported incidence of polyethylene-metal dissociation, screw breakage before bone ingrowth and clinical failure of cementless implants points out the need of achieving steady primary fixation to facilitate osseous integration of cementless prostheses. Recent publications have attempted to evaluate the quality and density of the bone in the glenoid cavity in order to provide information about the screws optimal location. Anglin et al. [53] through the study of cancellous bone's mechanical properties suggested that a deep fixation in the central region of glenoid cavity could allow a better initial fixation and this could be increased fixing the implant in the stronger regions of the glenoid cavity (posterosuperior and anterior zones).

Codsi *et al.* [54] suggested three locations to fix cementless implant through screws: in the superior glenoid the screw should be placed in a 5-mm area, in the middle glenoid in a 7-mm area and in the inferior glenoid in a 5-mm area.

Although alternative designs and new porous material have been introduced over the years, uncemented components do not have had significant improvements in clinical performance, while all-polyethylene components have shown to outperform cementless implants, so they remain the most reliable option in the TSA.

2.2 Glenoid loosening

Glenoid loosening has remained the primary complication and the major reason for failure since the introduction of Total Shoulder Arthroplasty in 1974 by Neer [55].
There are several factors that contribute to glenoid loosening [34]:

- *Glenoid malposition*: positioning the glenoid component in a right orientation is fundamental for implant long-term stability. A malpositioned component can prematurely loosen and clinically fail because of incomplete implant seating and inadequate bone support. Moreover, this can also influence significantly clinical outcomes [60]. The surgical techniques to minimize loosening consists of correcting the glenoid to neutral version and implanting the component in order to preserve bone and have a complete implant-bone contact [56].
  Yongpravat *et al.* [56] conducted a FEA to investigate cement mantle failure in the presence of several degree of glenoid correction. They demonstrated that considering only the implant orientation it is not possible to accurately predict the cement stress. In addition, maintaining cortical bone appeared to be more important than version correction when the glenoid presented high deformity. Another FE study was carried out by Hopkins *et al.* [57], which evaluated how glenoid alignment affected cement stresses considering normal and rheumatoid bone. They concluded that components implanted in a central position presented lowest failure rate. Furthermore, bone quality amplified loosening incidence due to component malposition. Several publications [58, 59] confirmed that glenoid retroversion led to eccentric loading and a significant increase in bone-cement interfacial stress and micromotions compared to glenoid implanted in a neutral position.

- *Glenoid mismatch*: "radial mismatch" is defined as the difference between the curvature radii of the glenoid component and the humeral head and it assumes an essential role in the TSA because it influences contact mechanics and humeral head translation [61]. However, an optimal mismatch value does not exist because perfectly conforming articulating surfaces reduce humeral head translation, but they lead to edge loading, whereas less conforming glenoids allow to avoid edge loading through humeral head translation, but they are at risk of point loading and polyethylene wear [63].

- *Rocking horse phenomenon*: it is a repetitive off-center loading of the implant [22]. The rocking motion occurs in the superior-inferior plane, in particular the glenoid component is edge loaded and it is compressed on the opposite side. This condition creates a torque on the fixation surface that lead to an increase of tensile stress and micromotions at the interfaces. At this point the interfacial failure and component-bone dissociation occur [22] [32].

- *Glenoid fixation failure*: glenoid loosening could be associated with the lack of good-quality fixation that does not allow bone ingrowth. Primary stability depends on several factors such as implant design, patient variables, implantation and surgical techniques. According to the used implant, initial fixation may be obtained through PMMA bone cement or screws. All-poly cemented glenoid components with pressurized cementing technique are considered a better solution than cementless fixation via screws to minimize glenoid loosening [72] [73].

- *Micromotions at bone-cement interface*: interfacial micromotions are essential for osseointegration and bone ingrowth [63]. Minimum interface micromotions promote bone ingrowth, while high relative micromotions between the bone and the implant induce fibrous connective tissue ingrowth instead of bone. The absence of bone ingrowth caused by too high bone-implant micromotions leads to cementless implants failure. It is necessary to quantify micromotions to improve cementless implant, given that bone ingrowth can only occur if relative micromotions at the bone-implant interface do not exceed a threshold that could be chosen between 20 and 150 μm [71].
  An experimental research [64] showed that micromotions equal to 75 μm led to fibrous tissue ingrowth, whereas micromotions of 40 μm allowed bone formation on a porous surface. Pilliar *et al.* [65] observed bone ingrowth in presence of micromotions less than 28 μm, but when micromotions exceeded a value of 150 μm the fixation was ensured only by mature connective tissue. In vivo studies [66] [67] [68] showed that micromotions were frequently above the limits of bone ingrowth, while other studies on porous-coated implants showed a great variability in bone ingrowth [69] [70].

- *High stresses in the cement mantle*: in the cemented components the generation of high stresses predispose patient to implant failure. In fact, stresses above a certain threshold induce the formation of microcracks. These last produce cement debris that may provoke an inflammatory reaction and so lead to bone-cement interface failure [31] [74].
  Literature [31] [56] [74] [75] suggests a threshold for cement failure initialization: 4 MPa is the endurance limit that avoids PMMA failure after one million loading cycles, stresses above such threshold lead to 75% risk of cement failure.

- *Lack of bone quantity and quality*: several shoulder diseases can damage bone quality and lead to a decrease of bone support for TSA. Surgical procedures (eccentric reaming, bone grafting) that allow to correct glenoid deformity involve the removing of normal bone. Although they allow a better forces distribution and a wider range of motions, they lead to a decrease bone support for the implant, a minor contact between bone-implant and to a possible risk of bone perforation due to fixation pegs or screws [76]. Glenoid components should be placed in the presence of sufficient bone support in order to promote bone ingrowth and ensure implant long-term survival. However, no quantitative limit has ever been provided to indicate the maximum value of the degree of posterior glenoid erosion that can be corrected ensuring the appropriate bone support for the implant [77].

Chapter 3
Finite Element Models

The implementation of numerical models of the shoulder seems to be a hard challenge throughout the entire process, starting from the design to the validation. This is due to the complexity of the shoulder joint that involves a wide range of motions and complex active and passive stabilizing mechanisms [78].

The increasing rate of injuries and the need to understand more thoroughly shoulder pathology to develop new therapeutic strategies have considerably encouraged the research activity. Numerical models of the shoulder allow to analyse and quantify features that would be difficult to achieve due to technical and ethical limits such as placement of sensors, lack of specimens, deterioration of tissue, etc.

Several modelling approaches exist according to clinical question to which surgeons want to answer and shoulder aspect to be analysed. They can be divided into three groups [78]:

- *deformable models*: this approach allows to address several problems within orthopaedics and biomechanics such as prostheses fixation and failure, joints degenerations and shoulder structures integrity, taking into account stress-strain distribution in the shoulder and the implants [79];
- *rigid body models*: this approach considers the shoulder and the humerus as solid bodies connected by kinematics constraints, while bodies deformations are neglected. Rigid body models allow to investigate ergonomics and joint kinematics thanks to simulations of collisions between entities, wrapping of the muscles over the bones and kinematics [80] [81];
- *muscle force estimation*: this approach is based on EMG-driven models and optimization methods that allow to estimate muscle force through the simulation of muscular action and joint reaction forces in order to face joint stability problems, muscular transfer and rehabilitation [78].

In the present work deformable models are used because, as already stated in section 1.4, the aim of the work is to study and give information about glenoid loosening in the presence of several type B2 bone erosions.

3.1 Preliminary assumptions

The first step for the implementation of the models was the definition of guidelines and assumptions of choosing the variables from the literature. Initially, the following hypothesis were made under the guidance of the co-operative surgeon from the KU Leuven:

I. *Component medialization has no influence on rotator cuff muscles*.

Reaming technique to correct the orientation of the glenoid cavity and to medialize loads affects rotator cuff stress. In particular, it may alter not only the amplitude of the joint reaction force, but also the direction of load in the glenoid cavity. Since, this condition is hard to evaluate, in this work the potential alteration of the rotator cuff muscles is not accounted.

II. *Quasi-static abduction in the frontal plane is considered*.

This means that the inertial effects are considered negligible and, among the wide range of shoulder motions, the only 90° abduction in the frontal plane is considered.

III. *The developed model is a mean shape scapula and simulates a worst-case scenario.*

Scapula model was obtained from a Computed tomography (CT) scan dataset of 66 healthy scapula without diseases. To simulate the worst-case scenario, maximal values from literature were used for loads.

3.2 Scapula

The three-dimensional geometry of the scapula was provided by IORT team from the KU Leuven as an orphan mesh (Figure 8a), its shape was obtained through different registration techniques able to elaborate a mean scapula shape based on a CT scan dataset of 66 healthy right scapula. In order to work with the model, the orphan mesh (STL file) was converted in CAD using 3-Matic (Materialise, Leuven, Belgium). Scapula's geometry and volume were created and the rim of glenoid was drawn (Figure 8b).

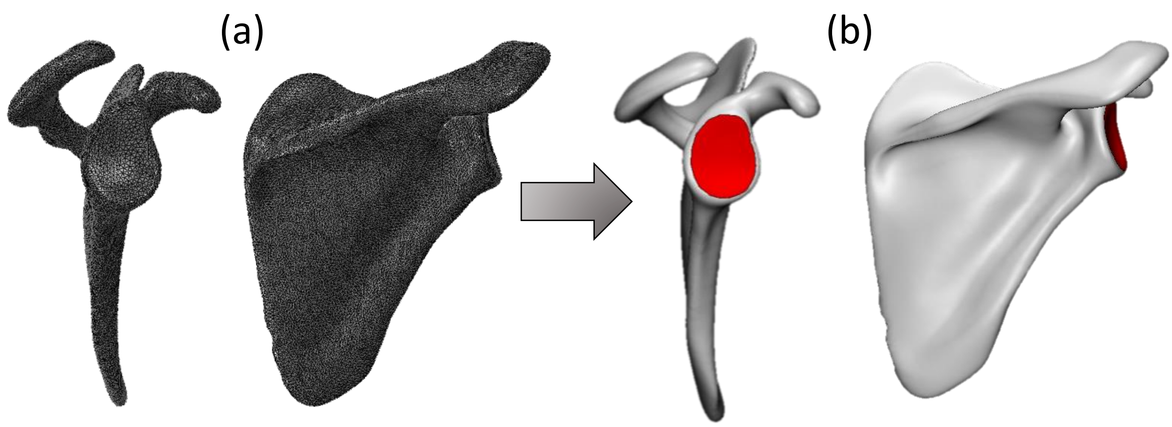

Figure 8 - Glenoid geometry: (a) orphan mesh in sagittal view (left) and posterior view (right); (b) scapula volume and glenoid rim in sagittal view (left) and posterior view (right).

3.2.1 Glenoid orientation

Shoulder's pathologies can lead to a distorted morphology of the scapula due to scapular bone loss. Obtaining scapular morphologic parameters is essential for TSA planning, since they influence implant survival and functionality [7] [58] [82] [83].

Therefore, scapular parameters such as reference points, axes and planes were defined to quantify glenoid orientation according to [84] [85] [86].

Three reference points were drawn on the scapular model (Figure 9a)):

i. *Trigonum Spinae (TS)*: it is the midpoint of the triangular surface placed on the medial border in line with the scapular spine;
ii. *Glenoid Center Point (GC)*: it is the point in the center of the glenoid fossa;
iii. *Angulus Inferior (AI):* it is the most causal point of the scapula.

Through defined points, four reference planes were achieved (Figure 9b and 9c):

i. *Glenoid Plane (GP)*: it is the least-square best-fit plane passing through the Glenoid Fossa and the Glenoid Center Point;
ii. *Scapular Plane (SP)*: it is the plane passing through Angulus Inferior, Glenoid Center Point and Trigonum Spinae;
iii. *Axial Plane (AP)*: it is the plane perpendicular to the Scapular Plane passing through Trigonum Spinae and Glenoid Center Point;
iv. *Glenoid Rim Plane (GRP)*: it is the plane parallel to the Glenoid Plane and tangent to the glenoid superior and inferior rim.

Finally, two reference axes were drawn on the model (Figure 9d):

i. *Glenoid Axis (GA)*: it is the axis normal to the Glenoid Plane passing through the Glenoid Center Point;
ii. *Centreline (CL)*: it is the axis passing through the Trigonum Spinae and the Glenoid Center Point and perpendicular to the Scapular Plane.

At this point, glenoid version and inclination were calculated according to [86]. The Glenoid Axis was projected on the scapular and axial planes. The angle formed by the centerline and the projection of the Glenoid Axes in the Scapular Plane is called glenoid version (Figure 10a), while the angle formed by the centerline and the projection of the Glenoid Axes in the Axial Plane is called glenoid inclination (Figure 10b). The values of glenoid version and inclination for the mean scapula shape are shown in Table 1:

Table 1 - Glenoid version and inclination.

Version	Inclination
-5.7°	-9.1°

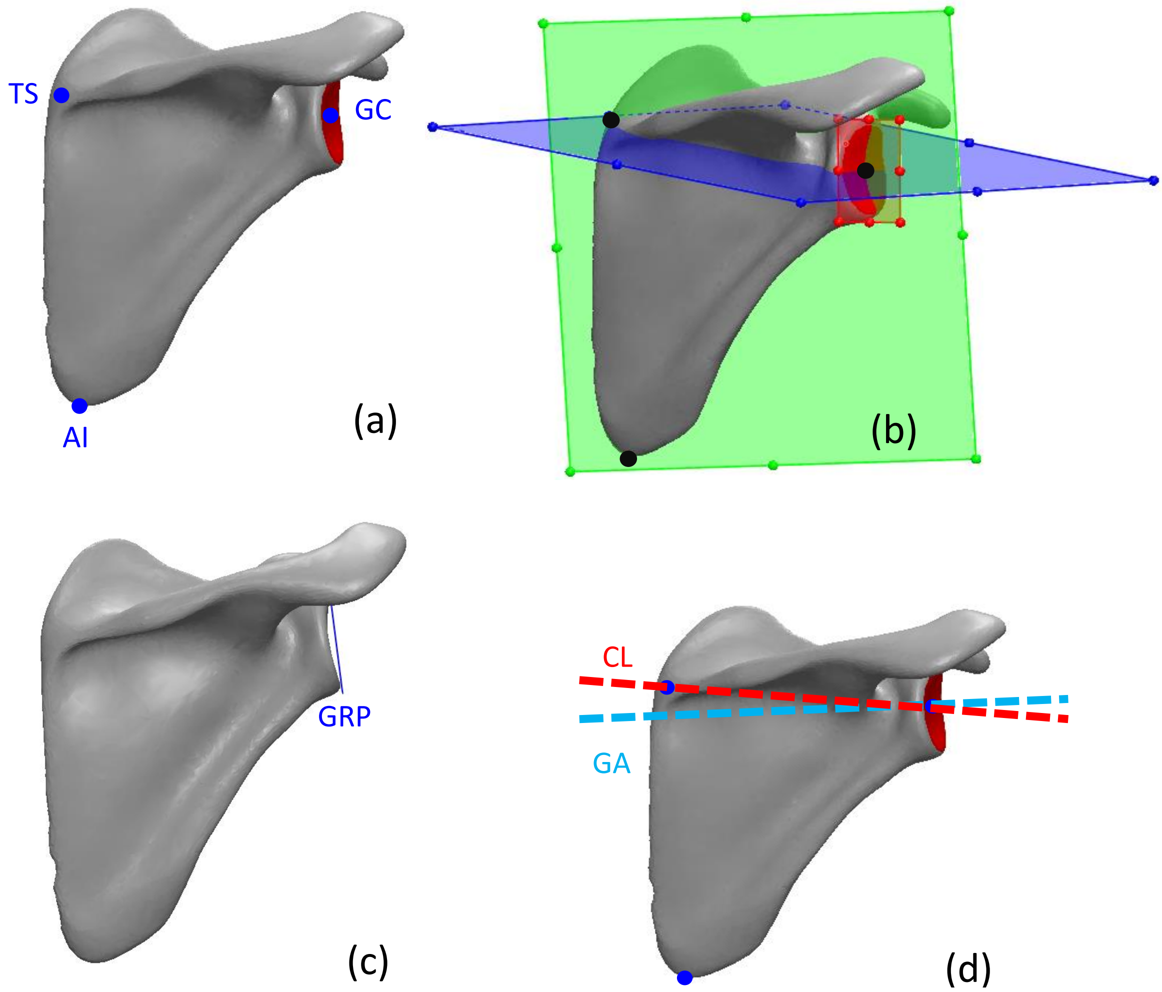

Figure 9 - Scapular morphologic parameters: (a) reference points; (b) glenoid plane (red), axial plane (blue) and scapular plane (green); (c) glenoid rim plane; (d) centreline (red) and glenoid axis (blue).

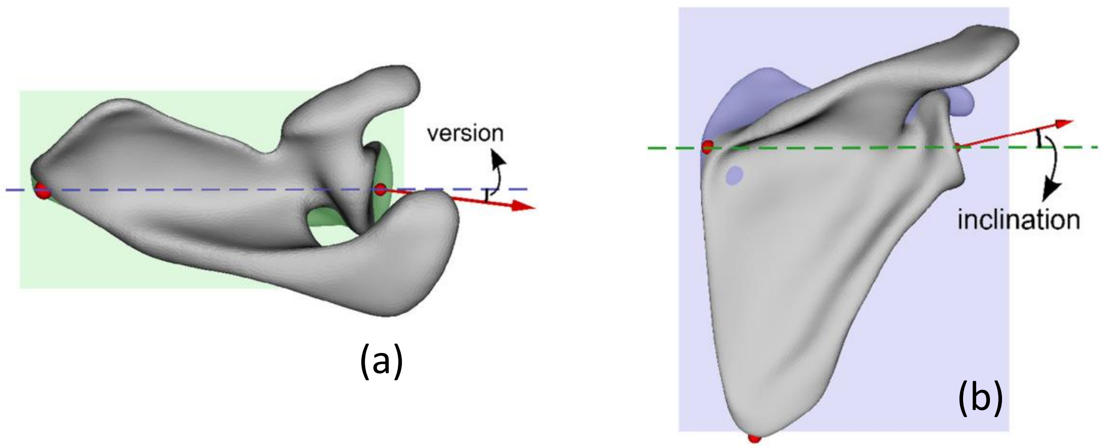

Figure 10 - Glenoid version (a) and inclination (b) [86].

Verhaegen *et al.* [86] have carried out direct 3D measurements on a contralateral scapula to understand if such scapula could be used as a reliable model to evaluate glenoid version and inclination and to help surgeons during preoperative planning of TSA. From the analysis of 100 scapulae they provided the mean values of glenoid version and inclination: -7° ± 4° for the version and -11° ± 4° for the inclination. The value calculated in this work are included within the range reported by Verhaegen *et al.* [86].

3.2.2 Scapular material properties

The used literature [87] suggests to model the scapula as an isotropic and homogeneous linear elastic material made up of cortical and cancellous bone with the mechanical properties reported in Table 2.

Since an orphan mesh of the scapula was provided, differentiating the cancellous bone from the cortical bone was difficult. For this reason, it was thought to assign mean values for Young’s modulus and Poison ratio to the scapula. Such mean values were obtained through a weighted average of cortical and cancellous values. To calculate such mean values, the following percentage was taken into account: 10% of cortical bone and 90% of cancellous bone. Material properties are shown in Table 2:

Table 2 - Bone properties.

	Material behaviour	**E (GPa)**	**ν**
Cortical Bone	Linear Elastic Isotropic	9.0 [87]	0.30 [87]
Cancellous Bone	Linear Elastic Isotropic	1.0 [87]	0.35 [87]
Mean Scapula	Linear Elastic Isotropic	1.8	0.31

3.3 Anatomical Shoulder Pegged and T.E.S.S. cementless components

In this work two type of glenoid components were considered: a cemented all polyethylene implant (Anatomical Shoulder Pegged, Zimmer Biomet Inc, Indiana, USA) and a metal-backed cementless component (T.E.S.S., Zimmer Biomet Inc, Indiana, USA). The components differ in their fixation technique, structure and materials.

Cementless implant consists of two components: a baseplate made in Porous Titanium TA6V Macrobond and Hydroxyapatite (Figure 11c); a PE insert (Figure 11b). Baseplate backside has a central convex surface and an external flat surface in order to maximise stability and besides to preserve bone stock, whereas the PE insert is fitted with a central peg in order to facilitate the positioning into the baseplate. T.E.S.S. shoulder system is directly inserted in the bone stock without requiring the use of cement, it is fixed through screws and spikes made in TA6V Titanium Alloy [88].

Anatomic Shoulder Pegged system is characterized by a single all PE component (Figure 11a) with four pegs and it is intended for cemented use only.

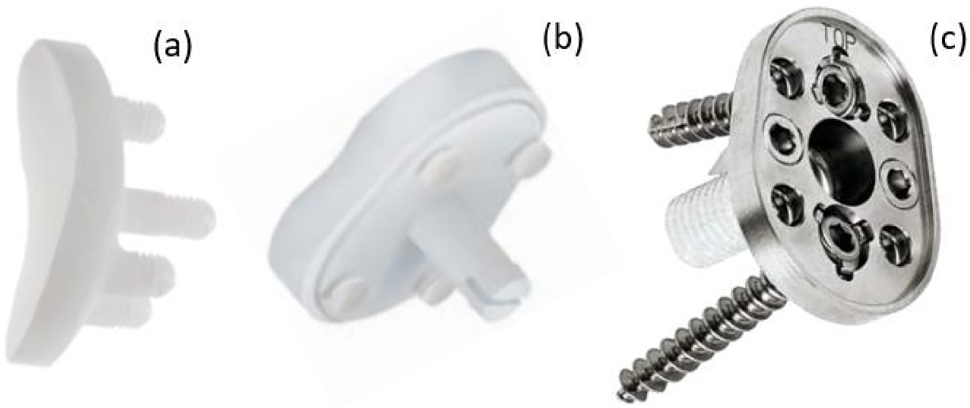

Figure 11 - Glenoid Components: (a) Cemented all PE implant [89]; (b) PE insert and (c) baseplate [88].

Components' sizes were chosen to fit properly the mean scapula shape, for both implants the small configuration was selected because it corresponded more closely to the glenoid cavity size. Glenoid cavity and implants sizes are reported in Table 3:

Table 3 - Components' size.

Component		**Height (mm)**	**Thickness (mm)**
Glenoid Cavity		32.5	-
All PE Implant		33	5
T.E.S.S.	Baseplate	33	4
	PE Insert	33	7

3.3.1 *Implant's material properties*

Prostheses materials were considered as homogeneous and isotropic linear elastic materials according to the used literature [75].

As previously observed, all PE implant requires the use of bone cement for fixation. According to Terrier et al. [31], the optimal cement thickness to minimize bone stress and to obtain a better stability should be 1.0 mm or 1.5 mm. For this reason, a 1.0 mm cement layer was created along the pegs of the all PE implant through Abaqus/Standard version 6.14-1 (Dassault Systèmes, Vélizy-Villacoublay, France). Figure 12a shows all PE implant with 1.0 mm cement mantle.

As regards material selection, Polymethyl Methacrylate (PMMA) properties were attributed to the bone cement, Ultra High Molecular Weight Polyethylene (UHWPE) properties were attributed to the cemented implant and the T.E.S.S. insert, while Trabecular Metal properties were attributed to T.E.S.S. baseplate (Figure 12a). Table 4Table 4 illustrates Young's modulus and Poisson's ratio for the implants and the cement mantle.

Table 4 - Cement and prostheses properties.

		Material	Behavoiur	E (GPa)	ν
Bone Cement		PMMA	Elastic Linear Isotropic	2.0 [56]	0.3 [56]
Cemented Implant		UHWPE	Elastic Linear Isotropic	1.2 [75]	0.4 [75]
T.E.S.S.	Baseplate	Trabecular Metal	Elastic Linear Isotropic	2.6 [90]	0.3 [90]
	Insert	UHWPE	Elastic Linear Isotropic	1.2 [75]	0.4 [75]

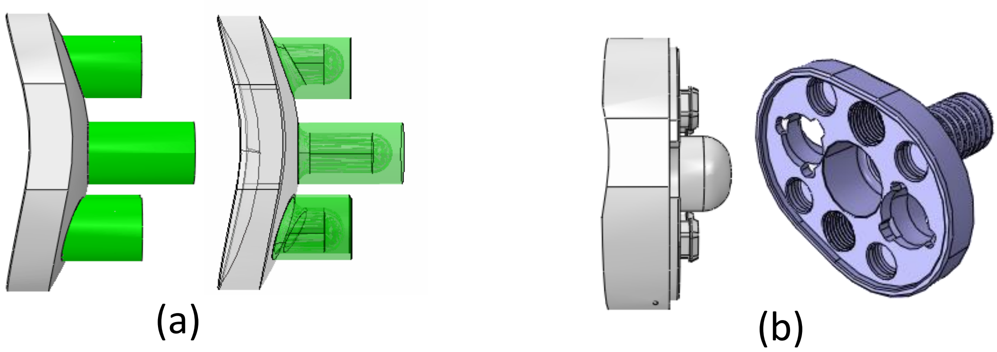

Figure 12 - Implants: (a) all PE implant with cement; (b) T.E.S.S. baseplate and insert.

3.4 Shoulder erosions

This work focuses on the type B2 bone erosion because it represents the most frequent erosion in osteoarthritis. Such erosion is characterized by a biconcavity in the postero-inferior quadrant of the glenoid [16]. Quantifying type B2 bone erosion is fundamental for TSA because it causes glenoid retroversion leading to eccentric loadings, generation of higher stresses and thus to glenoid loosening and failure.

On the request of surgeon, type B2 bone erosion was modelled according to Churchill *et al.* [16], which identified the "line of initial erosion" on a left shoulder. Such line represents the principal direction of erosion (Figure 13). Five different kinds of bone erosion (5°, 10°, 15°, 20° and 30°) were implemented from the reference model without any erosion through a 3D cutting procedure.

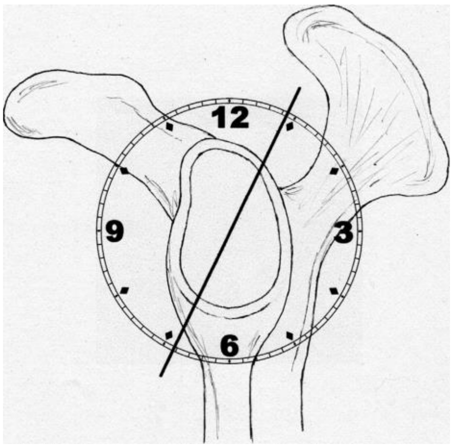

Figure 13 - Line of initial B2 erosion [16].

The references defined in section 3.2.1 were used to create the cutting planes in the main direction of erosion. The cutting techniques (Figure 14) consists of three steps:

i. rotation of the Scapular Plane around the Glenoid Axis by 30° anti-clockwise;
ii. creation of the intersection axis between the rotated Scapular Plane and the Glenoid Plane;
iii. rotation of the Glenoid Plane around the intersection axis to create 5°, 10°, 15°, 20° and 30° cutting planes.

Once the cutting procedure was performed, the volume of removed bone and the percentage of bone support were calculated for the five models of the scapula. For a mild erosion (5°) the volume of removed bone was equal to 147.6 mm^3 corresponding to a bone support of 98%, whereas for a severe erosion (30°) the volume of removed bone was equal to 2151.4 mm^3 corresponding to a bone support of 84%.

Since the scapula was modelled as a homogeneous material with mean values of Young's modulus and Poisson's ratio, it was not possible to evaluate directly from the models the percentage of bone support relating to the cortical bone and the cancellous one. Therefore, the percentages of removed cortical bone and cancellous one were estimated considering the 10% of cortical bone and the 90% of cancellous bone. The calculated values are shown in Table 5, the eroded models obtained using the described cutting technique are displayed in Figure 15.

Table 5 - Results of cutting procedure.

Degree of erosion	0°	5°	10°	15°	20°	30°
Volume of removed bone (mm^3)	-	147.6	326.3	567.6	1298.4	2151.4
% Bone support	100%	98%	97%	95%	90%	84%
% Cortical bone support	10%	9.8%	9.7%	9.5%	9.0%	8.4%
% Cancellous bone support	90%	88.2%	87.3%	85.5%	81%	75.6%

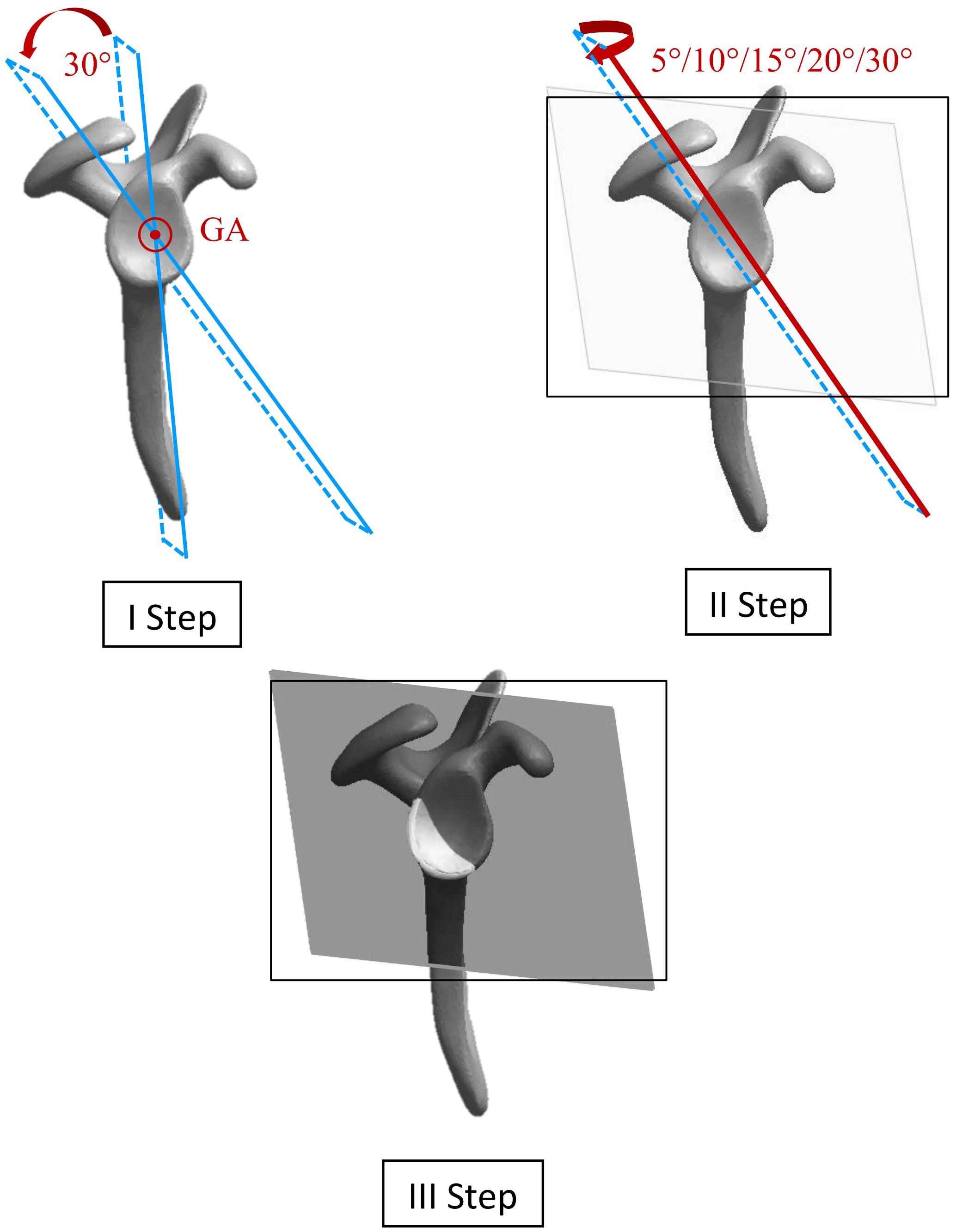

Figure 14 - Cutting technique.

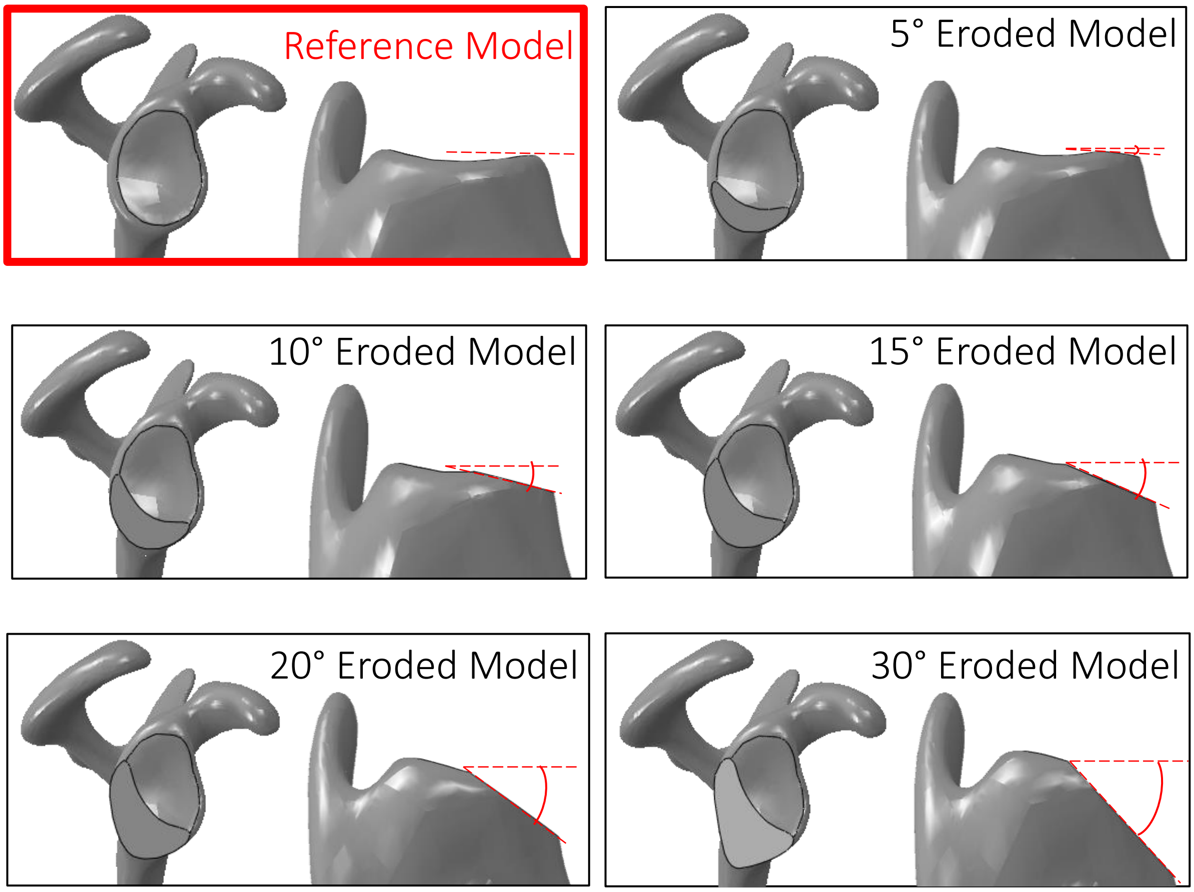

Figure 15 - Eroded models in sagittal (left) and posterior (right) views.

3.5 Implanted models

Positioning properly a glenoid implant is fundamental for its survival and for achieving positive functional results. Correct component fixation and placing are not easy to obtain and they are influenced by several factors, for instance surgeon experience and skills, implant type and accompanying instrumentation, patient's glenoid anatomy [91].

With the help of the co-operative surgeon, a virtual bone reaming was performed in order to obtain a perfect bone-implant contact. Subsequently, the implants described in section 3.3 were implanted in the eroded shoulders in such a way to have the same version and inclination of glenoid cavity. The eroded models with the all PE implant are displayed in Figure 16.

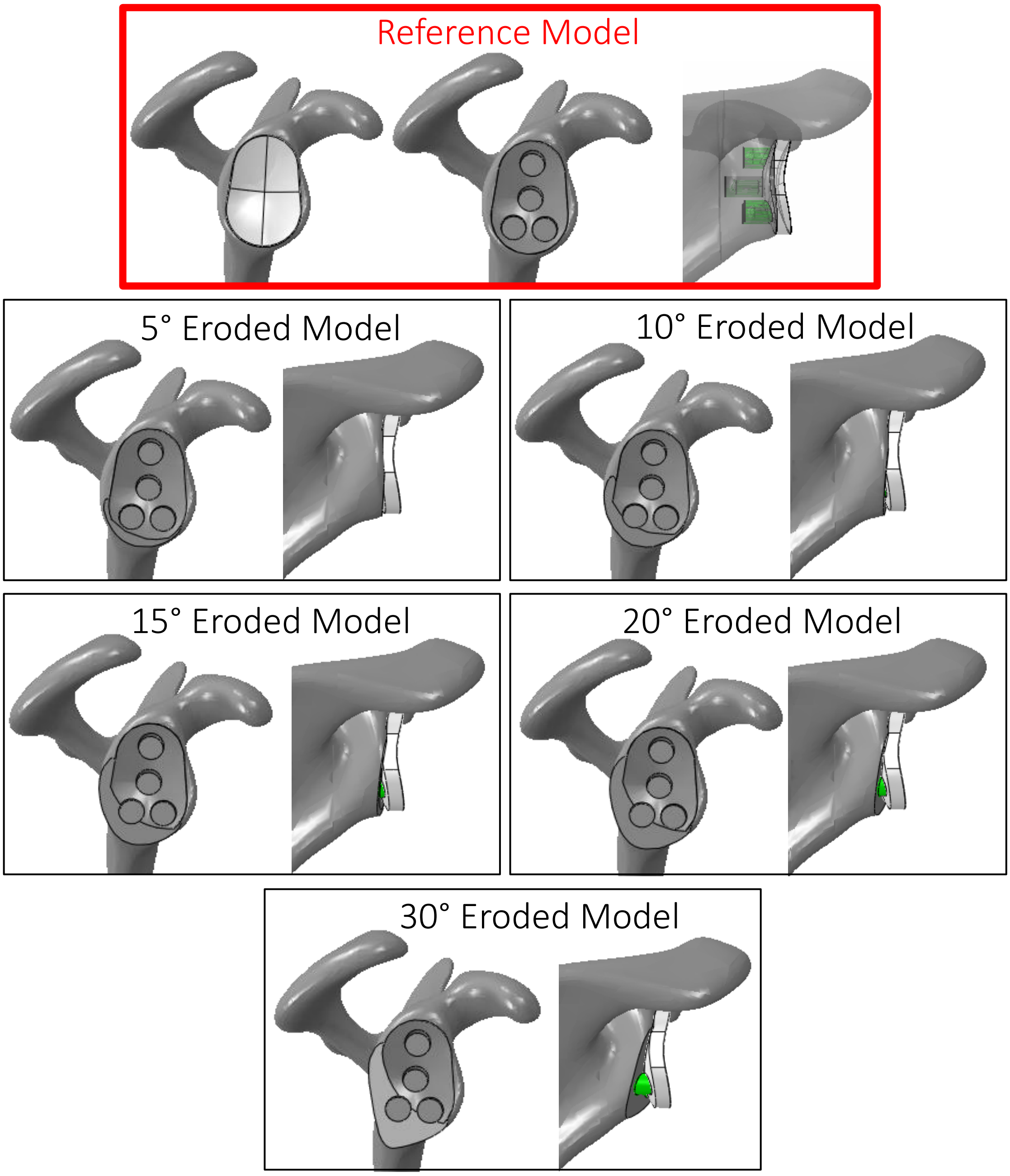

Figure 16 - Eroded models with the all PE component in sagittal (left) and posterior (right) views.

The eroded shoulders with the cementless implant are shown in Figure 17.

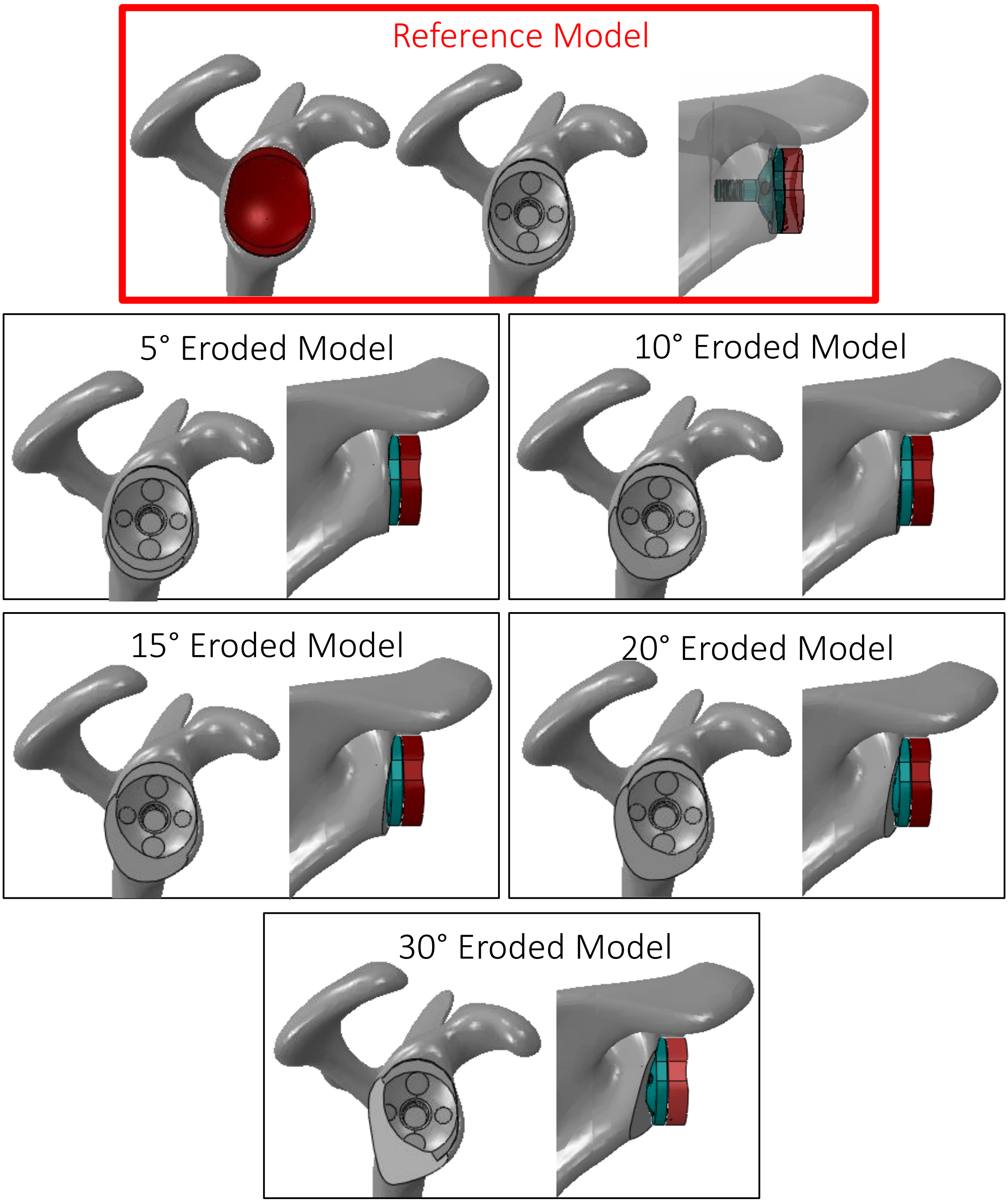

Figure 17 - Eroded models with T.E.S.S. in sagittal view (left) and posterior (right) views.

3.6 Contact properties

As previously mentioned in section 3.3, the glenoid components differ in fixation technique: the all PE implant requests the use of cement, which ensures good primary stability, while cementless implant is directly implanted in contact with the bone and fixed through screws for the purpose of promoting biological fixation [92]. For this reason, interfaces were modelled using different behaviour according to implant and materials (Table 6).

Models created with all PE implant show three interfaces because the bone cement were placed only along the four pegs. The three interfaces were set as non-bonded using a tangential behaviour penalty friction formulation. Friction coefficients for bone-cement, bone-implant and implant-cement interfaces were set respectively equal to 0.6 [34] [93], 0.2 [94], 0.6 [34] [93].

Models set up with T.E.S.S. are characterized by two interfaces: bone-baseplate and baseplate-insert interfaces. Baseplate-insert interface was set as perfectly bonded, whereas bone-baseplate interface was modelled as non-bonded to allow micromotions. Zhang *et al.* [50] provided values of friction coefficient for cortical bone-porous material and cancellous bone-porous material interfaces respectively equal to 1.75 and 0.88. In the present work the scapula was defined as a single homogeneous material, thus the friction coefficient of bone-baseplate interface was obtained as the weighted average of the two values considering the 10% of cortical bone and 90% of cancellous bone.

Table 6 - Contact properties.

	Interface	**Materials in contact**	**Friction coefficient**
All PE implant	Bone-Cement	Bone-PMMA	0.6
	Bone-Implant	Bone-UHMWPE	0.2
	Implant-Cement	UHMWPE-PMMA	0.6
T.E.S.S.	Bone-Baseplate	Bone-Trabecular Metal	0.97
	Baseplate-Insert	Trabecular Metal-UHMWPE	Perfectly bonded

3.7 Boundary conditions

In the present study the only abduction in the scapular plane is considered. During such movement the scapula is subject to several reaction, ligament and muscle forces. A great amount of research tried to estimate the joint reaction forces during upper limb abduction. Helm *et al.* [96] [97] assessed quality and quantitatively all forces acting on the scapula during abduction, providing the most complete dynamic model of the shoulder. The main muscles acting in shoulder abduction are the deltoid, the supraspinatus and the trapezius [98].

The main load acting in the glenoid region is the glenohumeral joint reaction force (GH-JRF), that presses humerus's proximal part into the glenoid socket in order to limit the humeral head translation and ensure stability. Such force ranges between 40-90% of body weight (BW) and grows with the increasing of the abduction angle, reaching peak values at 80°-90° abduction in the scapular plane [99].

To simulate a worst-case scenario on an average normal shoulder during a 90° abduction, the amplitude of GH-JRF was set equal to 750 N as recommended by literature [34] [56] [75] [97].

Therefore, the models were loaded through a 750 N compressive force applied perpendicularly to the glenoid plane through a continuum distributing coupling interaction. Two loading configurations were considered: concentric and eccentric loading mimicking the actual clinical situations [100]. Loading application points were obtained according to Wahab et al. [34] using a curvature radius of 35 mm (Figure 18). Concentric load was applied in the centre of the prosthesis considering a contact area of 3 cm^2, that corresponds to the 43% of the implant surface. The center of the eccentric load was determined rotating the radius of curvature of 20° in the superior direction and 10° in the posterior direction, as it is shown in figure. The contact area in the eccentric case was approximately 2 cm^2 corresponding to the 28% of the implant surface.

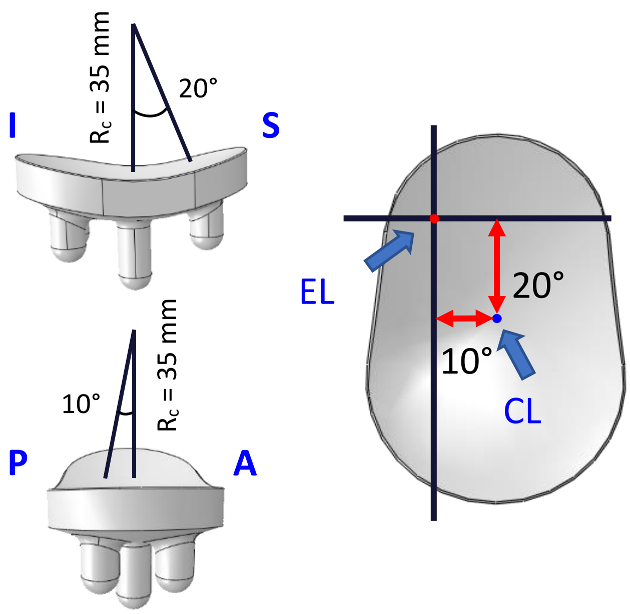

Figure 18 - Loading application point locations.

Scapula movement were avoided fixing its medial border. This situation corresponds to the physiological stabilization of the scapula during the abduction, accomplished by the trapezius muscle. The boundary conditions applied to the two implants are displayed in Figure 19:

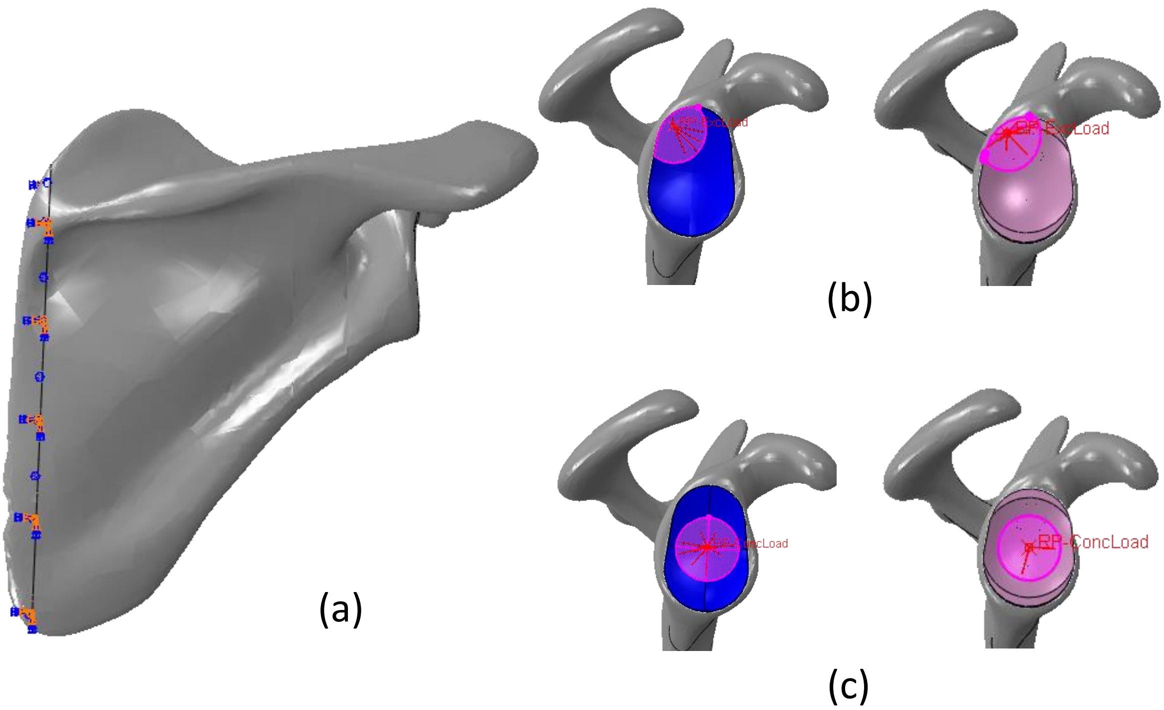

Figure 19 - Boundary conditions: (a) medial border fixed; (b) eccentric and (c) concentric conditions for all PE implant (left) and T.E.S.S. (right).

Table 7 shows an overview of the boundary conditions.

Table 7 - Boundary conditions summary.

Loads						
Type of Load	***Amplitude***	***Direction***	***Application Point***	***Contact Surface***	***Implant Surface***	***Interaction***
Eccentric Load	750 N	⊥ Glenoid plane	Superiorly off-centered [34]	Supero-posterior location	28%	Continuum distributing
Concentric Load	750 N	⊥ Glenoid plane	Centre of the implant [34]	Central location	43%	Continuum distributing
Constraints						
Type of constraint				**Fixed Region**		
Encastre				Medial border		

3.8 Mesh

The scapula is characterized by a complex shape and geometry. In order to achieve a better approximation of the geometry and a good compromise between accurate results and an acceptable computational time, it was thought to divide the scapula into three areas and to use different element size for the mesh (Figure 20).

The region of interest is the glenoid cavity, where the prostheses were implanted. It was picked considering a 2 mm distance from the longest peg. In the glenoid region a finer mesh with 1 mm linear tetrahedral elements was used to achieve reliable results. Moving in the medial direction, the intermediate scapular region and the medial scapular region can be found. This last was meshed using 15 mm linear tetrahedral elements because it is the less interesting region in which no results were calculated. The intermediate scapular region was picked considering a 15 mm distance from the glenoid region and it was meshed using an adaptive mesh (1-15 mm) (Figure 21a). The implants and the cement were meshed using 1 mm linear tetrahedral elements (Figure 21b). Table 8 shows an overview of the mesh sizes.

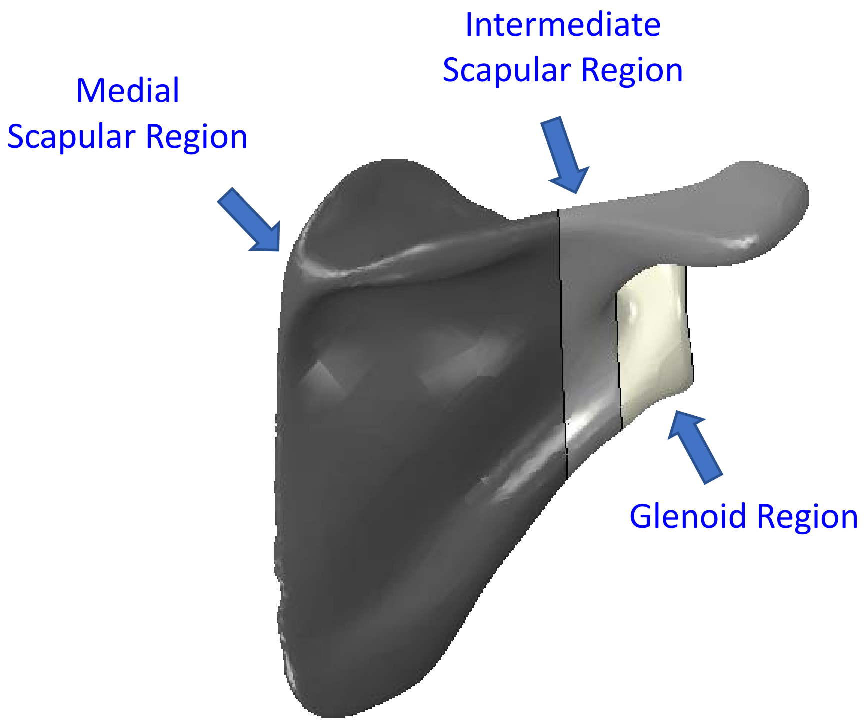

Figure 20 - Scapular areas.

Table 8 - Mesh size summary.

Loads			
	Region	***Element Type***	***Mesh Size***
Bone	Glenoid Region	Linear tetrahedral elements	1 mm
	Intermediate Scapular Region	Linear tetrahedral elements	Adaptive mesh (1-15 mm)
	Medial Scapular Region	Linear tetrahedral elements	15 mm
Implants	All PE Implant	Linear tetrahedral elements	1 mm
	Cement	Linear tetrahedral elements	1 mm
	T.E.S.S. Implant	Linear tetrahedral elements	1 mm

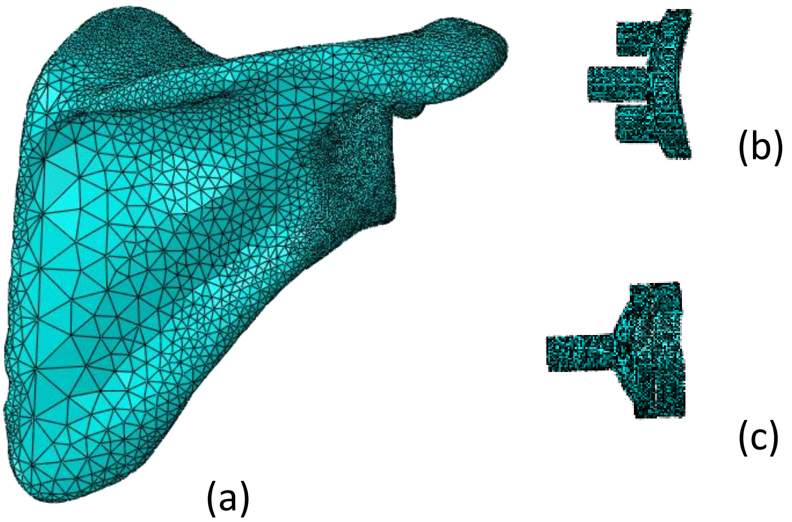

Figure 21 - Mesh: (a) scapula; (b) all PE implant and cement;
(c) T.E.S.S. baseplate and insert.

Chapter 4
Results

All simulations were performed on Abaqus/Standard version 6.14-1 (Dassault Systèmes, Vélizy-Villacoublay, France). Results were achieved considering two loading conditions (eccentric and concentric loads) for twelve models.

The variables considered in the present study were: quantity of bone support, type of glenoid component and GH-JRF contact location. All other variables were maintained constant during the simulations. Output variables were analysed in the glenoid region defined in section 3.8 and they are:

- cement stress and bone-cement interfacial contact pressure for the all PE implant;
- relative micromotions at the bone-implant interface and medial displacements for the cementless implant;
- bone strain and stress for both implants.

Peak and mean von Mises stresses were compared for the several models depending on bone support and type of implant. Furthermore, failure criteria were defined for bone stress and glenoid loosening. Bone failure was defined according to Chevalier *et al.* [75]. It was calculated the von Mises stress above which bone failure occurs:

$$\sigma_{yield}^{VM} = \sqrt{\frac{3}{2}\, E_{bone}\, \varepsilon_T} = 3.37 \text{ MPa} \qquad (1)$$

ε_T is the tensile bone tissue yield strain, picked equal to 0.41% [75]. Subsequently the percentage of bone in the glenoid cavity in which stresses overcome the threshold was calculated.

As already mentioned in section 2.2, failure initialization in the cement mantle occurs when stresses are higher than 4 MPa [31] [56] [74] [75], while cementless component failure takes place when relative micromotions at the bone-cement interface exceed a threshold range of 20 and 150 µm [71]. Thus, two parameters were defined to compare the two prostheses in terms of glenoid loosening:

- critical cement volume (CCV) [56]: it is the percentage of cement volume in which stresses are higher than 4 MPa;
- micromotions-threshold percentage ratio (MTPR): it is the percentage ratio between the relative micromotions and the threshold equal to 75 µm.

4.1 All PE Implant

In this section the results obtained from the FEA are shown in terms of cement stress, bone-cement interfacial contact pressure, bone stress and strain for the reference and the eroded models taking into account the two loading conditions.

4.1.1 Cement stress

In both loading conditions a global increase of von Mises stress in the cement mantle can be observed with the decreasing of bone support (Figure 22 and Figure 23). It is important to notice how the peak of von Mises stress remains constant, whereas the mean von Mises stress on each peg increases with the decreasing of bone support.

In the ***eccentric condition*** the peak of von Mises stress (15 MPa) is located in the posterior region of the superior peg, while it is located in the superior region of the inferior pegs for the ***concentric condition*** (7 MPa). The value obtained for the concentric case is approximately the half of those for the eccentric case.

To compare models, the mean von Mises stresses on each peg were evaluated for the eroded models and normalized to the mean von Mises stresses on each peg of the reference configuration. The mean von Mises stresses for all models in the two loading conditions are shown in Table 9.

Table 9 - Mean von Mises stress on each peg in function of bone support.

Eccentric load							
Bone support		100%	98%	97%	95%	90%	84%
Mean von Mises stress (MPa)	Superior peg	3.00	3.00	3.00	3.10	3.37	3.46
	Central Peg	1.54	1.54	1.54	1.57	1.57	1.59
	Posterior Peg	0.81	0.82	1.00	1.19	1.33	1.80
	Anterior Peg	0.24	0.24	0.24	0.3	0.31	0.45
Concentric load							
Bone support		100%	98%	97%	95%	90%	84%
Mean von Mises stress (MPa)	Superior peg	0.76	0.76	0.76	0.79	0.79	0.79
	Central Peg	2.28	2.28	2.29	2.29	2.29	2.30
	Posterior Peg	2.00	2.00	2.3	2.4	2.57	2.99
	Anterior Peg	1.37	1.37	1.39	1.4	1.4	1.45

The bar diagrams below (Graph 1 and Graph 2) show an evident increase of stress in the inferior pegs for the ***eccentric condition*** and in the posterior peg near the bone erosion fot the ***concentric***. In the ***eccentric condition*** the mean von Mises stress remains steady in the superior, central and anterior pegs until the 97% bone support, whereas starting from the 95% bone support an increase of stress occurs in the superior peg from 3% to 15%, in the central peg from 2% to 3% and in the anterior peg from 25% to 88%. The situation is different for the posterior peg because the mean stress rises from 23% to 122% starting from the 97% bone support. In the ***concentric condition*** the mean von Mises stress grows from 13% to 47% from a bone support of 97% to 84% in the posterior peg.

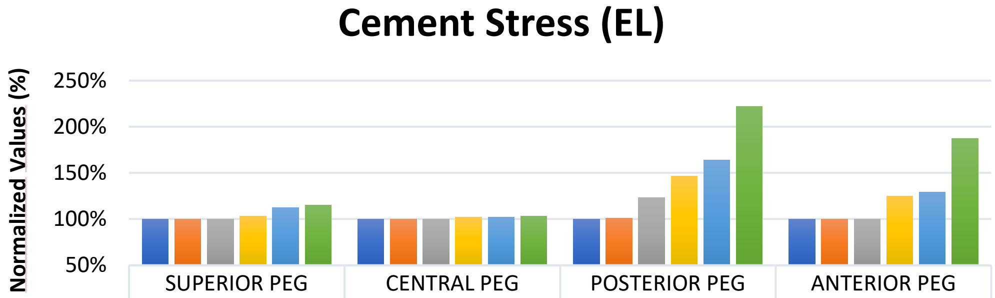

Bone Support (%)	SUPERIOR PEG	CENTRAL PEG	POSTERIOR PEG	ANTERIOR PEG
100%	100%	100%	100%	100%
98%	100%	100%	101%	100%
97%	100%	100%	123%	100%
95%	103%	102%	147%	125%
90%	112%	102%	164%	129%
84%	115%	103%	222%	188%

Graph 1 - Normalized cement stress in the eccentric condition.

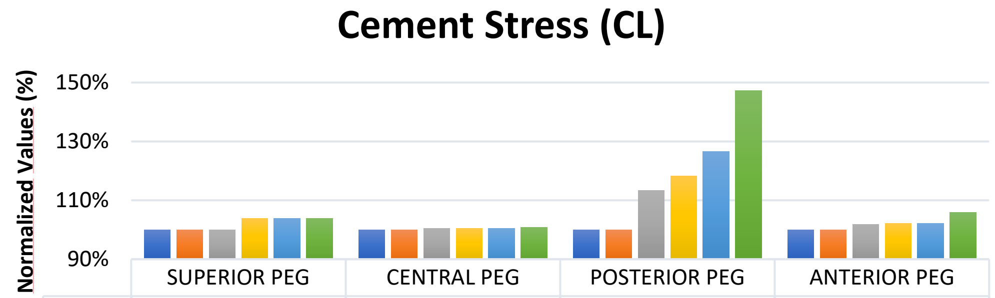

Bone Support (%)	SUPERIOR PEG	CENTRAL PEG	POSTERIOR PEG	ANTERIOR PEG
100%	100%	100%	100%	100%
98%	100%	100%	100%	100%
97%	100%	100%	113%	102%
95%	104%	100%	118%	102%
90%	104%	100%	127%	102%
84%	104%	101%	147%	106%

Graph 2 - Normalized cement stress in the concentric condition.

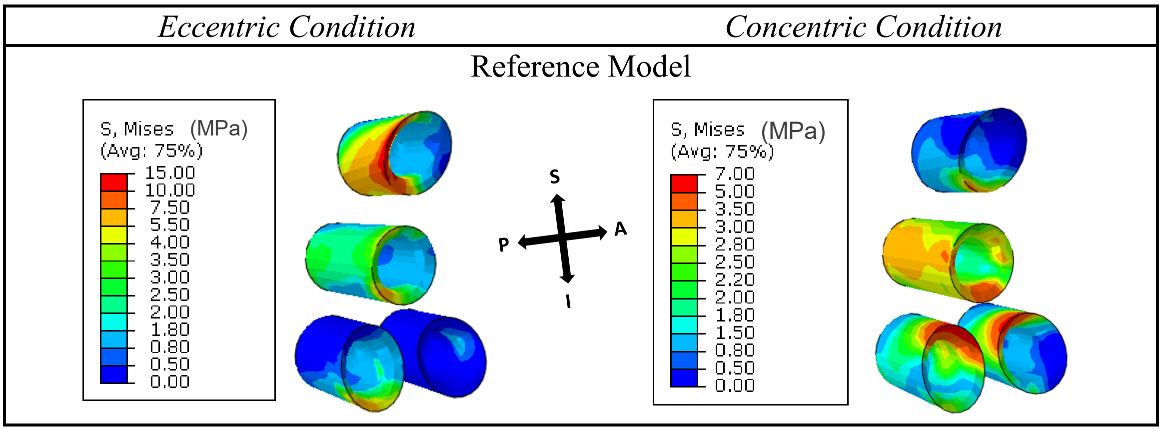

Figure 22 - Cement stress in the two loading conditions (reference model).

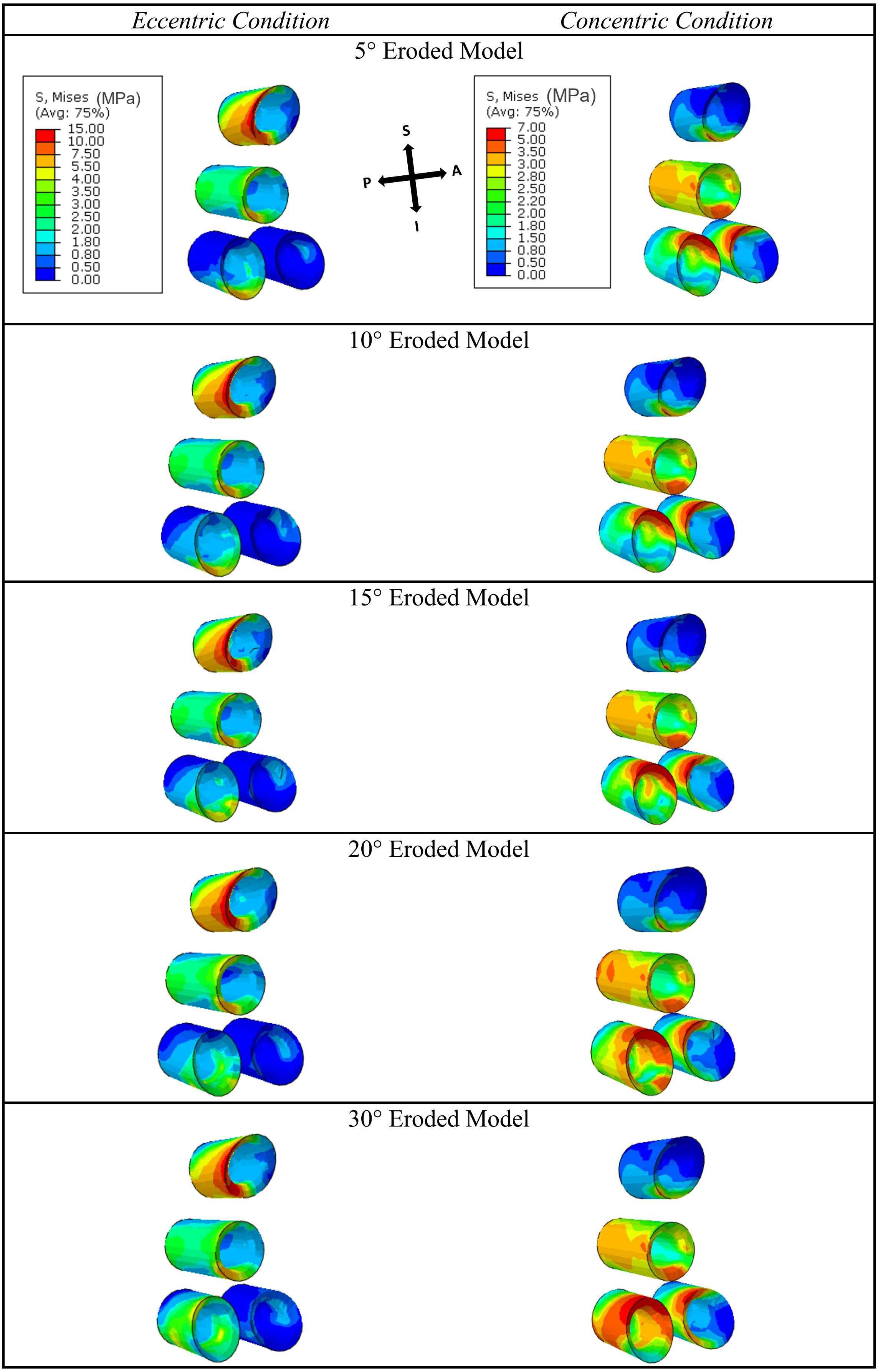

Figure 23 - Cement stress in the two loading conditions (eroded models).

4.1.2 Bone-Cement Interfacial Contact Pressure

There is an increase of contact pressure at the bone-cement interface with the increasing of bone erosion in both loading conditions (Figure 24 and Figure 25. The peak of contact pressure remains steady, while the mean pressure on each peg grows with the decreasing of bone support.

In the ***eccentric condition*** the maximum contact pressure (14 MPa) is located in the posterior region of the superior peg and at the base of the posterior peg with the increasing of erosion angle. In the ***concentric condition*** the peak of contact pressure (7 MPa) is located at the base of posterior peg corresponding to the erosion. Therefore, such value in the eccentric case is double of that in the concentric case.

To compare models, the mean contact pressure on each peg were evaluated for the eroded models and normalized to the mean contact pressure on each peg in the reference configuration. The mean values for all models in the two loading conditions are shown in Table 10.

Table 10 - Mean interfacial contact pressure on each peg in function of bone support.

Eccentric load							
Bone support		100%	98%	97%	95%	90%	84%
Mean contact pressure (MPa)	Superior peg	0.80	0.80	0.81	0.83	0.84	0.84
	Central Peg	0.66	0.66	0.67	0.69	0.7	0.7
	Posterior Peg	0.4	0.4	0.45	0.47	0.49	0.58
	Anterior Peg	0.07	0.07	0.07	0.09	0.09	0.1
Concentric load							
Bone support		100%	98%	97%	95%	90%	84%
Mean contact pressure (MPa)	Superior peg	0.18	0.18	0.18	0.19	0.20	0.20
	Central Peg	0.47	0.47	0.47	0.47	0.50	0.50
	Posterior Peg	0.49	0.49	0.49	0.50	0.50	0.80
	Anterior Peg	0.30	0.30	0.35	0.36	0.37	0.38

The normalized values (Graph 3 and Graph 4) illustrate a significant growth of interfacial pressure in the inferior pegs in the ***eccentric condition*** and in superior and anterior pegs in that ***concentric***.

In the ***eccentric condition*** the mean contact pressure remains steady in the superior, central and anterior pegs until a bone support of 97%, whereas starting from the 95% bone support an increase of pressure occurs in the superior peg from 4% to 5%, in the central peg from 5% to 6% and in the anterior peg from 29% to 43%. The situation is different for the posterior peg because the mean pressure rises from 13% to 45% starting from the 97% bone support.

In the ***concentric condition*** the mean interfacial contact pressure is approximatively constant in the posterior peg until the 90% bone support, but it considerably increases till 84% for the 84% of bone support. In the anterior peg the interfacial pressure rises from 17% to 27% starting from the 97% of bone support.

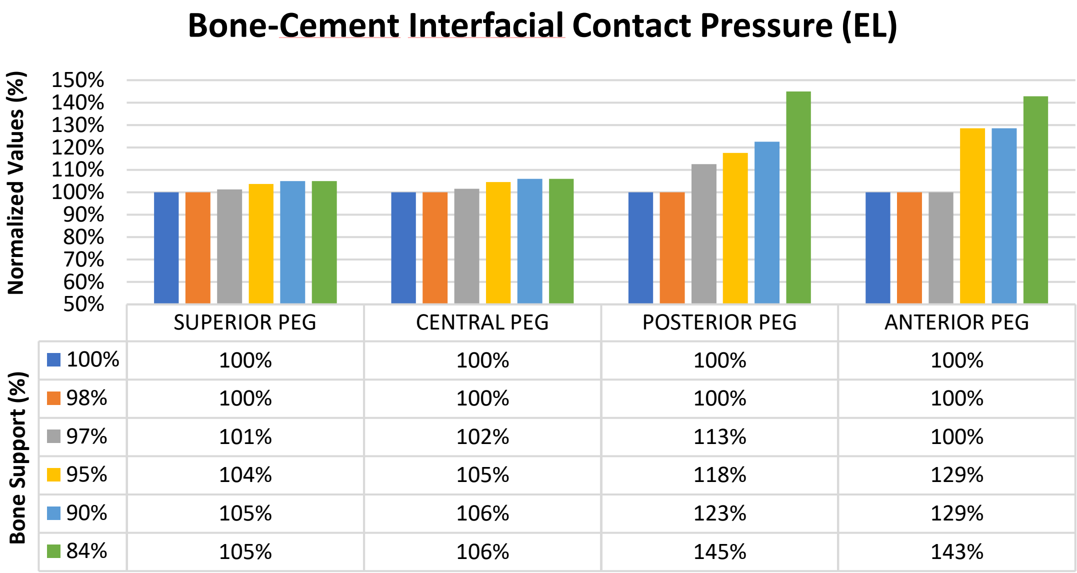

Bone Support (%)	SUPERIOR PEG	CENTRAL PEG	POSTERIOR PEG	ANTERIOR PEG
100%	100%	100%	100%	100%
98%	100%	100%	100%	100%
97%	101%	102%	113%	100%
95%	104%	105%	118%	129%
90%	105%	106%	123%	129%
84%	105%	106%	145%	143%

Graph 3 - Bone-cement interfacial contact pressure in the eccentric condition.

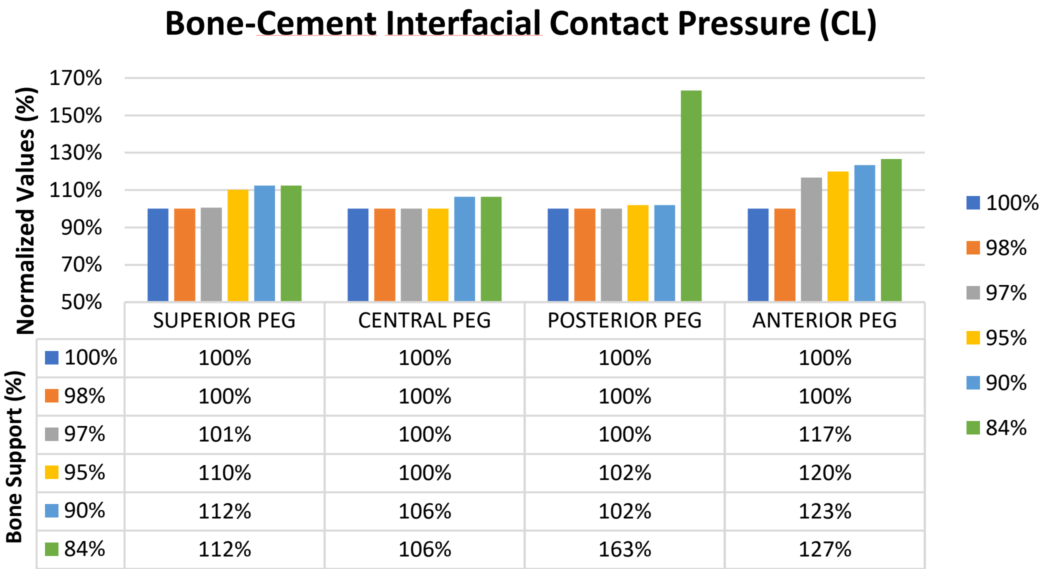

Bone Support (%)	SUPERIOR PEG	CENTRAL PEG	POSTERIOR PEG	ANTERIOR PEG
100%	100%	100%	100%	100%
98%	100%	100%	100%	100%
97%	101%	100%	100%	117%
95%	110%	100%	102%	120%
90%	112%	106%	102%	123%
84%	112%	106%	163%	127%

Graph 4 - Bone-cement interfacial contact pressure in the concentric condition.

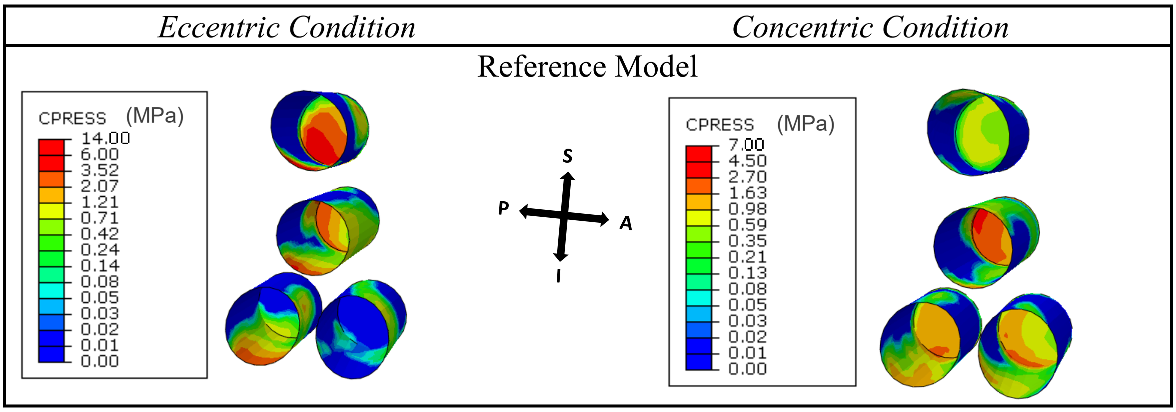

Figure 24 - Bone-Cement interfacial contact pressure in the two loading conditions (reference models).

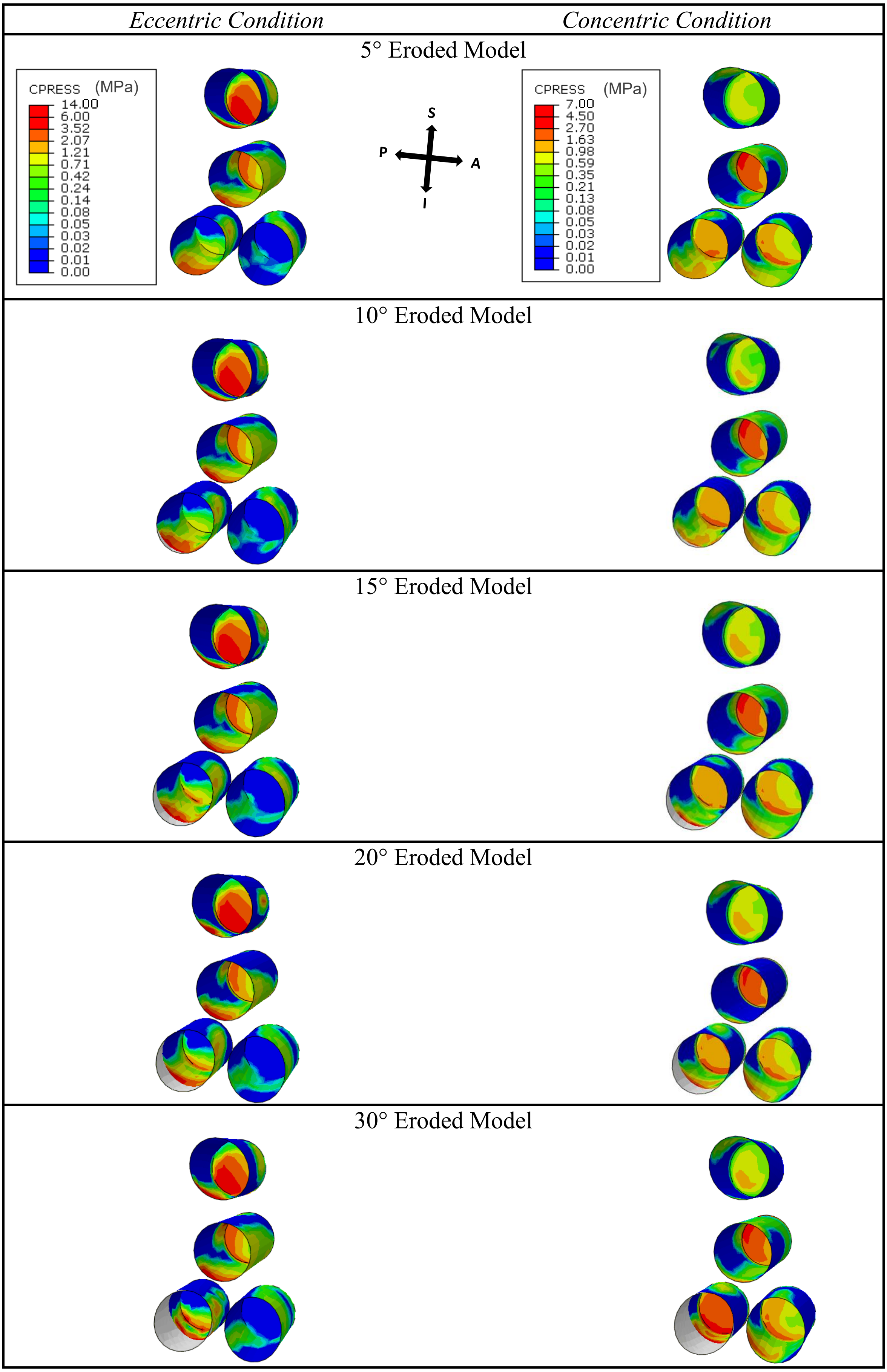

Figure 25 - Bone-Cement interfacial contact pressure in the two loading conditions (eroded models).

4.1.3 Bone Stress

The bone stress was analysed in the glenoid cavity defined in section 3.8. There is a slight increase of stress with the decreasing of bone erosion in both loading conditions (Figure 26 and Figure 27).

The peak of von Mises stress (15 MPa) can be observed in the supero-posterior region of the glenoid cavity and in the posterior region of the scapula for the ***eccentric condition***, while it is located in the central region of the glenoid cavity and in the posterior region of the scapula for the ***concentric condition*** (6.5 MPa).

The peak of von Mises stress does not change between the models, to compare them the mean von Mises stress in the glenoid cavity was calculated for the eroded models and normalized to the mean von Mises stresses of the reference configuration. The mean von Mises stresses for all models in the two loading conditions are shown in Table 11.

Table 11 - Mean bone stress in function of bone support with all PE implant.

Eccentric load						
Bone support	100%	98%	97%	95%	90%	84%
Mean bone stress (MPa)	1.94	1.94	1.96	1.97	2.00	2.10
Concentric load						
Bone support	100%	98%	97%	95%	90%	84%
Mean bone stress (MPa)	1.10	1.10	1.10	1.10	1.11	1.12

The bar diagrams below (Graph 5) illustrate that in the ***eccentric condition*** the mean von Mises stress in the bone rises till 8% with the 84% bone support, while in the ***concentric condition*** a lesser increase of mean stress occurs, it rises until 2% with the 84% bone support.

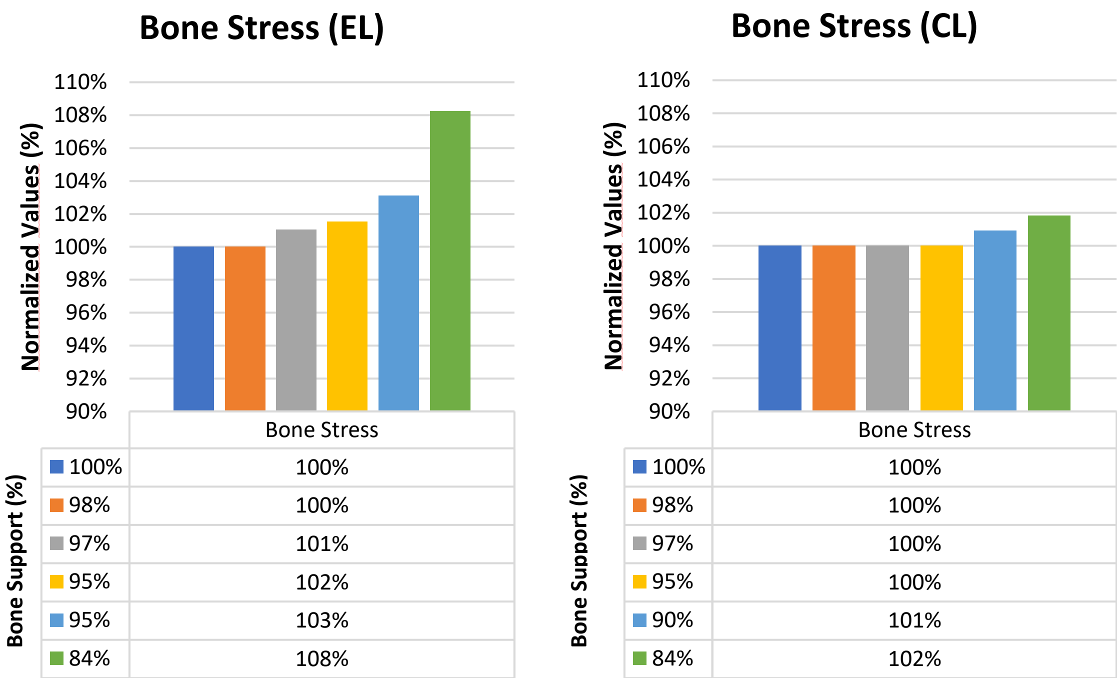

Graph 5 - Bone stress with all PE implant in the eccentric (left) and concentric (right) conditions.

Taking into account the failure criteria defined in section 0, the percentages of failed bone in the glenoid cavity were calculated (Table 12). It appears to be greater for the eccentric than concentric condition. In the eccentric case the failed bone volume ranges from 17.3 to 18.6%, whereas in the concentric case it ranges from 1.4 to 3.0% with the decreasing of bone support.

Table 12 - Failed bone volume in function of bone support with all PE implant.

Eccentric load						
Bone support	100%	98%	97%	95%	90%	84%
Failed Bone Volume	17.3%	17.3%	17.6%	17.9%	18.1%	18.6%
Concentric load						
Bone support	100%	98%	97%	95%	90%	84%
Failed Bone Volume	1.4%	1.4%	1.7%	1.8%	2.5%	3.0%

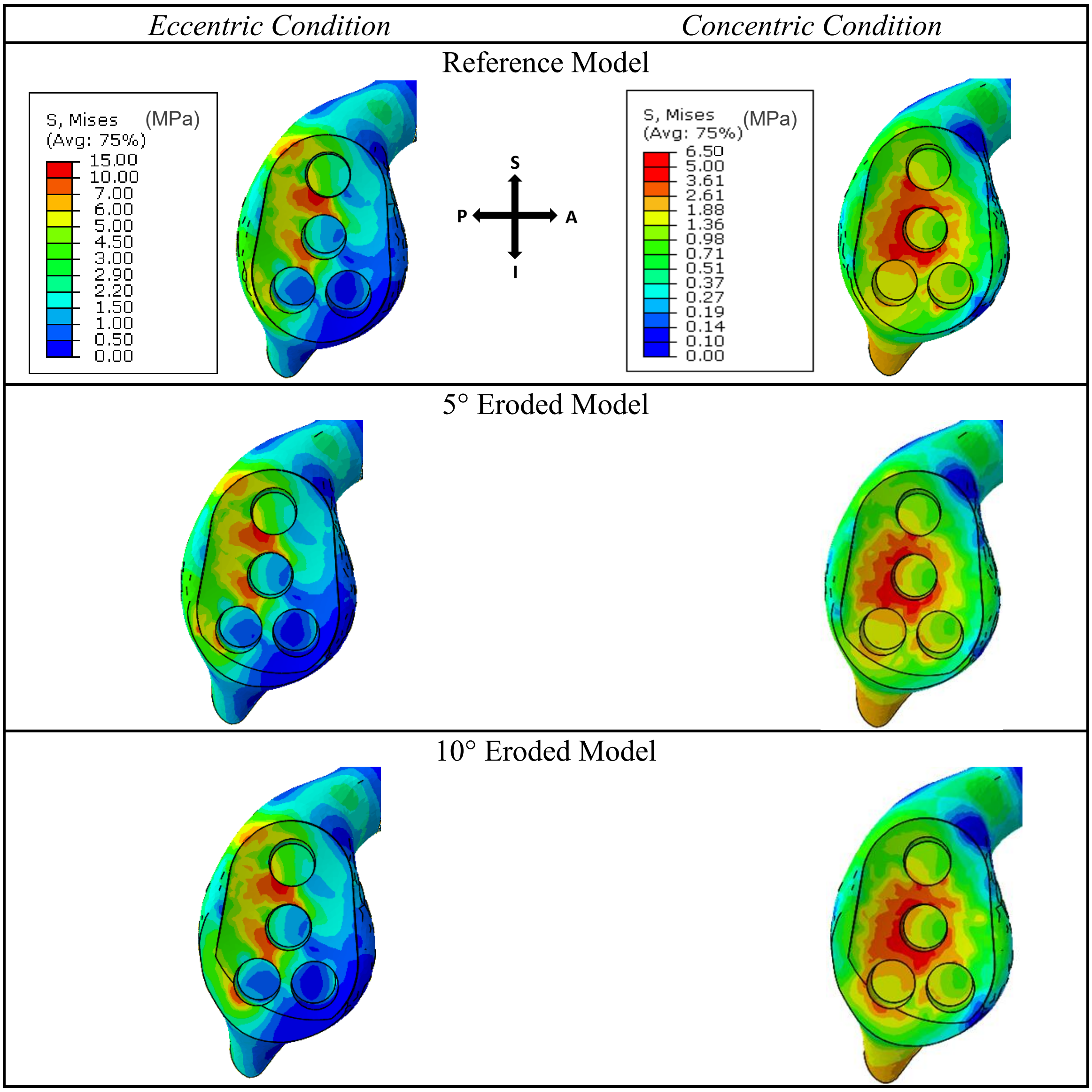

Figure 26 - Bone stress in the two loading conditions with cemented implant (reference, 5°, 10° eroded models).

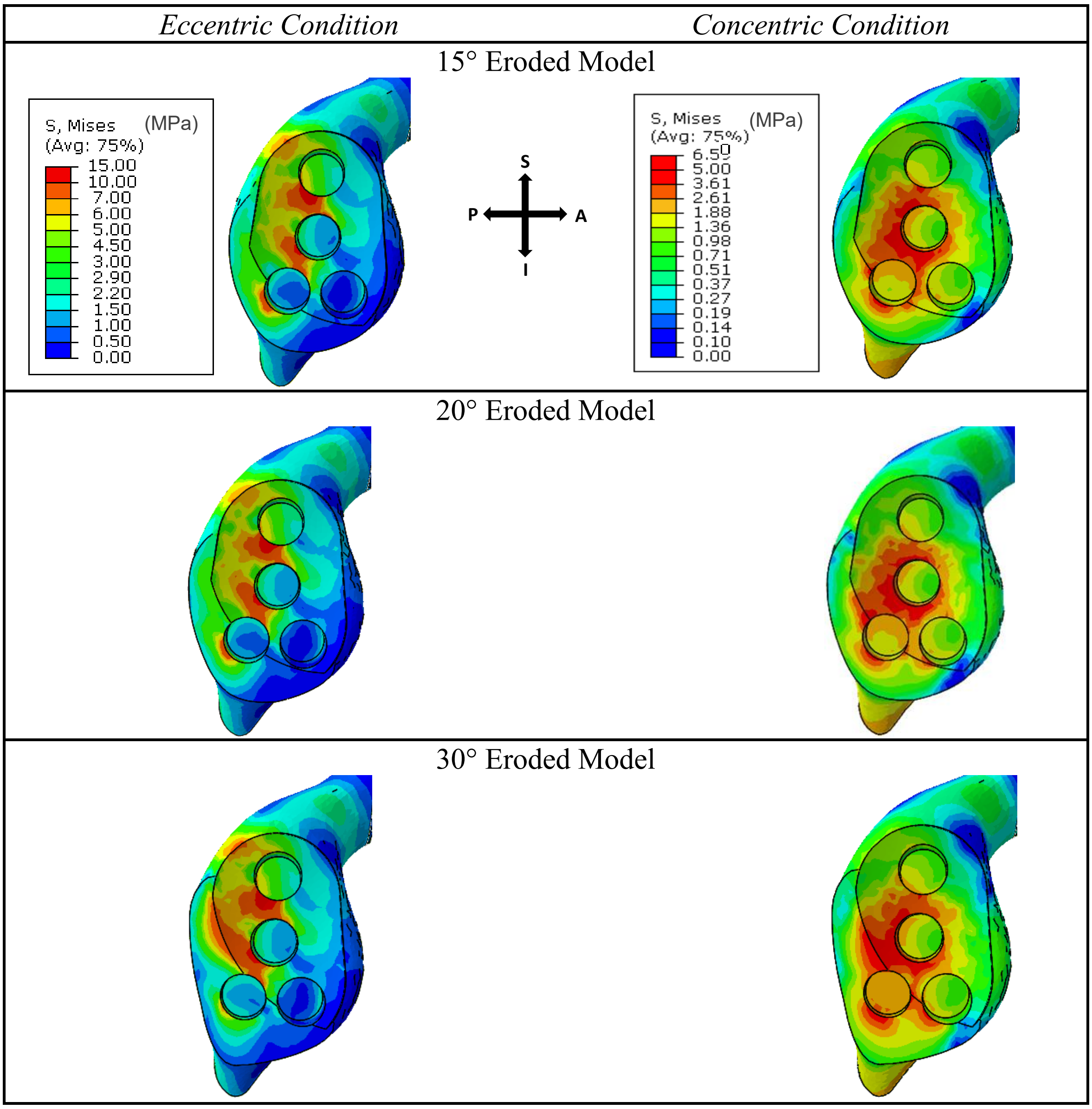

Figure 27 - Bone stress in the two loading conditions with cemented implant (15°, 20°, 30° eroded models).

4.1.4 Bone Strain

Bone strain slightly grows with the increasing of bone erosion in both loading conditions (Figure 28 and Figure 29. The maximum strain (7000 µstrain) is located in the supero-posterior region of the glenoid cavity for the ***eccentric condition***, whereas it can be observed in the central region of the glenoid cavity and in the posterior region of the scapula for the ***concentric condition*** (1900 µstrain).

The maximum strain does not change between the models, to compare them the mean strain in the glenoid cavity was calculated for the eroded models and normalized to the mean strain of the reference configuration. The values for all models in the two loading conditions are shown in Table 13.

Table 13 - Mean bone strain in function of bone support with all PE implant.

Eccentric load						
Bone support	100%	98%	97%	95%	90%	84%
Mean bone strain (μstrain)	730	730	731	732	740	751
Concentric load						
Bone support	100%	98%	97%	95%	90%	84%
Mean bone strain (μstrain)	350	350	350	350	352	360

The normalized values (Graph 6) show that the mean strain in the glenoid region rises till 3% with the 84% bone support in both loading conditions.

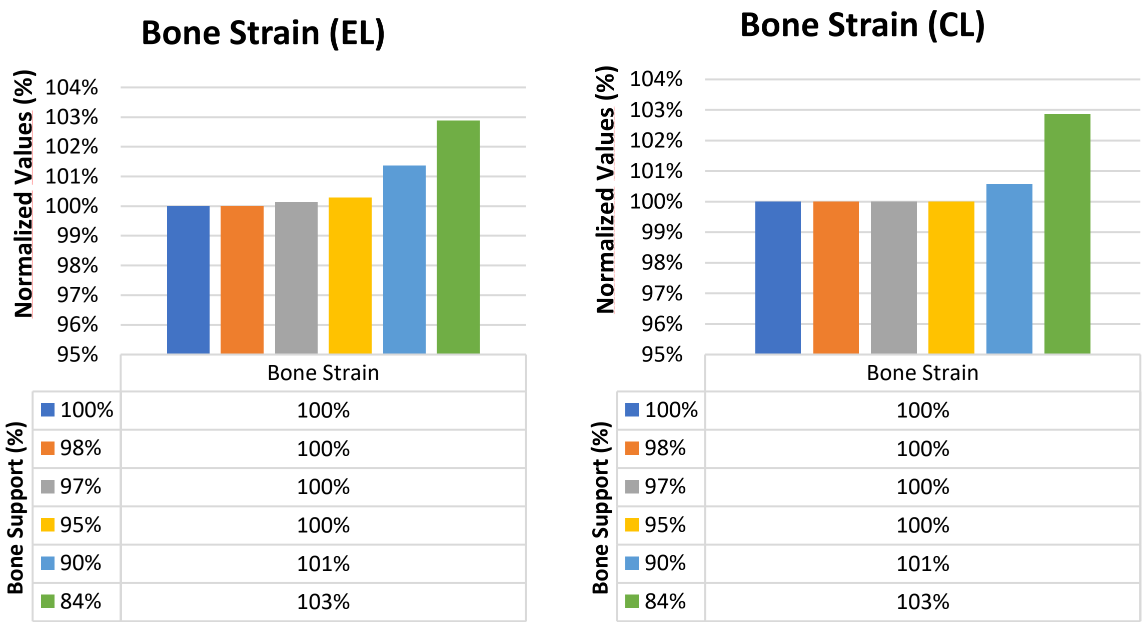

Graph 6 - Bone strain with all PE implant in the eccentric (left) and concentric (right) conditions.

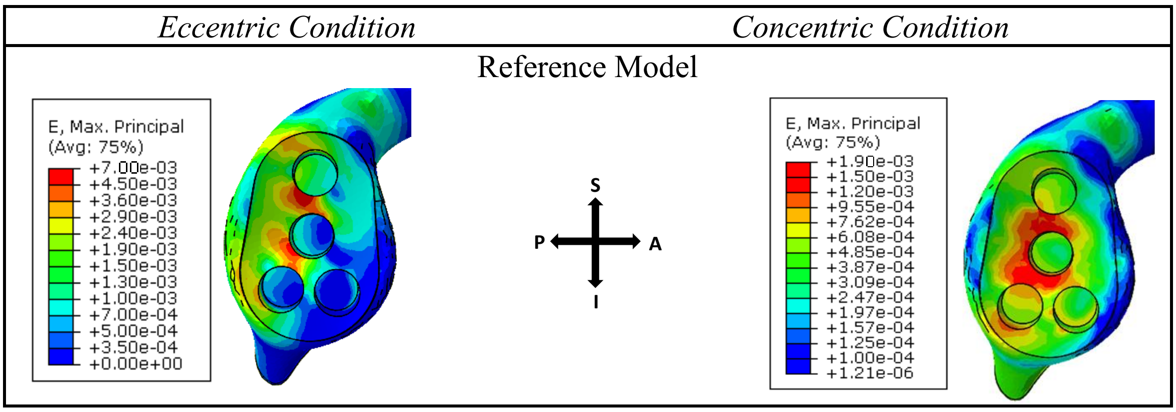

Figure 28 - Bone strain in the two loading conditions with cemented implant (reference model).

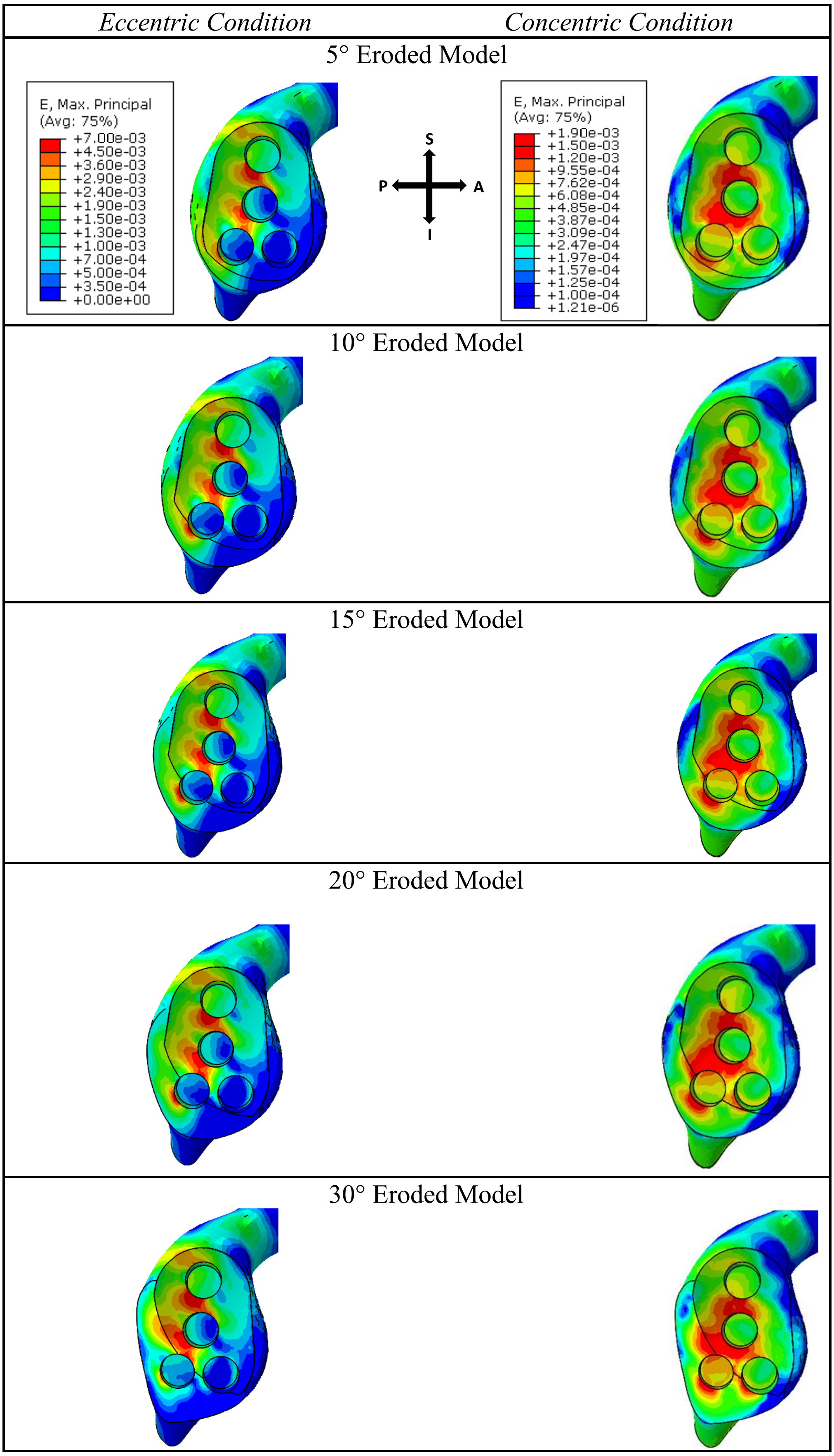

Figure 29 - Bone strain in the two loading conditions with cemented implant (eroded models).

4.2 Cementless implant

In this section the results obtained from the FEA are analysed in terms of micromotions at the bone-implant interface, medial displacements, bone stress and strain for the reference and the eroded models taking into account the two loading conditions.

4.2.1 Relative Micromotions

In both loading conditions relative micromotions at the bone-implant interface were obtained considering the difference between the mean displacements in tangent direction of four points in the centre of glenoid cavity and four points in the centre on the implant's baseplate. An increase of relative micromotions can be noted with the decreasing of bone support for both loading conditions (Figure 30, Figure 31, Figure 32 and Figure 33).

To compare models, the obtained values for eroded models were normalized to the relative micromotion of the reference configuration. The relative micromotions for all models in the two loading conditions are shown in Table 14.

Table 14 - Relative micromotions in function of bone support.

Eccentric load						
Bone support	100%	98%	97%	95%	90%	84%
Relative micromotions (µm)	1.20	1.20	1.30	1.50	1.60	1.90
Concentric load						
Bone support	100%	98%	97%	95%	90%	84%
Relative micromotions (µm)	1.17	1.17	1.20	1.31	1.43	1.50

The normalized values (Graph 7) show that the relative micromotions do not change till the 98% bone support for both loading conditions. In the ***eccentric condition*** relative micromotions increase till 58% with the 84% bone support, whereas in the ***concentric condition*** they rise until 28% with the 84% bone support.

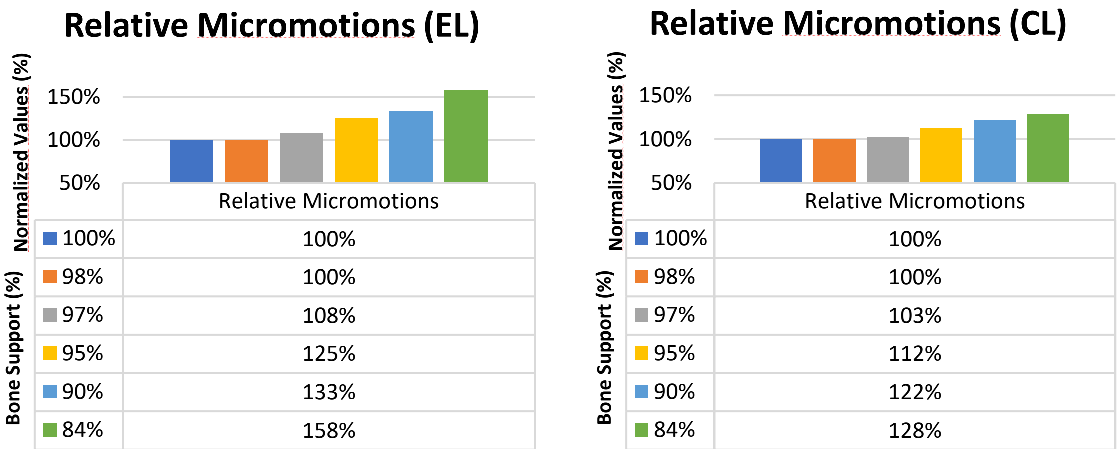

Graph 7 - Normalized relative micromotions in the eccentric (left) and concentric (right) conditions.

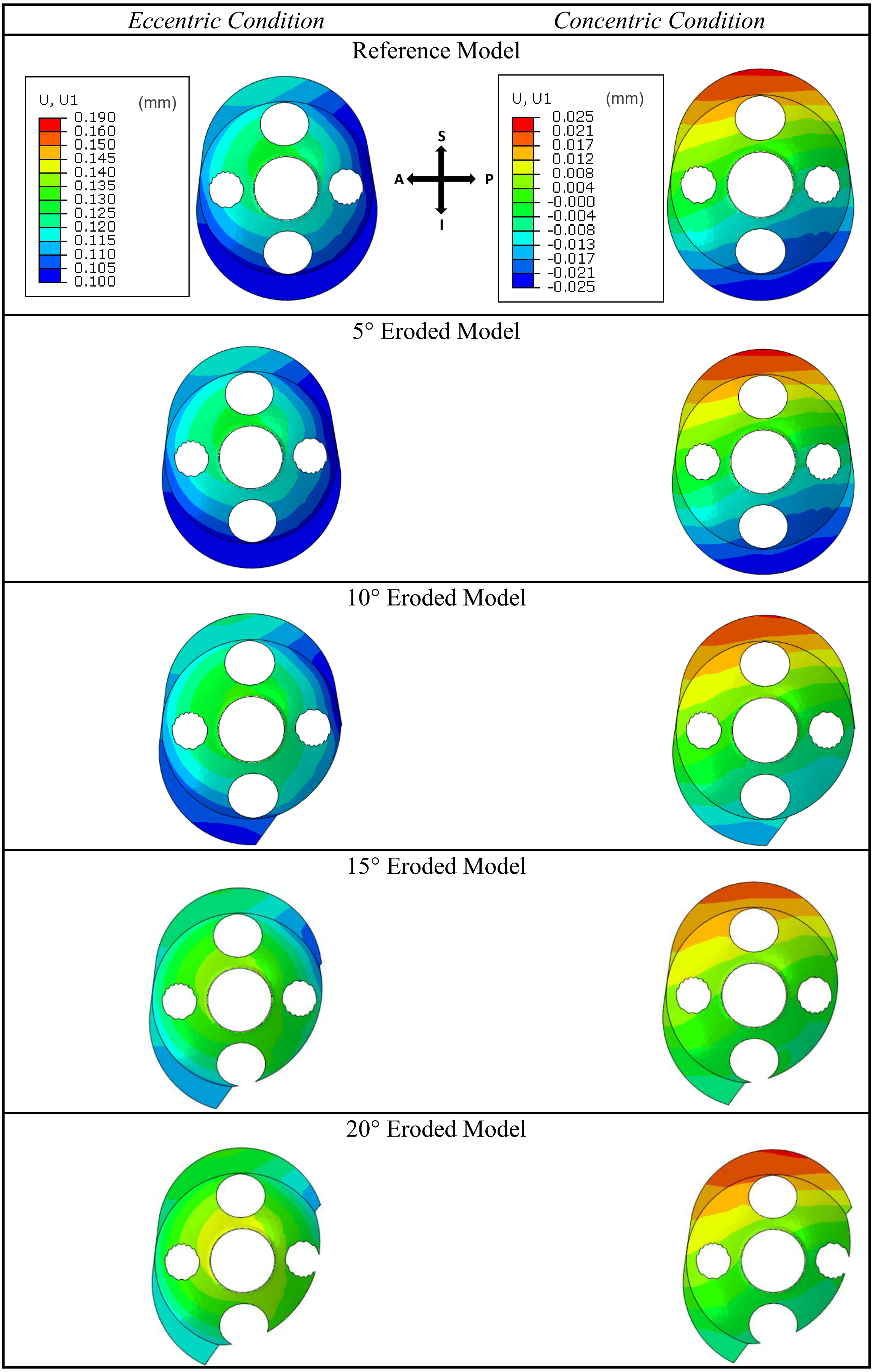

Figure 30 - Tangent-to-glenoid plane micromotions in the implant backside (reference, 5°, 10°, 15°, 20° eroded models).

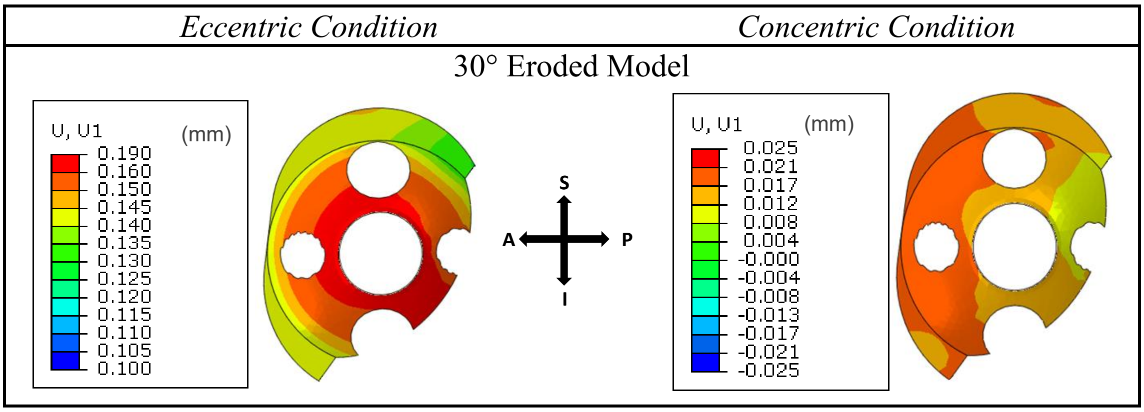

Figure 31 - Tangent-to-glenoid plane micromotions in the implant backside (30° eroded models).

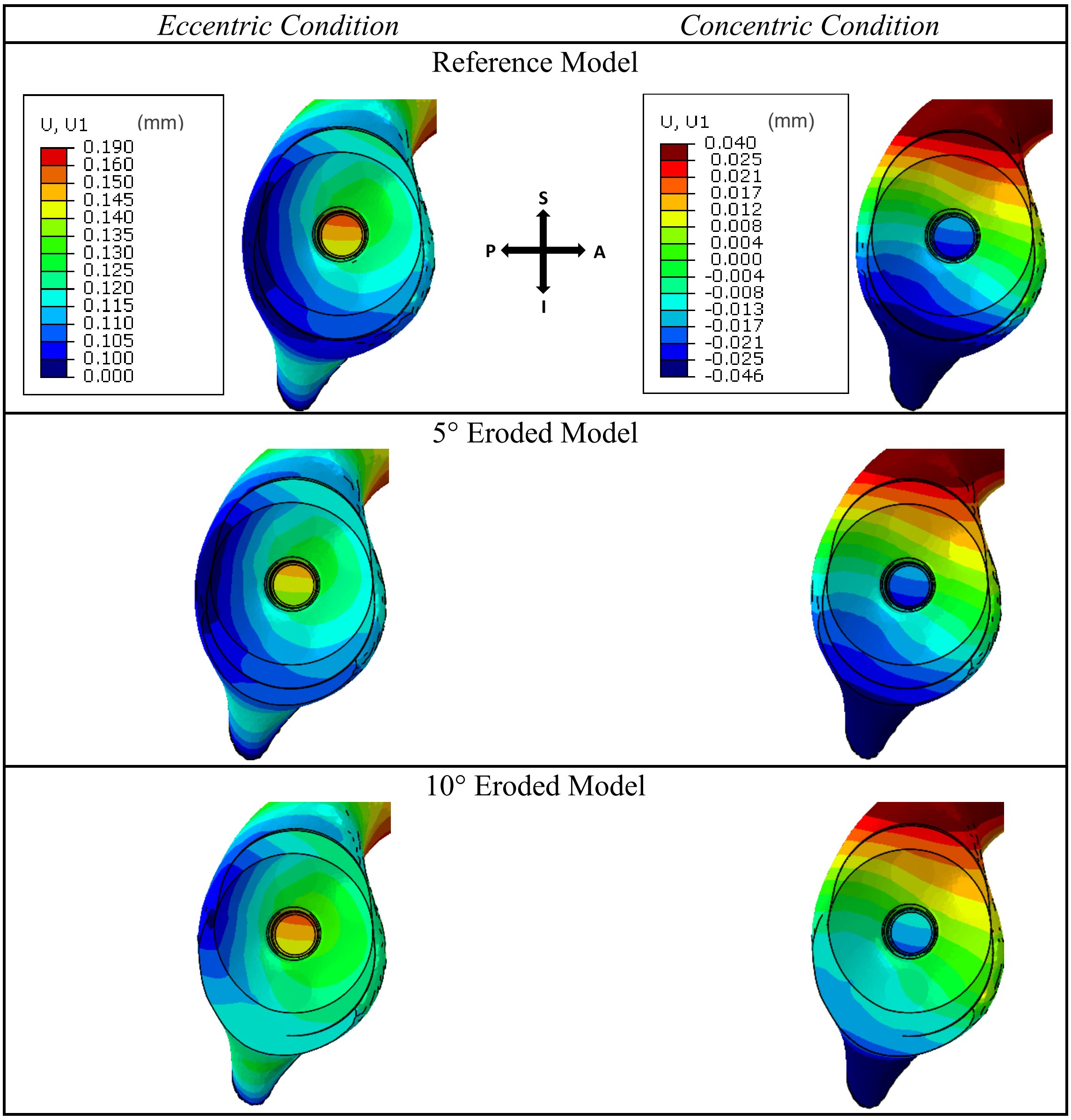

Figure 32 - Tangent-to-glenoid plane micromotions in the glenoid region (reference, 5°, 10° eroded models).

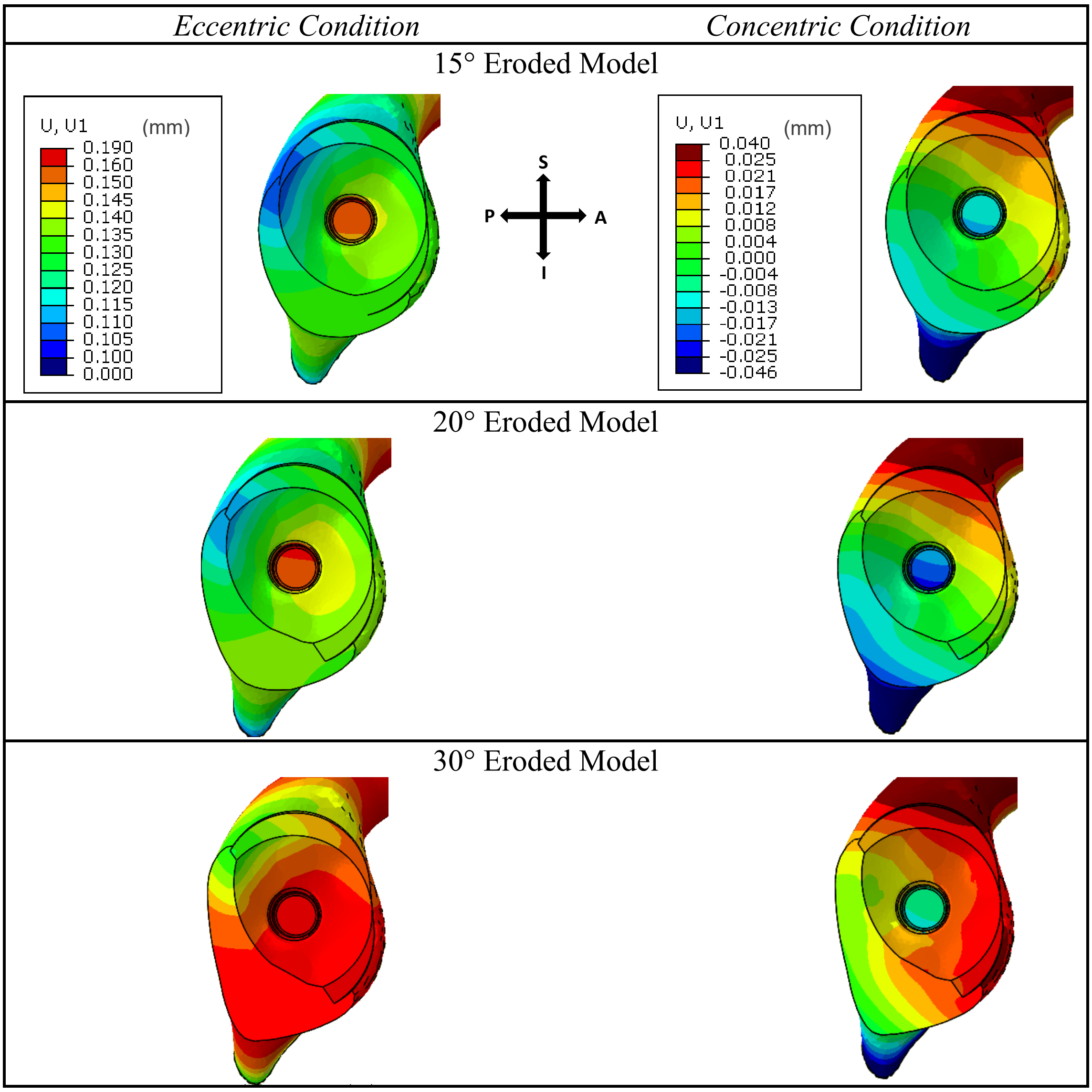

Figure 33 - Tangent-to-glenoid plane micromotions in the glenoid region (15°, 20°, 30° eroded models).

4.2.2 *Medial displacements*

In both loading conditions implant medial displacement was obtained considering the mean displacement of four points at the bottom of the keel. An increase of medial displacements can be noted with the decreasing of bone support for both loading conditions (Figure 34 and Figure 35).

To compare models, the obtained values for eroded models were normalized to the mean displacement of the reference configuration. The medial displacements for all models in the two loading conditions are shown in Table 15.

Table 15 - Medial displacement of the cementless implant in function of bone support.

Eccentric load						
Bone support	100%	98%	97%	95%	90%	84%
Medial displacement (µm)	135	135	136	137	137.5	146
Concentric load						
Bone support	100%	98%	97%	95%	90%	84%
Medial displacement (µm)	135	135	135.5	136	137.6	146

The normalized values (Graph 8) show the same increase for both loading conditions. In fact, the values in Table 15 are similar. The medial displacements rise till 8% with the 84% bone support in the ***eccentric*** and ***concentric conditions***.

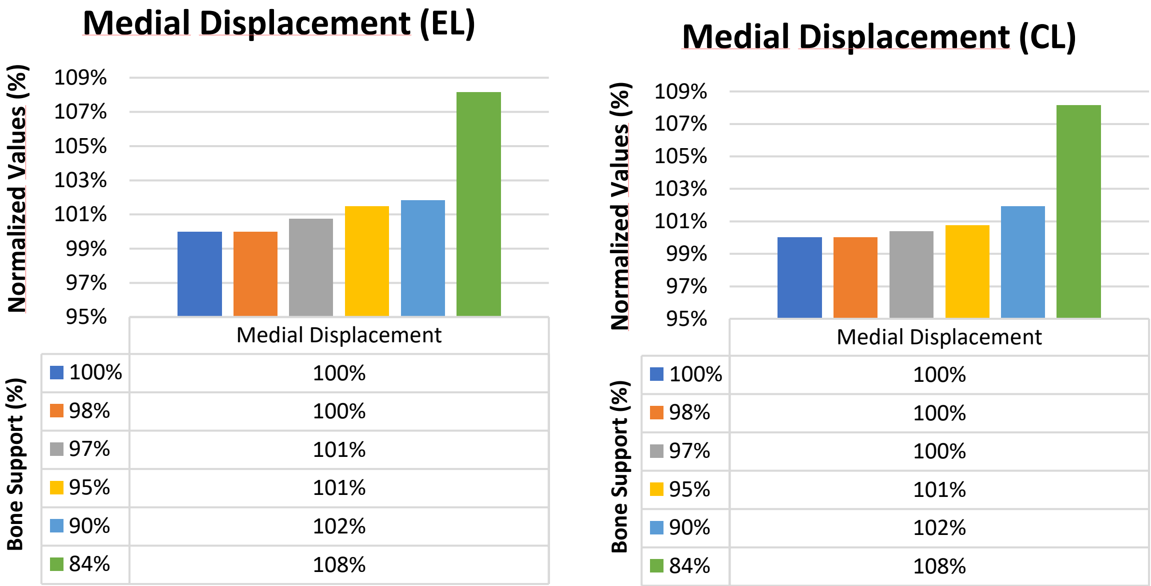

Graph 8 - Normalized medial displacement in the eccentric (left) and concentric (right) conditions.

Eccentric Condition	*Concentric Condition*

Reference Model

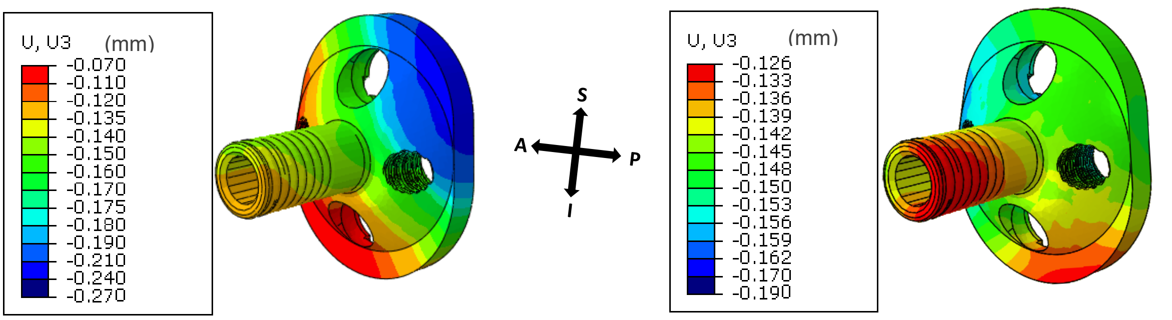

Figure 34 - Medial displacement of the cementless implant (reference model).

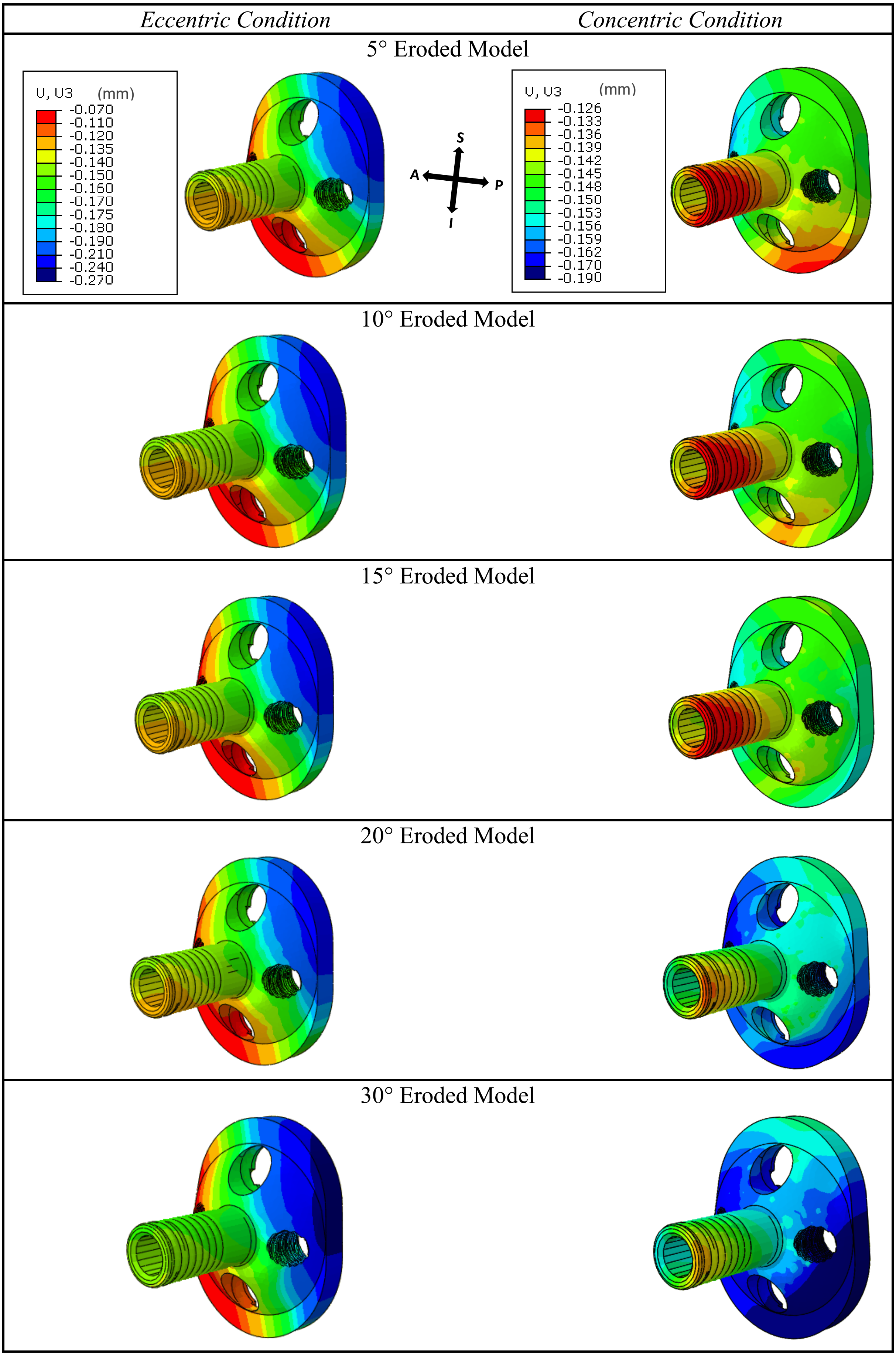

Figure 35 - Medial displacement of the cementless implant (eroded models).

4.2.3 Bone stress

The bone stress was analysed in the glenoid cavity defined in section 3.8. It is important to notice with the second type of implant that the peak of von Mises remains steady till the 90% bone support, while it increases with the 84% bone support. Furthermore, the mean von Mises stress in the bone slightly rises with the decreasing of bone erosion in both loading conditions (Figure 36 and Figure 37).

In the ***eccentric condition*** the peak of von Mises stress can be observed in the posterior region of the scapula for all model, in the glenoid cavity it is located only in the supero-posterior region till the 97% bone support, with the decreasing of support it extends to all posterior region of the glenoid cavity. In the ***concentric condition*** the peak of von Mises stress can be seen in the posterior region of the scapula for all model, in the glenoid cavity it is located only in the central region till the 97% bone support, with the decreasing of support it extends to infero-posterior region of the glenoid cavity.

To compare models the mean von Mises stress in the glenoid cavity was calculated for the eroded models and normalized to the mean von Mises stresses of the reference configuration. The peak and the mean von Mises stresses for all models in the two loading conditions are shown in Table 16.

Table 16 - Peak and mean bone stress in function of bone support with cementless implant.

Eccentric load						
Bone support	100%	98%	97%	95%	90%	84%
Peak bone stress (MPa)	8	8	8	8	8	10
Mean bone stress (MPa)	1.68	1.71	1.72	1.74	1.76	1.84
Concentric load						
Bone support	100%	98%	97%	95%	90%	84%
Peak bone stress (MPa)	6	6	6	6	6	8.5
Mean bone stress (MPa)	1.15	1.15	1.16	1.18	1.19	1.23

The bar diagrams below (Graph 9) illustrate that in the ***eccentric condition*** the mean von Mises stress in the bone grows already starting from the 98% bone support, whereas in the ***concentric condition*** it increases from the 97% bone support. In the ***eccentric condition*** the mean von Mises stress rises till 10% with the 84% bone support, while in the ***concentric condition*** a lesser increase of mean stress occurs, it rises until 7% with the 84% bone support.

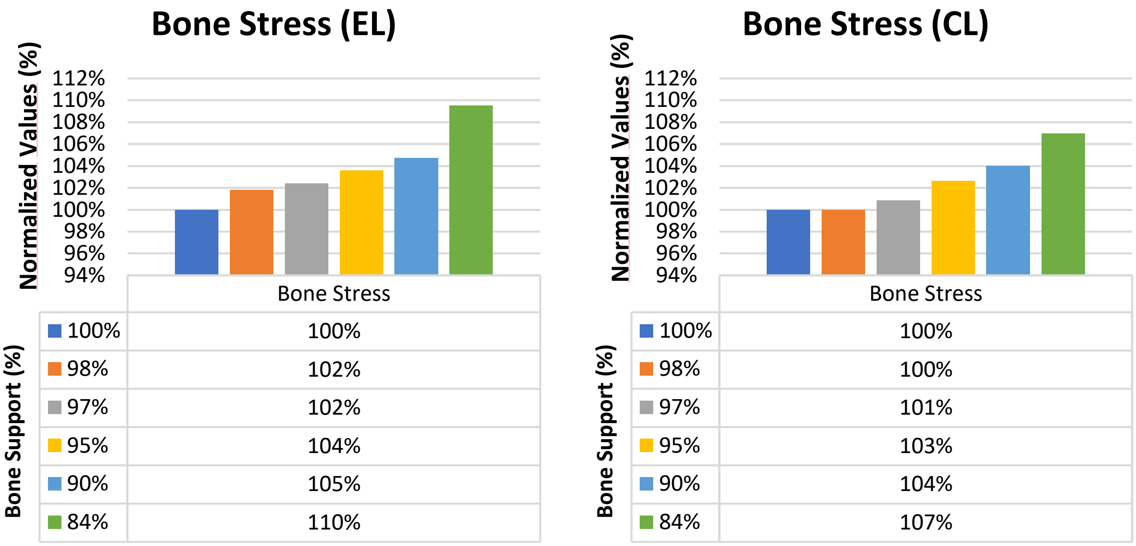

Graph 9 - Normalized bone stress with T.E.S.S. in the eccentric (left) and concentric (right) conditions

As for the cemented implant, the percentages of failed bone in the glenoid cavity were evaluated (Table 17). Failed bone volume is higher for the eccentric than concentric condition. In the eccentric case the failed bone volume ranges from 13.5 to 16.7%, whereas in the concentric case it ranges from 1.5 to 4.5% with the decreasing of bone support.

Table 17 - Failed bone volume in function of bone support with T.E.S.S.

Eccentric load						
Bone support	100%	98%	97%	95%	90%	84%
Failed Bone Volume	13.5%	13.7%	14.1%	15.7%	15.5%	16.7%
Concentric load						
Bone support	100%	98%	97%	95%	90%	84%
Failed Bone Volume	1.5%	1.5%	1.7%	2.3%	2.8%	4.5%

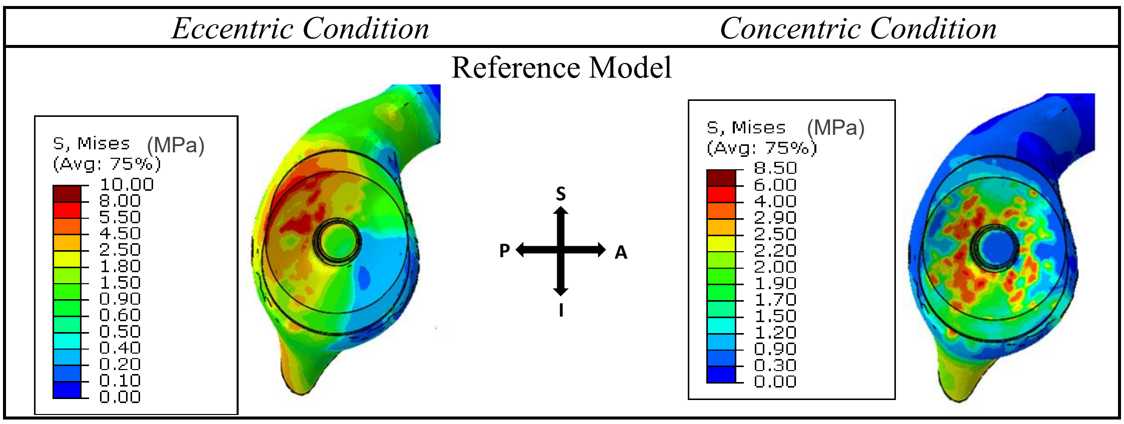

Figure 36 - Bone stress in the two loading conditions with cementless implant (reference model).

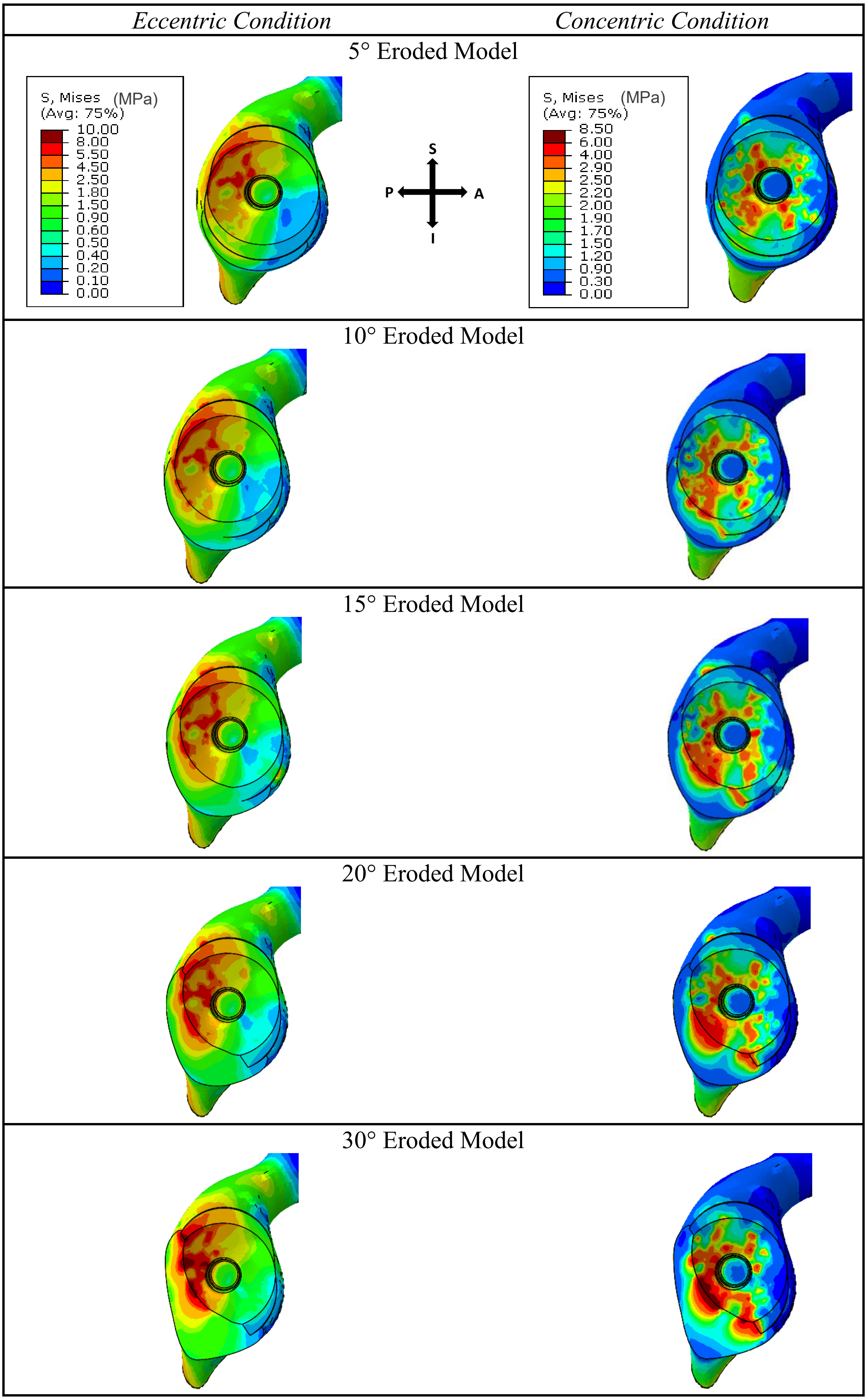

Figure 37 - Bone stress in the two loading conditions with cementless implant (eroded models).

4.2.4 Bone Strain

Bone strain slightly increases with the decreasing of bone support in both loading conditions. The maximum strain with the second type of implant remains steady till the 90% bone support, while it rises with the 84% bone support. Furthermore, the mean bone strain slightly increases with the decreasing of bone erosion in both loading conditions (Figure 38 and Figure 39).

In the ***eccentric condition*** the maximum strain can be observed in the posterior region of the scapula for all model, in the glenoid cavity it is located only in the central-posterior region till the 97% bone support, with the decreasing of support it extends to all posterior region of the glenoid cavity. In the ***concentric condition*** the maximum strain is located in the posterior region of the scapula for all model, in the glenoid cavity it is located only in the central region till the 97% bone support, with the decreasing of support it extends to infero-posterior region of the glenoid cavity.

To compare models the mean strain in the glenoid cavity was calculated for the eroded models and normalized to the mean von Mises stresses of the reference configuration. The maximum and the mean bone strain for all models in the two loading conditions are shown in Table 18.

Table 18 - Peak and mean bone strain in function of bone support with cementless implant.

Eccentric load						
Bone support	100%	98%	97%	95%	90%	84%
Max bone strain (µstrain)	2500	2500	2500	2500	2500	4000
Mean bone strain (µstrain)	582	582	584	596	600	626
Concentric load						
Bone support	100%	98%	97%	95%	90%	84%
Max bone strain (µstrain)	1400	1400	1400	1400	1400	2000
Mean bone strain (µstrain)	480	480	488	490	510	540

The normalized values (Graph 10) show that in the ***eccentric condition*** the mean bone strain grows till 8% with the 84% bone support, whereas in the ***concentric condition*** it rises until 12% with the 84% bone support.

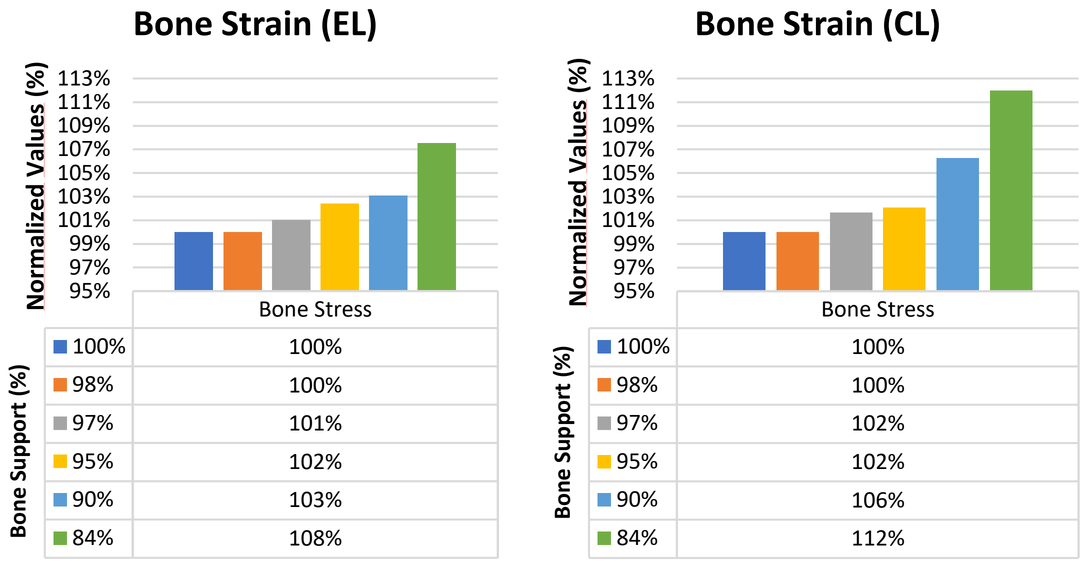

Graph 10 - Normalized bone strain with T.E.S.S. in the eccentric (left) and concentric (right) conditions.

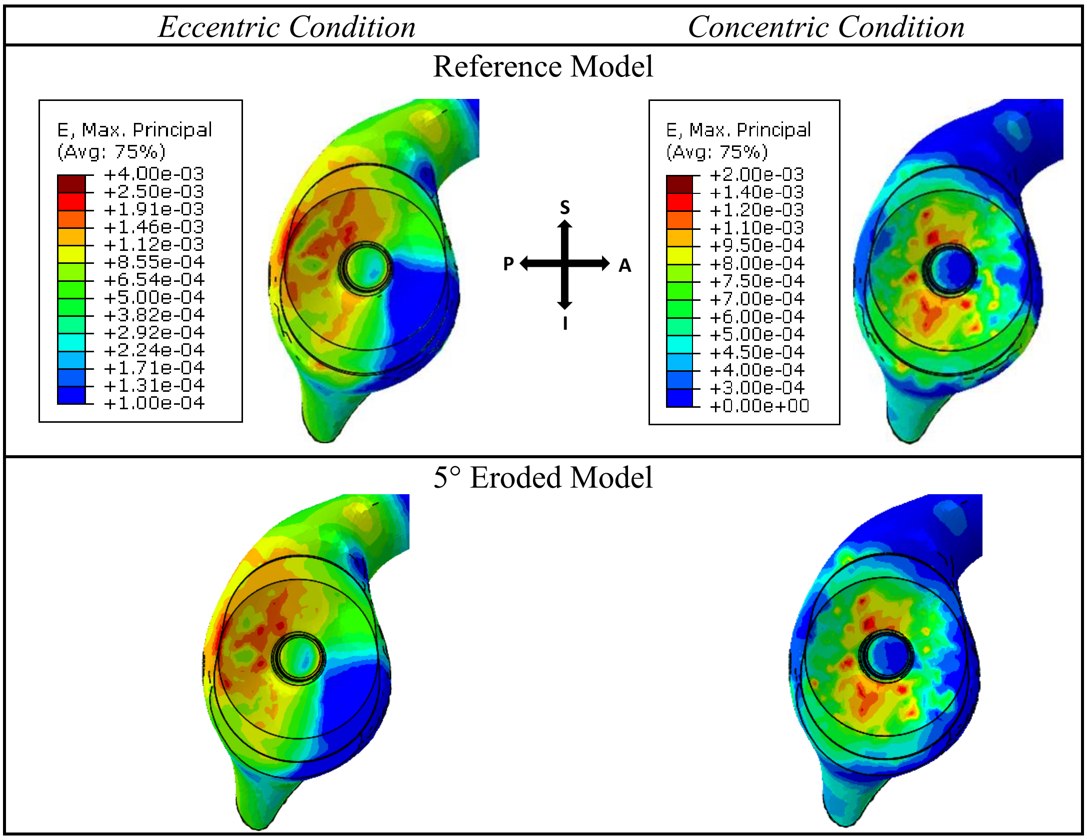

Figure 38 - Bone strain in the two loading conditions with cementless implant (reference, 5° eroded models).

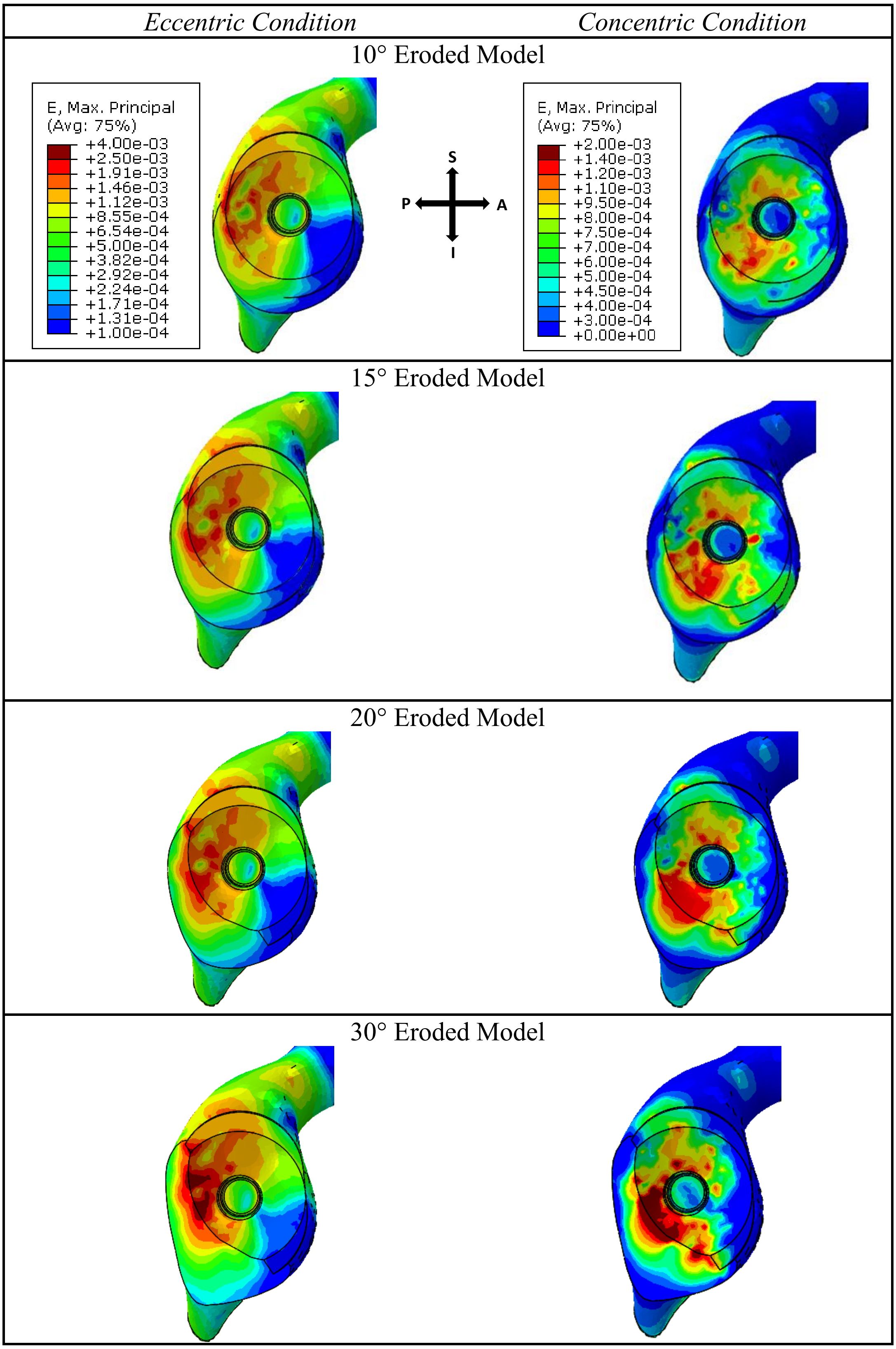

Figure 39 - Bone strain in the two loading conditions with cementless implant (10°, 15°, 20°, 30° eroded models).

4.3 All PE implant vs T.E.S.S.

In this section the results obtained for the all PE implant and the cementless component are compared in terms of bone stress, strain and glenoid loosening taking into account the two loading conditions.

4.3.1 Bone stress and strain

In the ***eccentric condition*** glenoid mean strain and stress are higher for models with the all PE implant than those obtained with the cementless component. In the ***concentric condition*** an opposite situation occurs: the results with the cementless implant are higher than those with the all PE component.

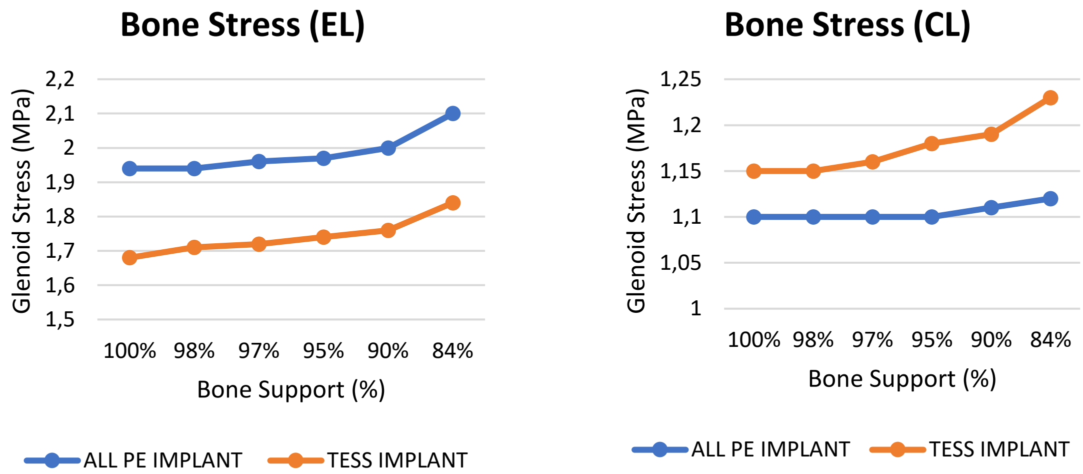

Graph 11 - Comparison of bone stress in all PE implant and T.E.S.S. in the two loading conditions.

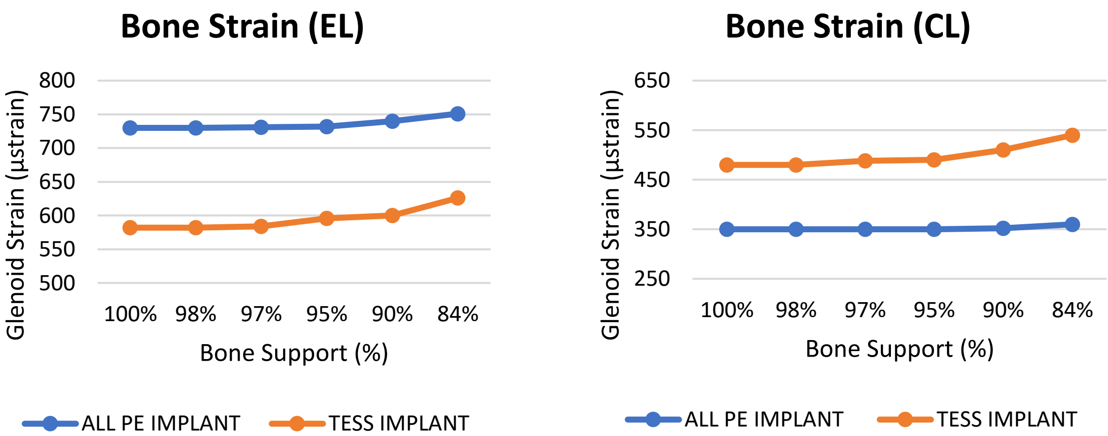

Graph 12 - Comparison of bone strain in all PE implant and T.E.S.S. in the two loading conditions.

In the ***eccentric condition*** mean stress slightly increases with the decreasing of bone support for both implants, in models with T.E.S.S. glenoid mean stress is always below 2 MPa.

In the ***concentric condition*** mean stress remains constant till the 95% bone support for models with cemented implant, while it rises starting from the 97% bone support for models with cementless component. There is a slight growth of bone mean strain for both components in the ***eccentric conditions***. Bone strain remains constant till the 90% bone support for cemented implant, whereas it rises starting from the 97% bone support for cementless component in the ***concentric condition.***

Comparing the percentages of failed bone (Graph 13), it can be noted that volume of failed bone is higher in models with all PE implant for the eccentric case, while it is higher in models with cementless component for the concentric case.

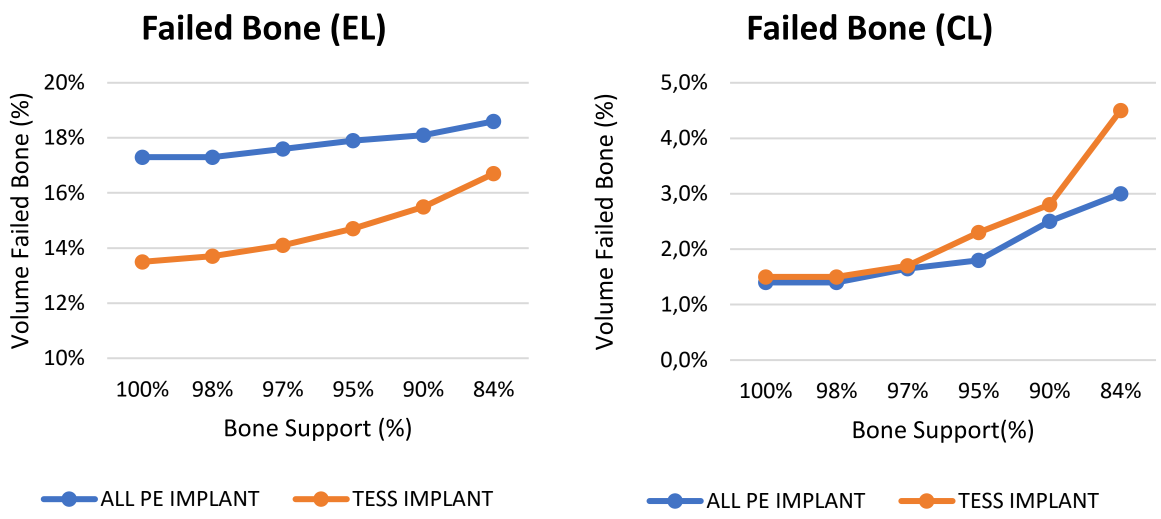

Graph 13 - Comparison of failed bone in all PE implant and T.E.S.S. in the two loading conditions.

4.3.2 Glenoid loosening

The two types of implants were compared in terms of loosening defining two parameters. The critical cement volume (CCV) and the micromotions-threshold percentage ratio (MTPR) were calculated in order to quantify the glenoid loosening of two components. The obtained values are shown in Table 19.

Table 19 - CCV and MTPR in function of bone support.

Eccentric load						
Bone support	100%	98%	97%	95%	90%	84%
CCV	34.40%	34.40%	34.90%	35.10%	39.00%	44.00%
MTPR	1.60%	1.60%	1.70%	2.00%	2.10%	2.50%
Concentric load						
Bone support	100%	98%	97%	95%	90%	84%
CCV	4.10%	4.10%	4.20%	4.30%	4.50%	5.00%
MTPR	1.56%	1.56%	1.60%	1.75%	1.91%	2.00%

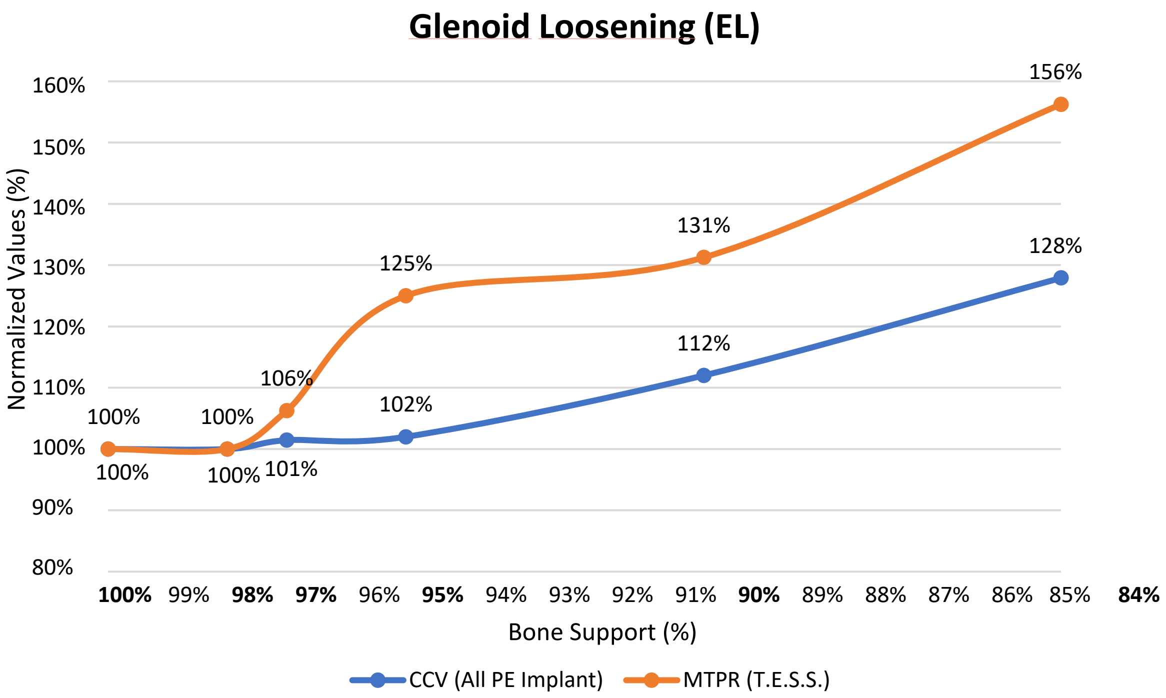

Graph 14 - Normalized CCV and MTPR in the eccentric condition.

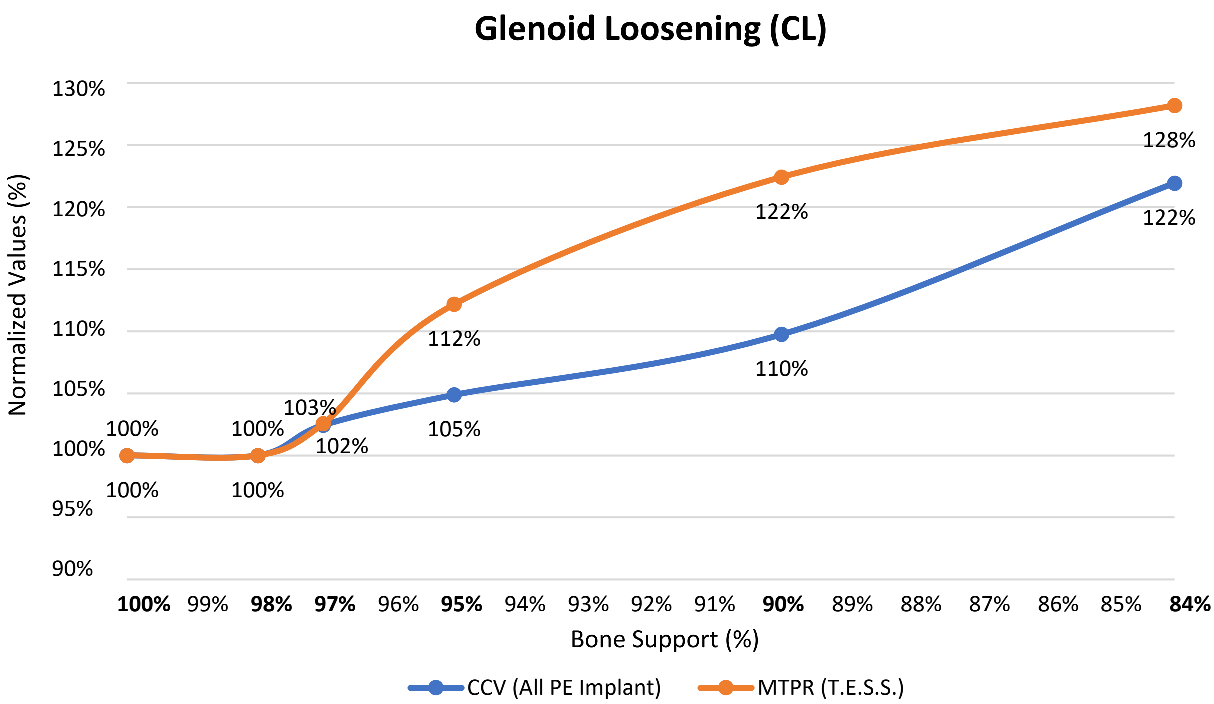

Graph 15 - Normalized CCV and MTPR in concentric condition.

The CCV is higher for the eccentric than concentric condition, in the first case it ranges from 34.40 to 44.00%, whereas in the second one it increases from 4.10 to 5.00% with the decreasing of bone support. The MTPR is characterized by similar values for both conditions, the obtained values are extremely low (under 3%) because the relative micromotions are far below the threshold of 75 μm. The results were normalized to the values of the reference models in order to compare the two glenoid components (Graph 14 and Graph 15).

It is evident that the cemented component is less affected by the decreasing of bone support because the loosening increases till 28% and 22% respectively in the eccentric and concentric conditions with the 84% bone support. In models with cementless implant the glenoid loosening rapidly increases until 56% and 28% respectively in the eccentric and concentric conditions with the 84% bone support.

Chapter 5
Discussion

Loosening of glenoid component represents the main problem to face in aTSA [59] since it jeopardies stability and survival of the implant. Posterior glenoid erosion is commonly found in some patients affected by osteoarthritis. That type of disorder can lead to an increase of complications and component loosening, affecting negatively on clinical outcomes after an aTSA [14] [15]. Therefore, predicting the possible consequences of implanting an anatomic component with incomplete bone support is crucial for long term stability of implant.

Some studies demonstrated that with the decreasing of bone support an increase of bone-cement stresses and interface micromotions occurs [56] [101]. However, not all of these studies used finite element models and no one compared the results of different implants and fixations. The purpose of the present study was to investigate the effects of decreasing bone support on the glenoid component stability when two kinds of anatomical shoulder prostheses are implanted in order to provide guidelines for aTSA planning. Several parameters were analysed through FEA considering two loading conditions: cement layer stress, bone-cement interfacial contact pressure, bone stress and strain and interface micromotions.

As previously observed in section 0, a global increase of considered parameters compared to the reference model can be noted with the decreasing of bone support for both loading conditions. Moreover, the values obtained for the eccentric condition are always higher than those for the concentric case for both implants.

5.1 All PE implant

For the all PE implant the results of the reference model are consistent with some previous studies [34] [56]. Wahab *et al.* [34] obtained peaks of von Mises stress in the cement layer equal to 18 and 7 MPa for the eccentric and concentric loads, in the present study peaks of von Mises stress are 15 and 7 MPa respectively for the eccentric and concentric conditions. Maximum von Mises stress is located in the posterior region of the superior peg for the eccentric case, whereas it is located in the superior region of the inferior pegs for the concentric condition. These repetitive stresses could generate the rocking horse phenomenon, compromising component stability. With the decreasing of bone support it was noticed that the peak of von Mises stress remains constant, while the mean von Mises stress on each peg increases. In the eccentric condition the higher increase occurs in the inferior pegs: in the posterior peg mean stress increases till 122%, while in the anterior peg it rises until 88% with the 84% bone support. In the concentric condition mean stress increases mainly in the posterior peg: 47% with the 84% of bone support.

Cement is a material weak in tension (25 MPa) [102], but stronger in compression (100 MPa) [31]. Results show that the stresses in the cement layer are below cement failure strength (tensile), but they can provoke crack initiation in the cement mantle because they are higher than the chosen threshold of 4 MPa.

Terrier *et al.* [31] found peak values of contact pressure at the bone-cement interface equal to 15 and 6 MPa for the eccentric and concentric loading conditions, in the present study peak values of contact pressure are 14 and 7 MPa respectively with the eccentric and concentric loads. Maximum contact pressure is found in the posterior region of the superior peg and at the base of the posterior peg for the eccentric case, whereas it is found at the base of posterior peg for the concentric condition. With the increasing of bone erosion, the maximum contact pressure remains steady, while the mean contact pressure at the interface rises. The higher increase occurs in the inferior pegs in both loading conditions. The mean pressure increases till 45% and 43% respectively in the posterior and anterior pegs with the eccentric load, whereas it rises until 63% and 27% respectively in the posterior and anterior pegs with the concentric load.

Peaks of von Mises stress in bone cannot be directly compared with literature because in this work a homogenous scapula was considered. Chevalier *et al.* [75] obtained for the cortical bone peaks of 6 and 4 MPa respectively in the eccentric and concentric conditions, whereas they obtained for the trabecular bone peaks of 15 and 8 MPa. In this study a single peak of von Mises stress was achieved: 15 and 6.5 MPa respectively for the eccentric and concentric conditions. These values do not change with the decreasing of bone support and exceed the chosen failure criterion, in particular the percentage of failure bone in the glenoid cavity appears to be greater for the eccentric than concentric condition. In the eccentric case the failed bone volume ranges from 17.3 to 18.6%, whereas in the concentric case it ranges from 1.4 to 3.0% with the decreasing of bone support.

Maximum strains do not change with the decreasing of bone support: they are 7000 and 1900 μstrain respectively for the eccentric and concentric conditions. Their location depends on the applied load. With the increasing of bone erosion, the mean bone strain slightly increases in both loading conditions (till 3% with the 84% bone support).

5.2 Cementless implant

For the cementless implant the results of the reference model cannot be directly compared with literature because only few FEA were conducted on metal-backed glenoid components.

Relative micromotions and medial displacements are not consistent with other studies because the used method is different from others. In fact, the aim of this work is not to focus on the absolute values of the parameters, but to analyse how they change with the decreasing of bone support. For instance, Suarez *et al.* [103] assessed the tangent- and normal-to interface micromotions for different degrees of GH-joint conformity. They considered a cementless implant with a central screw and two loads in order to simulate the rocking-horse phenomenon, obtaining micromotions of 50 μm or more. In another study [104] micromotions at bone-implant interface were estimated for different configurations of screws using a compressive and a cyclic "subluxation" force. Results showed micromotions of 5 μm or more.

In the present work relative micromotions at the bone-implant interface were obtained considering the difference between the mean displacements in the tangent direction of four points in the centre of glenoid cavity and four points in the centre on the implant's baseplate. In addition, no screws were taken into account and only a compressive force was considered. Relative micromotions ranges from 1.20 to 1.90 μm for the eccentric case, whereas they are between 1.17 and 1.50 μm for the concentric case. In both loading conditions they are far below the threshold of 75 μm. With the decreasing of bone support, in the eccentric condition the relative micromotions increase till 58% with the 84% bone support, whereas in the concentric condition they rise until 28% with the 84% bone support.

Medial displacements were obtained likewise, considering the mean displacement in normal direction of four points at the bottom of the keel. They range from 135 to 146 μm, rising till 8% with the 84% bone support in both loading conditions.

Peaks of von Mises stress in glenoid region change with the decreasing of bone support. In the eccentric condition the maximum von Mises stress is 8 MPa till the 90% bone support, whereas it increases (10 MPa) with the 84% bone support. In the concentric condition the peak von Mises stress is 6 MPa until the 90% bone support, whereas it rises (8.5 MPa) with the 84% bone support. Maximum stresses overcome the failure criterion: the percentages of failure bone in the glenoid region is lower in the concentric than eccentric condition. Failed bone volume ranges from 1.5 to 4.5% and from 13.5 to 16.7% respectively in the concentric and eccentric conditions.

A similar situation exists for bone strain. In the eccentric condition maximum strain is 2500 μstrain till the 90% bone support, whereas it increases (4000 μstrain) with the 84% bone support. In the concentric condition maximum strain is 1400 μstrain until the 90% bone support, whereas it increases (2000 MPa) with the 84% bone support. These values are lower than strain calculated by Suarez *et al.* [104] (4300 ÷ -4600 μstrain) and Bayraktar *et al.* [105] (6200 ÷ -10400 μstrain). In such studies the presence of screws, cortical and trabecular bones were taken into account. In the present study it was notice that with the decreasing of bone support, in the eccentric case the mean bone strain increase till 8%, whereas in the concentric condition it grows until 12% with the 84% bone support.

5.3 All PE implant vs T.E.S.S.

In literature few studies were carried out in order to compare the two fixation techniques. Finite Element Analyses [51] [52] demonstrated that cemented all PE implants provided a more physiologic stress distribution, whereas metal-backed cementless implant allowed to achieve lower stresses in the glenoid cavity under the implant. In the present work a similar situation was found. In the eccentric condition the mean bone stress and strain are lower in models with cementless component than those with cemented implant. The mean bone stress is always below 2 MPa with T.E.S.S., while it ranges from 1.94 to 2.10 MPa in models with all PE implant. Similarly for the mean bone strain: it is always below 650 µstrain with T.E.S.S., while it ranges from 730 to 751 µstrain in models with all PE implant. This shows that all PE component transfers stress more effectively to the underlying bone, whereas T.E.S.S. provides a greater stress shielding in the bone, which could affect long term results.

In the concentric case a different situation occurs because the values with the cementless implant are higher than those with the all PE component. The mean bone stress is always below 1.15 MPa with all PE component, while it is between 1.15 and 1.23 MPa in models with cementless component. The mean bone strain is always below 400 µstrain with cemented prosthesis, while it ranges from 450 to 540 µstrain in models with metal-backed implant. In such loading configuration, the results might be due to the presence of four cement pegs, which shield stress by preventing an appropriate interaction between the PE implant and the bone.

Comparing the percentages of failed bone, it can be noted that volume of failed bone is higher in models with all PE implant for the eccentric case, while it is higher in models with cementless component for the concentric case. In addition, volume of failed bone always increases more quickly in models with T.E.S.S. than models with all PE implant with the decreasing of bone support.

In terms of glenoid loosening, the two implants were compared through two failure criteria: CCV and MTPR. CCV is higher for the eccentric than concentric configuration, in the first case it ranges from 34.40 to 44.00%, whereas in the second one it rises from 4.10 to 5.00% with the decreasing of bone support. MTPR takes values extremely low (under 3%) because the relative micromotions are far below the threshold of 75 µm in both loading conditions. The two parameters (CCV and MTPR) cannot be directly compared because they represent different quantity. Therefore, it was thought to compare the normalized values to the reference model. In this way it can be noted that the all PE cemented component is less affected by the decreasing of bone support because the loosening increases till 28% and 22% respectively in the eccentric and concentric condition with the 84% bone support. In models with cementless implant the glenoid loosening rapidly increases until 56% and 28% respectively in the eccentric and concentric conditions with the 84% bone support.

5.4 Limitations

In this section unavoidable limits of the present Finite Element Analysis are reported in order to allow a better understanding and to avoid that the results are not overestimate.

I. *Bone quality was not considered.*

   To develop this project, it was not considered an osteoarthritic scapula, but only an healthy scapula, whose morphology was based on 66 CT scan data in order to mimic the mean scapular morphology of the population. Therefore, it was chosen to generate bone defects in line with a literature-based description of the most frequent and relevant type of erosion in case of osteoarthritis.

II. *No distinction between cortical and cancellous bones.*

   Since an orphan mesh of the scapula was provided, differentiating the cancellous from the cortical bone was difficult. For this reason, mean values of the mechanical properties of the scapula were considered. Therefore, simulations were done considering bone as a homogenous material.

III. *Debonding interface between all PE implant and cement.*

   Although micromotions at the interface were not evaluated for the all PE implant, PE-cement interface was considered debonded. Such choice was done because initially a perfectly bonded interface was set, in spite of that the obtained results did not show differences between some eroded models. This could be associated to a too stiff model.

IV. *Specific all PE design.*

   In the present work a specific cemented all PE design was considered, namely pegged implant.

Chapter 6
Conclusions and Future Developments

Anatomic total shoulder arthroplasty (aTSA) has markedly developed in the decades thanks to its efficacy in relieving pain and restoring function of the arthritic shoulders [106] [107]. The main reason of its failure is glenoid component loosening, chiefly in shoulders with preoperative erosion [15]. Eroded shoulders are difficult to deal with and correct because the glenoid components need sufficient bone support for the implantation so as to promote osseous integration or cement layer long-term survival. The adequate bone support to limit glenoid loosening has not yet been defined [56]. Thus, the objective of the present work was to obtain guidelines in terms of bone support for aTSA planning.

For the first time a FEA was carried out to investigate the effects of bone support decrease on glenoid component loosening. The clinical relevance of this study is clear: bone support is a key factor in glenoid component stability. All considered parameters (cement layer stress, bone-cement interfacial contact pressure, bone stress and strain, interface micromotions) show an upward trend compared to the reference model with the decreasing of bone support for both loading conditions. Even though, the values obtained for the eccentric condition are always higher than those for the concentric case for both implants.

For the all PE implant a decrease of the backside support until 95% had no relevant effect on cement stress, however the high degree of CCV for the reference model should raise concern. In case of a cementless component the interfacial micromotions increased starting from the 97% bone support. Consequently, all of which leads to the conclusion that an anatomic glenoid component should always be implanted with full backside support. In case this is not possible without jeopardising other outcome related factors like glenoid orientation, other options should be investigated. Future studies that include bone quality parameters and different implant designs (augmented components) and an experimental validation will provide improved insights for glenoid component placement in eroded glenoids.

Bibliography

[1] Funk L. *Shoulder Anatomy*. Available: https://frozenshoulderclinic.com/shoulder anatomy/

[2] University of Bristol. *Shoulder girdle anatomy*. Available: https://www.ole.bris.ac.uk/bbcswebdav/institution/Faculty%20of%20Health%20Sciences/MB%20ChB%20Medicine/Year%203%20MDEMO%20%20Hippocrates/Hippocrates/shoulder%20pain%20etutorial/shoulder_girdle_anatomy.html

[3] Healthline Media. *Muscles*. Available: https://www.healthline.com/human-body-maps/shoulder-muscles#1

[4] Amacsports. *The shoulder joint*. Available: http://amactraining.co.uk/resources/handy-information/free-learning-material/level-3-exercise-and-fitness-knowledge-index/level-3-70 -exercise-and-fitness-knowledge-the-shoulder-joint/

[5] Zaffagnini S., Marcheggiani Muccioli G. M., Neri M. P., et al. *Spalla: La protesi di spalla*. Available: http://www.ior.it/curarsi-al-rizzoli/spalla-la-protesi-di-spalla

[6] Khatib O., Onyekwelu I., Yu S., Zuckerman J.D., *Shoulder Arthoplasty in New York State, 1991 to 2010: changing patterns of utilization.* J Shoulder Elbow Surg 2015; 24(10): 286-291.

[7] Walch G., Young A.A., Melis B., Gazielly D., Loew M., Boileau P. *Results of a convex-back cemented keeled glenoid component in primary osteoarthritis: multicenter study with a followup greater than 5 years.* J Shoulder Elbow Surg 2011; 20: 385–394.

[8] Pomwenger W., Entacher K., Resch H., Schuller-Götzburg P. *Need for CT-based bone density modelling in finite element analysis of shoulder arthroplasty revealed through a novel method for result analysis.* Biomed. Eng. 2014; 59(5): 421-430.

[9] Gruppo Giomi. Available: http://www.giomi.com/Portals/Giomi/Pubblicazioni/Acta/Volume39_2016/acta% 20n.%2039%202016%20De%20Cupis.pdf.

[10] Origimm Biotechnology GmbH. *Background: implant-associated infections*. Available: http://www.origimm.com/rd-programs/implant-associated-infections-2/implant- associated-infections/

[11] Pinkas D., Wiater B., Wiater J.M. *The glenoid component in anatomic shoulder arthroplasty*. J Am Acad Orthop Surg. 2015;23:317–26.

[12] Walch G., Badet R., Boulahia A., Khoury A. *Morphologic study of the glenoid in primary glenohumeral osteoarthritis*. J Arthroplasty 1999; 14:756-60.

[13] Jones, R. B. *Addressing glenoid erosion in anatomic total shoulder arthroplasty.* Bull Hosp Jt Dis 71 2013;suppl 2:S46–50.

[14] Chin PC, Hachadorian ME, Pulido PA, Munro ML, Meric G, Hoenecke HR Jr. *Outcomes of anatomic shoulder arthroplasty in primary osteoarthritis in type B glenoids*. J Shoulder Elbow Surg 2015;24:1888- 93.

[15] Walch G., Moraga C., Young A., Castellanos-Rosas J. *Results of anatomic nonconstrained prosthesis in primary osteoarthritis with biconcave glenoid*. J Shoulder Elbow Surg 2012;21:1526-33

[16] Churchill R.S., Spencer E.E., Fehringer E.V., *Quantification of B2 glenoid morphology in total shoulder arthroplasty*. J Shoulder Elbow Surgery 2015; 24(8).

[17] Walch G., Young A.A., Boileau P., Loew M., Gazielly D., Molé, D. *Patterns of Loosening of Polyethylene Keeled Glenoid Components After Shoulder Arthroplasty for*

Primary Osteoarthritis. Results of a Multicenter Study with More Than Five Years of Follow-up". J Bone Joint Surg Am 2012; 94(2): 145-50.
[18] Walch G., Young A.A., Melis B., Gazielly D., Loew M., Boileau P. *Results of a convex-back cemented keeled glenoid component in primary osteoarthritis: multicenter study with a follow-up greater than 5 years*. J Shoulder Elbow Surg 2011; 20(3): 385-94.
[19] Donohue KW, Ricchetti ET, Iannotti JP. *Surgical management of the biconcave (B2) glenoid*. Curr Rev Musculoskelet Med. 2016;9(1):30–9.
[20] Neer CS II, *Replacement Arthroplasty for Glenohumeral Osteoarthritis*. J Bone Joint Surg Am 1974;56(1):1-13.
[21] Physiopedia. *Total Shoulder Arthtoplasty*. Available: https://www.physio-pedia.com/Total_Shoulder_Arthroplasty
[22] Anglin C., Wyss U.P., Pichora D.R. *Mechanical testing of shoulder prostheses and recommendations for glenoid design*. J Shoulder Elbow Surg 2000;9:323-31.
[23] Iannotti J.P., Spencer E.E., Winter U., Deffenbaugh D., Williams G. *Prosthetic positioning in total shoulder arthroplasty*. J Shoulder Elbow Surg 2005;14(1 suppl S). 111e21S.
[24] Medical EXPO, *Cemented glenoid cavity prosthesis.* Available: http://www.medical-expo.com/prod/tornier/product-74846-656081.html
[25] Edwards TB, Labriola JE, Stanley RJ, O'Connor DP, Elkousy HA, Gartsman GM. *Radiographic comparison of pegged and keeled glenoid components using modern cementing techniques: A prospective randomized study.* J Shoulder Elbow Surg 2010;19(2):251-257.
[26] Lazarus MD, Jensen KL, Southworth C, Matsen FA III, *The radiographic evaluation of keeled and pegged glenoid component insertion*. J Bone Joint Surg Am 2002;84(7): 1174-1182.
[27] Friedman R.J., LaBerge M., Dooley R.L., O'Hara A.L. *Finite Element Modeling of the Glenoid Component: Effect of Design Parameters on Stress Distribution*. J. Shoulder Elbow Surg. 1992;1:261–270.
[28] Orr T. E., Wong B. E., Maw K., Ashmore W. P., Mason M. D. *The Effect of Component Fixation Design on the Performance of Glenoid Prostheses*. 43rd Meeting ORS, San Francisco 1997;881.
[29] Lacroix D., Murphy L.A., Prendergast P.J. *Three-dimensional finite element analysis of glenoid replacement prostheses: a comparison of keeled and pegged anchorage systems*. J Biomech Eng. 2000;122(4):430–6.
[30] Strauss E.J., Roche M.S., Flurin P., Wright T., Zuckerman J.D. *The glenoid in shoulder arthroplasty*. J Shoulder Elbow Surg 2009;18(5):819-833.
[31] Terrier A., Buchler P., Farron A. *Bone-cement interface of the glenoid component: stress analysis for varying cement thickness*. Clin Biomech (Bristol, Avon) 2005;20:710-7.
[32] Anglin C., Wyss U.P., Nyffeler R.W., Gerber C. *Loosening performance of cemented glenoid prosthesis design pairs*. Clin Biomech 2001;16:144–150.
[33] Giori NJ, Beaupre GS, Carter DR. *The influence of fixation peg design on the shear stability of prosthetic implants*. J Orthop Res 1990;8:892-8.
[34] Wahab A.H.A., Kadir M.R.A., Harun M.N. et al. *Number of pegs influence focal stress distributions and micromotion in glenoid implants: a finite element study*. Med Biol Eng Comput 2017;55:439.
[35] Katz D., Sauzières P., Valenti P., Kany J. *The case for the metal-backed glenoid design in total anatomical shoulder arthroplasty*. Eur J Orthop Surg Traumatol 2012;22:9–16.
[36] Brems J. *The glenoid component in total shoulder arthroplasty*. J Should Elbow Surg 1993;2:47–54

[37] Barrett WP, Thornhill TS, Thomas WH, Gebhart EM, Sledge CB. *Nonconstrained total shoulder arthroplasty in patients with polyarticular rheumatoid arthritis*. J Arthroplast 1989;1:91–96

[38] Tammachote N., Sperling J.W., Vathana T., Cofield R.H., Harmsen W.S., Schleck C.D. *Long-term results of cemented metal-backed glenoid components for osteoarthritis of the shoulder*. J Bone Joint Surg Am 2009;91:160-6.

[39] Cofield R.H. *Total shoulder arthroplasty with the Neer prosthesis*. J Bone Joint Surg 1984;66:899–906

[40] Cofield R.H. *Uncemented total shoulder arthroplasty: a review*. Clin Orthop 1994;307:86–93 56.

[41] Budge MD, Nolan EM, Heisey MH, Baker K, Wiater JM. *Results of total shoulder arthroplasty with a monoblock porous tantalum glenoid component: a prospective minimum 2-year follow-up study*. J Shoulder Elbow Surg. 2013;22:535–541.

[42] Castagna A., Randelli M., Garofalo R., Maradei L., Giardella A., Borroni M. *Midterm results of a metal-backed glenoid component in total shoulder replacement.* J Bone Joint Surg (Br) 2010; 92(10):1410-15.

[43] Stone KD, Grabowski JJ, Cofield RH, Morrey BF, An KN. *Stress analyses of glenoid components in total shoulder arthroplasty*. J Shoulder Elbow Surg 1999;8:151-8.

[44] Cofield R.H., Daly P.J. *Total shoulder arthroplasty with a tissue ingrowth glenoid component*. J Shoulder Elbow Surg 1992;1:77-85.

[45] McElwain JP, English E. *The early results of porous-coated total shoulder arthroplasty*. Clin Orthop 1987;218:217-24

[46] Roper BA, Paterson JM, Day WH. *The Roper-Day total shoulder replacement*. J Bone Joint Surg Br 1990;72:694-7.

[47] Boileau P., Avidor C., Krishnan S.G., Walch G., Kempf J.F., Mole D. *Cemented polyethylene versus uncemented metal-backed glenoid components in total shoulder arthroplasty: a prospective, double-blind, randomized study*. J Shoulder Elbow Surg 2002;11:351-9.

[48] Wallace AL, Phillips RL, MacDougal GA, Walsh WR, Sonnabend DH. *Resurfacing of the glenoid in total shoulder arthroplasty. A comparison, at a mean of five years, of prostheses inserted with and without cement*. J Bone Joint Surg Am 1999;81:510-8.

[49] Martin S.D., Zurakowski D., Thornhill T.S. *Uncemented glenoid component in total shoulder arthroplasty. Survivorship and outcomes*. J Bone Joint Surg Am 2005;87:1284-92.

[50] Taunton M.J., McIntosh A.L., Sperling J.W., Cofield R.H. *Total shoulder arthroplasty with a metal-backed, bone-ingrowth glenoid component. Medium to long-term results*. J Bone Joint Surg Am 2008;90:2180-8.

[51] Gupta S., van der Helm F.C., van Keulen F. *The possibilities of uncemented glenoid componentea finite element study*. Clin Biomech (Bristol, Avon) 2004;19:292-302.

[52] Stone KD, Grabowski JJ, Cofield RH, Morrey BF, An KN. *Stress analyses of glenoid components in total shoulder arthroplasty*. J Shoulder Elbow Surg 1999;8:151-8.

[53] Anglin C., Tolhurst P., Wyss U.P., Pichora D.R. *Mechanical properties of glenoid cancellous bone*. Proceedings of the First Conference of the International Shoulder Group. 1996:77-82.

[54] Codsi M.J., Bennetts C., Powell K., Iannotti J.P. *Locations for screw fixation beyond the glenoid vault for fixation of glenoid implants into the scapula: an anatomic study*. J Shoulder Elbow Surg 2007;16(3 suppl):S84-9.

[55] Neer CS, Watson KC, Stanton FJ. *Recent experience in total shoulder replacement*. J Bone Jt Surg Am Vol 1982; 64: 319e37.

[56] Yongpravat C., Kim H.M., Gardner T.R., Bigliani L.U., Levine W.N., Ahmad C.S. *Glenoid implant orientation and cement failure in total shoulder arthroplasty: a finite element analysis*. J Shoulder Elbow Surg 2013;22:940–947.
[57] Hopkins A.R., Hansen U.N., Amis A.A., Emery R. *The effects of glenoid component alignment variations on cement mantle stresses in total shoulder arthroplasty*. J Shoulder Elbow Surg 2004;13:668-75.
[58] Farron A., Terrier A., Buchler P. *Risks of loosening of a prosthetic glenoid implanted in retroversion*. J Shoulder Elbow Surg 2006;15: 521-6.
[59] Shapiro T.A., McGarry M.H., Gupta R, Lee Y.S., Lee T.Q. *Biomechanical effects of glenoid retroversion in total shoulder arthroplasty*. J Shoulder Elbow Surg 2007;16(3 suppl):S90-5.
[60] Yian EH, Werner CM, Nyffeler RW, Pfirrmann CW, Ramappa A, Sukthankar A, et al. *Radiographic and computed tomography analysis of cemented pegged polyethylene glenoid components in total shoulder replacement*. J Bone Joint Surg Am 2005;87:1928-36.
[61] Sins L., Tétreault P., Nuño N., Hagemeister N. *Effects of Prosthetic Mismatch and Subscapularis Tear on Glenohumeral Contact Patterns in Total Shoulder Arthroplasty: A Numerical Musculoskeletal Analysis*. Journal of Biomechanical Engineering. 2016;138(12):121007.
[62] Ghazala C.G. et al. *Anatomic shoulder arthroplasty*. Orthopaedics and Trauma, Volume 32, Issue 3,171-177
[63] Kienapfel H. S., et al. *Implant fixation by bone ingrowth*. The Journal of arthroplasty 1999;14, 3: 355–368.
[64] Burke DW, Bragdon CR, O'Connor DO, et al. *Dynamic measurement of interface mechanics in vivo and the effect of micromotion on bone ingrowth into a porous surface device under controlled loads in vivo*. Trans Orthop Res Soc 1991;16:103.
[65] Pilliar RM, Lee JM, Maniatopoulos C. *Observations on the effect of movement on bone ingrowth into porous-surfaced implants*. Clin Orthop 1986;208:108.
[66] Kienapfel H., Sprey S., Meudt P., et al. *The effect of hydroxyapatite coating on the implant micromotion in non-cemented porous coated total knee arthroplasty*. In Niwa et al (eds): Reconstruction of the knee joint. Springer-Verlag, Tokyo, 1996.
[67] Ryd L., Lindstrand A., Stenstrom A., Selvik G. *The influence of metal backing in unicompartmental tibial component fixation: an in vivo roentgen stereophotogrammetric analysis of micromotion*. Arch Orthop Trauma Surg 1992;111:148.
[68] Karrholm J., Malchau H., Snorrason F., Herberts P. *Micromotion of femoral stems in total hip arthroplasty: a randomized study of cemented, hydroxyapatire-coated, and porous-coated stems with roentgen stereophotogrammetric analysis*. J Bone Joint Surg Am 1994;76:1692.
[69] Sumner D.R., Jasty M., Jacobs J.J., et al. *Histology of porous-coated acetabular components: 25 cementless cups retrieved after arthroplasty*. Acta Orthop Scand 1993;64:619.
[70] Collier JP, Bauer TW, Bloebaum RD, et al. *Results of implant retrieval from postmortem specimens in patients with well-functioning, long-term total hip replacement*. Clin Orthop 1992;274:97.
[71] Suárez D.R., Nerkens W., Valstar E.R., Rozing P.M., van Keulen F. *Interface micromotions increase with less-conforming cementless glenoid components*. J. Shoulder Elbow Surg. 2012;21 474–482. 10.1016
[72] Klepps S., et al. *Incidence of early radiolucent glenoid lines in patients having total shoulder replacements*. Clin. Orthop. Relat. Res. 435 2005;118–125.

[73] Papadonikolakis A., Neradilek M.B., Matsen F.A. 3rd. *Failure of the glenoid component in anatomic total shoulder arthroplasty: a systematic review of the English-language literature between 2006 and 2012.* J. Bone Joint Surg. 2013;Am. 95(24):2205–2212.

[74] Verdonshot, N., and Huiskes, R. *The effects of cement-stem debonding in tha on the long-term failure probability of cement*. Journal of Biomechanics 1997;30, 8:795–802.

[75] Chevalier Y., et al. *Bone density and anisotropy affect periprosthetic cement and bone stresses after anatomical glenoid replacement: A micro finite element analysis*. Journal of Biomechanics 2016;49:1724–1733.

[76] Hermida J.C., Flores-Hernandez C., Hoenecke H.R., D'Lima D.D. *Augmented wedge-shaped glenoid component for the correction of glenoid retroversion: a finite element analysis*. J Shoulder Elbow Surg 2014;23:347–354.

[77] Clavert P., Millett P.J., Warner J.J.P. *Glenoid resurfacing: What are the limits to asymmetric reaming for posterior erosion?* Journal of Shoulder and Elbow Surgery 2007;16(6):843–848.

[78] Favre P., et al. *Numerical modelling of the shoulder for clinical applications*. Philosophical Transcations of the Royal Society 367 2009;2095–2118.

[79] Huiskes R., Hollister, S. J. *From structure to process, from organ to cell: recent developments of FE-analysis in orthopaedic biomechanics*. J. Biomech. Eng. 1993;115: 520–527.

[80] Johnson, G.R., Gill, J.M. *Prediction of the range of hand positions available to a patient with movement restrictions at the joints of the upper limb—a mathematical model*. Int. J. Rehabil. Res. 1987;10: 291–297.

[81] Engin, A.E., Tumer, S.T. *Three-dimensional kinematic modelling of the human shoulder complex—part I: physical model and determination of joint sinus cones*. J. Biomech. Eng. 1989;111:107–112.

[82] Gregory T.M., Sankey A., Augereau B., Vandenbussche E., Amis A., Emery R., et al. *Accuracy of glenoid component placement in total shoulder arthroplasty and its effect on clinical and radiological outcome in a retrospective, longitudinal, monocentric open study*. PLoS ONE 2013;8:2-8.

[83] Ho JC, Sabesan VJ, Iannotti JP. *Glenoid component retroversion is associated with osteolysis*. J Bone Joint Surg Am 2013;95:e82.

[84] Wu G., van der Helm F.C., Veeger H.E., Makhsous M., Van Roy P., Anglin C., Nagels J., Karduna A.R., McQuade K., Wang X., Werner F.W., Buchholz B. *ISB recommendation on definitions of joint coordinate systems of various joints for the reporting of human joint motion - Part II: Shoulder, elbow, wrist and hand*. Journal of Biomechanics. 2005;38(5):981-992.

[85] Amadi, H.O., et al. *An optimised method for quantifying glenoid orientation*. International journal of shoulder surgery 2008;2,2,25.

[86] Verhaegen F., Plessers K., Verborgt O., Scheys L., Debeer P. *Can the contralateral scapula be used as a reliable template to reconstruct the eroded scapula during shoulder arthroplasty?* J Shoulder Elbow Surg. 2018 Feb 23.

[87] Chae S.W. et al. *Primary stability of inferior tilt fixation of the glenoid component in reverse total shoulder arthroplasty: a finite element study. Journal of Orthopedic research* 2015;34:1061–1068.

[88] Zimmer Biomet. Available: http://www.biomet.co.uk/userfiles/files/Extremities/BMET0892_0%20TESS%20Bro-chure%20ENG.pdf

[89] Zimmer Biomet. Available: http://www.zimmer.com/content/dam/zimmer-web/documents/en-US/pdf/surgical-techniques/shoulder/anatomical-shoulder-glenoid-surgical-technique.pdf

[90] Beckmann N. A. et al. *Mechanical properties of a cemented porous implant interface*. Acta orthopaedica 2014;85, 5:531–537.

[91] Saltzman MD, Chamberlain AM, Mercer DM, Warme WJ, Bertelsen AL, Matsen FA. *Shoulder hemiarthroplasty with concentric glenoid reaming in patients 55 years old or less*. J Shoulder Elbow Surg. 2011;20:609–615.

[92] Matassi F., Carulli C., Civinini R., Innocenti M. *Cemented versus cementless fixation in total knee arthroplasty*. Joints. 2014;1(3):121–125.

[93] Terrier, A., et al. *Influence of glenohumeral conformity on glenoid stresses after total shoulder arthroplasty*. Journal of Shoulder and Elbow Surgery 2006;15, 515-520.

[94] J. Fisher, D. Dowson, H. Hamdzah, H.L. Lee. *The effect of sliding velocity on the friction and wear of UHMWPE for use in total artificial joints*. Wear, 1994;175:219-225

[95] Zhang Y., et al. *Interfacial frictional behavior: Cancellous bone, cortical bone, and a nover porous tantalum biomaterial*. Journal of Musculoskeletal Research 1999;3,4:245–251.

[96] Van der Helm F.C.T. *Analysis of the kinematic and dynamic behaviour of the shoulder mechanism*. Journal of Biomechanics 1994;27:527–550.

[97] Van der Helm, F.C.T. *A finite element musculoskeletal model of the shoulder mechanism*. Journal of Biomechanics 1994;27:551–569.

[98] Quental C. et al. *A multibody biomechanical model of the upper limb including the shoulder girdle*. Multibody System Dynamics 2012;28:83–108.

[99] Yanagawa, T., Pandy, M. G., Shelburne, K. B., Hawkins, R. J., and Torry, M. R. *Estimation of muscle and joint reaction forces at the glenohumeral joint during arm abduction: A musculoskeletal modelling approach*. Summer Bioengineering Conference. Key Biscayne, Florida 2003

[100] Massimini D.F., Li G., Warner J.P. *Glenohumeral contact kinematics in patients after total shoulder arthroplasty*. Journal of Bone and Joint Surgery - Series A 2010; 92(4):916–926.

[101] Formaini N.T., Everding N.G., Levy J.C., Santoni B.G., Nayak A.N., Wilson C., Cabezas A.F.. *The effect of glenoid bone loss on reverse shoulder arthroplasty baseplate fixation*. Journal of Shoulder and Elbow Surgery 2015;1–5.

[102] Gupta S.,van der Helm, Frans & Keulen, Fred. *Stress analysis of cemented glenoid prostheses in Total Shoulder Arthroplasty*. Journal of biomechanics 2004;37. 1777-86.

[103] Suarez, D. et al. *Interface micromotions increase with less conforming cementless glenoid components*. Journal of Shoulder and Elbow Surgery 2012;21:474–482.

[104] Suarez D. R., Valstar, E. R. Rozing, P. M., Keulen F. van. *Fracture risk and initial fixation of a cementless glenoid implant: The effect of numbers and types of screws*. Proceedings of the Institution of Mechanical Engineers, Part H: Journal of Engineering in Medicine 2013;227(10):1058–1066.

[105] Bayraktar HH, Morgan EF, Niebur GL, et al. *Comparison of the elastic and yield properties of human femoral trabecular and cortical bone tissue*. J Biomech 2004; 37(1): 27–35.

[106] Issa K., Pierce C.M., Pierce T.P., Boylan M.R., Zikria B.A., Naziri Q. et al. *Total Shoulder Arthroplasty Demographics, Incidence, and Complications-A Nationwide Inpatient Sample Database Study*. Surgical technology international 2016;29:240–246.

[107] Norris TR, Iannotti JP. *Functional outcome after shoulder arthroplasty for primary osteoarthritis: A multicenter study. Journal of Shoulder and Elbow Surgery*. 2002;11(2):130–135.